



HAL
open science

Indoor geo-location static and dynamic geo-location of mobile terminals in indoor environments

Mustapha Dakkak

► **To cite this version:**

Mustapha Dakkak. Indoor geo-location static and dynamic geo-location of mobile terminals in indoor environments. Other [cs.OH]. Université Paris-Est, 2012. English. NNT : 2012PEST1070 . tel-00794586

HAL Id: tel-00794586

<https://theses.hal.science/tel-00794586>

Submitted on 26 Feb 2013

HAL is a multi-disciplinary open access archive for the deposit and dissemination of scientific research documents, whether they are published or not. The documents may come from teaching and research institutions in France or abroad, or from public or private research centers.

L'archive ouverte pluridisciplinaire **HAL**, est destinée au dépôt et à la diffusion de documents scientifiques de niveau recherche, publiés ou non, émanant des établissements d'enseignement et de recherche français ou étrangers, des laboratoires publics ou privés.

UNIVERSITE PARIS-EST

ECOLE DOCTORALE MATHÉMATIQUES ET STIC
(MSTIC, E.D. 532)

THESE DE DOCTORAT EN INFORMATIQUE

par

Mustapha Dakkak

Géo-localisation des terminaux mobiles en
environnement fermé

soutenue le 29 novembre 2012

Jury:

Alexandre CAMINADA	Professeur des Universités	Belfort	Rapporteur
Jean-Marie GORCE	Professeur des Universités	INSA Lyon	Rapporteur
Francis LEPAGE	Professeur des Universités	Nancy	Examineur
Nacer M'SIRDI	Professeur des Universités	Marseille	Examineur
Boubaker DAACHI	Maître de Conférences	UPEC Vitry	Co-directeur
Amir NAKIB	Maître de Conférences	UPEC Vitry	Co-directeur
Patrick SIARRY	Professeur des Universités	UPEC Vitry	Directeur de thèse

Remerciements

Je voudrais tout d'abord remercier Patrick Siarry, Directeur de l'équipe Traitement de l'Image et du Signal du Laboratoire Images, Signaux et Systèmes Intelligents, et Directeur de cette thèse, ainsi que Amir Nakib et Boubaker Daachi, pour m'avoir donné la possibilité de faire cette thèse, et pour leur encadrement parfait. Ils ont toute ma gratitude pour m'avoir laissé une grande liberté dans mes recherches, aidé et encouragé dans les moments difficiles et m'avoir consacré leur temps malgré leurs occupations.

Je tiens à exprimer ma gratitude à Alexandre Caminada et à Jean-Marie Gorce pour avoir accepté d'être les rapporteurs de cette thèse. Je voudrais également remercier Francis Lepage pour avoir accepté de présider mon jury. Je remercie aussi Nacer M'Sirdi pour avoir accepté d'examiner mes travaux. J'adresse un grand merci à tous les membres de mon jury, pour avoir ainsi marqué leur intérêt pour mon travail, et pour les remarques qu'ils ont apportées durant la relecture et la soutenance de ma thèse.

Je souhaite également exprimer ma reconnaissance envers tous les membres du LiSSi, pour m'avoir accueilli chaleureusement, et pour toutes les conversations scientifiques ou non que l'on a pu avoir. Un grand merci à Patricia Jamin, Sandrine David et Frédéric Dumont, pour m'avoir aidé à surmonter toutes sortes de problèmes. Je remercie également Brigitte David, de l'ancienne Ecole Doctorale SIMME, et Sylvie Cach, de la nouvelle ED MSTIC.

Je remercie tous mes collègues doctorants, pour la bonne ambiance et leur amitié. Merci en particulier à Abbas El Dor, Noureddine Belgacem et Julien Lepagnot. Un grand merci à vous trois, pour tous les bons moments que nous avons eu au sein et à l'extérieur du labo.

Je remercie mes amis, Arij, Fadwa, Oussama AL Chami et Khaled Abu Hijleh, pour la bonne ambiance et leur amitié. Merci en particulier à Lina, Lama, Amro et Sami, toujours présents lorsque j'ai besoin d'eux.

Je remercie ma grande famille, que je remercie tout particulièrement. Un grand merci à mes parents et à mes soeurs et frères.

Ce travail n'aurait pas pu être réalisé sans le soutien de ma petite famille, que je remercie tout particulièrement. Un grand merci à mon épouse Sumaya et à mes enfants Obada et Sarah, toujours présents lorsque j'ai besoin d'eux.

Et enfin, comme il y a sans doute des trous dans mon énumération, je conclurai par ces quelques mots, merci à tous !

Résumé

Récemment, la localisation statique et dynamique d'un objet ou d'une personne est devenue l'une des plus importantes fonctionnalités d'un système de communication, du fait de ses multiples applications. En effet, connaître la position d'un terminal mobile (MT), en milieu extérieur ou intérieur, est généralement d'une importance majeure pour des applications fournissant des services basés sur la localisation. Ce développement des systèmes de localisation est dû au faible coût des infrastructures de réseau sans fil en milieu intérieur (WLAN). Les techniques permettant de localiser des MTs diffèrent selon les paramètres extraits des signaux radiofréquences émis entre des stations de base (BSs) et des MTs. Les conditions idéales pour effectuer des mesures sont des environnements dépourvus de tout obstacle, permettant des émissions directes entre BS et MT. Ce n'est pas le cas en milieu intérieur, du fait de la présence continue d'obstacles dans l'espace, qui dispersent les rayonnements. Les mesures prises dans ces conditions (NLOS, pour *Non Line of Sight*) sont imprévisibles et diffèrent de celles prises en condition LOS. Afin de réduire les erreurs de mesure, différentes techniques peuvent être utilisées, comme la mitigation, l'approximation, la correction à priori, ou le filtrage.

En effet, l'application de systèmes de suivi (TSs) constitue une base substantielle pour la navigation individuelle, les réseaux sociaux, la gestion du trafic, la gestion des ressources mobiles, etc. Différentes techniques sont appliquées pour construire des TSs en milieu intérieur, où le signal est bruité, faible, voire inexistant. Les systèmes de localisation globaux (GPS) et les travaux qui en découlent fonctionnent bien hors des bâtiments. Par contre, le suivi d'utilisateurs en milieu intérieur est bien plus problématique. De ce fait, le problème de prédiction reste un obstacle essentiel à la construction de TSs fiables dans de tels environnements. Une étape de prédiction est inévitable, en particulier, dans le cas où l'on manque d'informations. De multiples approches ont été proposées dans la littérature, la plupart étant basées sur un filtre linéaire (LF), un filtre de Kalman (KF) et ses variantes, ou sur un filtre particulaire (PF). Les filtres de prédiction sont souvent utilisés dans des problèmes d'estimation et l'application de la dérivation non entière peut limiter l'impact de la perte de performances.

Ce travail présente une nouvelle approche pour la localisation intérieure par WLAN utilisant un groupement des coordonnées. Ensuite, une étude comparative des techniques déterministes et des techniques d'apprentissage pour la localisation intérieure est présentée. Enfin, une nouvelle approche souple pour les systèmes de suivi en milieu intérieur, par application de la dérivation non entière, est présentée.

Mots clés: *localisation statique en milieu intérieur, regroupement de coordonnées, réseaux de neurones, les K plus proches voisins, localisation dynamique en milieu intérieur, filtres de prédiction, intégration non entière.*

Abstract

Recently, the static and dynamic geo-location of a device or a person has become one of the most important aspects of communication systems because of its multiple applications. In general, knowing the position of a mobile terminal (MT) in outdoor or indoor environments is of major importance for applications providing services based on the location. The development of localization systems has been mainly driven by the availability of the affordable cost of indoor wireless local area network (WLAN) infrastructure. There exist different techniques to localize MT_s with the differences mainly depending on the type of the metrics extracted from the radio frequency signals communicated between base stations (BS_s) and MT_s . Ideal measurements are taken in environments which are free of obstacles and in direct ray tracings between BS and MT . This is not the case in indoor environment because the daily use of permanent obstacles in the work space scatters the ray tracings. Measurements taken in Non Line Of Sight (NLOS) are unpredictable and different from those taken in LOS. In order to reduce measurement errors, one can apply different techniques such as mitigation, approximation, prior correction, or filtering.

Tracking systems (TSs) have many concrete applications in the space of individual navigation, social networking, asset management, traffic management, mobile resource management, etc. Different techniques are applied to build TSs in indoor environments, where the signal is noisy, weak or even non-existent. While the Global Positioning System (GPS) devices work well outside buildings and in urban canyons, tracking an indoor user in a real-world environment is much more problematic. The prediction problem remains an essential obstacle to construct reliable indoor TSs. Then lack of reliable wireless signals represents the main issue for indoor geo-location systems. This obviously calls for some sort of predictions and corrections to overcome signal reliability, which unavoidably open the door for a multitude of challenges. Varieties of approaches were proposed in the literature. The most used are the ones based on prediction filters, such as Linear Filter (LF), Kalman Filter (KF) and its derivatives, and Particle Filters (PF). Prediction filters are often used in estimation problems and applying Digital Fractional Differentiation can limit the impact of performance degradations.

This work presents a novel approach for the WLAN indoor geo-location by using coordinates clustering. This approach allows overcoming the limitations of NLOS methods without applying any of mitigation, approximation, prior correction, or filtering approaches. Then a comparison study of deterministic and learning techniques for indoor geo-location is presented. Finally, we propose a novel soft approach for indoor tracking system by applying digital fractional integration (DFI) to classical prediction filters.

Keywords: *static indoor localization, coordinate clustering, artificial neural networks, K-nearest neighbor, soft computing, dynamic indoor localization, prediction filters, digital fractional differentiation/integration (DFD/DFI), short-archive principle.*

Table of contents

Acronyms	1
Introduction	3
1 State of the art: mobile terminal geo-location	6
1.1 Introduction	6
1.2 Indoor geo-location: different measurements and techniques	7
1.2.1 Range-based techniques	9
1.2.1.1 Distance-based techniques	9
1.2.1.1.a Time Of Arrival (TOA)	9
1.2.1.1.b Time Difference Of Arrival (TDOA)	10
1.2.1.1.c Received Signal Strength (RSS)	12
1.2.1.1.d Round-Trip Time (RTT)	14
1.2.1.1.e Received Signal Phase (RSP)	15
1.2.1.2 Angle-based techniques: Angle Of Arrival (AOA)	16
1.2.2 Range-free techniques	17
1.2.2.1 Associated Cell (CellId)	17
1.2.2.2 Location patterning techniques	19
1.2.2.2.a Probabilistic methods	20
1.2.2.2.b K-nearest neighbors (KNN)	22
1.2.2.2.c Artificial neural networks (ANN)	23
1.2.2.2.d Support vector machine (SVM)	24
1.2.2.2.e Smallest M-vertex polygon (SMP)	25
1.3 Tracking systems and prediction filters	25
1.3.1 Tracking systems	25
1.3.2 Prediction filters	26
1.3.2.1 Kalman filter	26
1.3.2.1.a Kalman filter modeling	27
1.3.2.2 Particle filter	29
1.3.2.2.a Particle filter modeling	30
1.4 Location systems: architectures and requirements	32
1.5 Conclusion	34
2 Our indoor location based on TOA and AOA using coordinates clustering	36
2.1 Introduction	36
2.2 Clustering and problem formulation	36
2.2.1 Cluster analysis	37
2.2.2 Measurements choice	37
2.2.3 Problem formulation	37

2.3	Proposed method	39
2.3.1	Two dimensional environment case	39
2.3.2	Extension to three dimensional environment case	44
2.4	Experimental results and discussion	45
2.4.1	Case study	45
2.4.2	Two dimensional case	47
2.4.3	Thresholds impact	48
2.4.4	Three dimensional case	48
2.5	Comparison	49
2.6	Conclusion	52
3	A comparison of learning and deterministic range-free techniques for indoor geo-location	54
3.1	Introduction	54
3.2	Artificial neural networks (ANN)	56
3.2.1	Definition	56
3.2.2	Neural network topologies	57
3.2.2.1	Feedforward neural networks	57
3.2.2.2	Recurrent neural networks	58
3.2.2.3	Hybrid neural networks	58
3.2.3	Neural network training (learning)	59
3.2.3.1	Supervised learning	59
3.2.3.2	Unsupervised (adaptive) learning	60
3.2.3.3	Reinforcement learning	60
3.2.4	Neural network applications	60
3.3	Proposed ANN approach for indoor location	61
3.3.1	Case study and fingerprint collection	61
3.3.1.1	Case study	61
3.3.1.2	Fingerprint collection	62
3.3.2	ANN-based proposed algorithm for indoor location	63
3.3.3	ANN experimental results	63
3.3.3.1	Impact of hidden layers number	65
3.3.3.2	Impact of heterogeneous fingerprints	67
3.3.3.3	Impact of fingerprint database resolution	67
3.4	K-nearest neighbor (KNN)	68
3.4.1	Proposed KNN-based algorithm for indoor location	70
3.4.2	KNN-based experimental results	70
3.4.2.1	Impact of nearest neighbor number K	70
3.4.2.2	Impact of the chosen metric: δ -nearest neighbor (δ -NN)	71
3.4.2.3	Impact of heterogeneous fingerprints	72
3.4.2.4	Impact of fingerprint database resolution	73
3.5	ANN vs KNN: comparison and discussion	74
3.6	Conclusion	75
4	Mobile tracking based on fractional integration	77
4.1	Introduction	77
4.2	Digital fractional integration: characteristics and applications	78
4.2.1	Fractional integration	79

4.2.2	Properties of the fractionally integrated trajectory	81
4.2.2.1	Regularity	81
4.2.2.2	Statistical analysis of the fractionally integrated path	82
4.2.2.2.a	Average value of the differentiated function	82
4.2.2.2.b	Autocorrelation	83
4.2.3	The short-memory principle	86
4.3	Our proposed method	87
4.4	Results and discussion	88
4.4.1	Enhancement of the path prediction using DFI	91
4.4.2	On the decrease of archive size	92
4.4.2.1	The linear predictor (LP) case	93
4.4.2.2	The Kalman filter case	95
4.4.3	The short-memory principle	96
4.5	Conclusion	96
 Conclusion and perspectives		 104
 References		 115

Acronyms

2D	Tow Dimensional
3D	Three Dimensional
ANN	Artificial Neural Network
ARPS	Active Remote Positioning System
AOA	Angle Of Arrival
AP(s)	Access Point(s)
APS	Ad hoc Positioning System
BS(s)	Base Station(s)
BPNN	Back-Propagation Neural Network
CellID	Celle Identifier
CN	Closest Neighbor
DFD	Digital Fractional Differentiation
DFI	Digital Fractional Integration
DMLP	Dynamic Multi-Layer Perceptron
DOA	Direction Of Arrival
DSSS	Direct Sequence Spread-Spectrum
DTS	Dynamic Tracking System
EBP	Error BackPropagation
FFNN	Feed Forward Neural Network
GPS	Global Positioning System
ILP	Indoor location system
KNN	K-Nearest Neighbors
LBA	Location-Based Applications
LBS	Location-Based Sevices
LMS	Least Mean Square
LOB(s)	Line(s) Of Bearing
LOS	Line Of Sight

MT(s)	Mobile Terminal(s)
NLOS	Non Line Of Sight
NN	Neural Network
OINNSS	Oriented Independent Nearest Neighbor Signal Strength
PNMC	Prior NLOS Measurement Correction
POA	Phase Of Arrival
PRPS	Passive Remote Positioning System
PSO	Particle Swarm Optimization
RF	Radio Frequency
RIPS	Radio-Interferometric Positioning System
RPS	Remote Positioning System
RPSim	Radiowave Propagation Simulator
RSP	Received Signal Phase
RSS	Received Signal Strength
RSSI	Received Signal Strength Indicator
RTOF	Round-Time Of Flight
RTLS	Real-Time Location System
RTT	Round-Trip Time
RWGH	Residual WeiGHting
SMP	Smallest M-vertex Polygon
SVM	Support Vector Machine
SVR	Support Vector Regression
TDOA	Time Difference Of Arrival
TCAS	Traffic alert and Collision Avoidance Systems
TOA	Time Of Arrival
UPEC	Université Paris-Est Créteil
UWB	Ultra Wide Band
WA	Weighted Average
WAP	Wireless Access Points
WLAN	Wireless Local Area Network

Introduction

To meet and satisfy users needs, location-based applications and services (LBA, LBS) need to provide a relatively high level of accuracy. Locating the mobile terminal (MT) in outdoor environments is achieved with good accuracy using GPS systems, where there is a line of sight between satellites and MT s in most situations. This accuracy is about a few meters for civilian applications. However, in tunnels, forests, and urban canyons, the performance of GPS degrades or may not work at all due to the weakness of received signals, or because of the absence of the visibility between the system elements (satellites and MT).

Indoor geo-location is a useful application because it can be effectively used in airports, hotels, hospitals, museums, etc. for tracking and safety of humans and goods. The development of geo-location systems has been mainly driven by the novel standards such as IEEE 802.11, IEEE 802.15.4a or Zigbee. These internal networks, which are deployed into the buildings, allow us to improve the geo-location process. One of the major problems for such systems is that the daily use of permanent obstacles in the work space scatters the signals between base stations and mobile terminals, which means the MT is rarely in line of sight (LOS) of the base station, an accurate triangulation here is much more challenging. Although several metrics are supplied by WLAN access points, the angle of arrival (AOA), the time of arrival (TOA), the round trip time (RTT), the received signal strength (RSS) and other metrics, geo-location of MT has never been an objective in WLAN design. Fortunately, some of the above mentioned metrics can be exploited to design an indoor geo-location system with an accuracy level that can satisfy most of the indoor LBS applications.

The different geo-location techniques could be classified into two essential categories, range-based and range-free categories. The range-based technique category is based on positioning the MT by calculating distances and angles contributed between BS_s and MT or between MT_s themselves. On the other hand, the second technique relies on identifying the MT location using its fingerprint or by applying pattern recognition or probabilistic models. The notion of received signal strength is related to signal propagation laws and the attenuation of the signal is proportional to the distance between BS and MT . On the other hand, RSS fingerprint map

could be determined in the indoor environment, which means the available information of RSS can be used to establish the geo-location process using a range-base or a range-free technique.

Locating a *MT* depends on the available metrics and other information which characterizes the test-bed. Techniques which exploit more than one metric or rely on several technologies to position the *MT* are called hybrid techniques. Because each technique has its own advantages and shortcomings, hybrid techniques aim to combine the advantages of their principal techniques and cancel out their disadvantages. Such solutions could lead to the best estimation of the *MT* location.

The so-called soft approaches have been proposed as an underlying technology to build reliable indoor tracking systems, particularly in the lack of reliable signals. The most used approach is that based on prediction filters, such as linear filters (LF), Kalman filters (KF) and its derivatives, and particles filters (PF). To enhance the performance of these predictors, the digital fractional integration (differentiation) DFI (DFD) has been applied. The theory of fractional derivatives was primarily developed as a theoretical field of mathematics. More recently, fractional differentiation is found in various areas: in control theory, it is used to determine a robust command control; it is also used to solve the inverse heat conduction problem; other applications are reported for instance in neuronal modeling, image processing for edge detection, and biomedical signal processing.

The main contributions of this thesis are:

- a novel hybrid method for indoor geo-location based on AOA and TOA measurements. A new type of clustering will be introduced to classify the location estimates, called coordinate clustering. Our proposed method for indoor geo-location allows overcoming the limitations of NLOS methods.
- An objective study of two range-free techniques, artificial neural network learning technique and K-nearest neighbor deterministic technique. Range-free techniques provide an alternative solution to locate the mobile terminal in critical blind areas.
- A novel soft approach to enhance the performance of classical prediction filters. The main idea takes advantage from the properties of the DFI to increase the performance without any complexity.

This thesis is organized as follows.

The first chapter presents the set of existing geo-location technologies and techniques. Some of these methods (e.g., GPS) have been intensively studied, while other technologies have received a limited coverage in the relevant literature. Although the GPS method dominates the tracking systems in outdoor environments, this chapter shows that neither of the geo-location techniques dominates the indoor environment geo-location process for location-based applications/services (LBA/LBS). Hence, the interest of our work in this research domain.

The second chapter proposes a novel hybrid indoor geo-location method using a coordinate clustering technique. This method exploits two metrics, time of arrival (TOA) and angle of arrival (AOA). The coordinate clustering technique helps to restrict the geo-location process by reducing the number of observations at each coordinate level. Finally, we show in this chapter that it is better in some situations not to consider the above techniques if an error occurs in a multipath environment as a result of Non Line Of Sight (NLOS).

In the third chapter, a comparative study of artificial neural network (learning) method and K-nearest neighbor (deterministic) method for indoor geo-location is presented. Definition, topologies, and different learning approaches are explored in detail in this chapter. Several simulations on the same test-bed are also conducted here to assess the impact of different variants of each technique and compare their performances using homogeneous and heterogeneous fingerprint databases with different resolutions.

In the fourth chapter, we show and prove under some assumptions that the digital fractional integration allows to increase the autocorrelation of a path. Then, we present a novel soft approach to enhance the performance of the classical predictors using digital fractional differentiation/integration (DFD/DFI) to predict a MT trajectory. Intensive study of short-archive principle has been done to prove the superiority of DFI predictors using only the last few locations.

To conclude this thesis, we summarize our contributions and we propose interesting future research directions based on the work performed within this thesis.

STATE OF THE ART: MOBILE TERMINAL GEO-LOCATION

1.1 Introduction

Recently, the location of a mobile terminal (MT) has become one of the most important features of communication systems because of its multiple applications. Indoor location is a useful application as it can be effectively used in airports, hotels, hospitals, etc. to track goods and to provide safety services. An important number of techniques have been developed for indoor location purposes, where GPS is not applicable because of the coverage limitation and its low level of precision. There are two main categories of positioning systems, static or memoryless positioning systems and dynamic positioning (tracking) systems (DTSs). The first category assumes that the MT remains stationary [Dakk 11a; Kush 07; Yin 08; Yous 05; Bahl 00b; Kaem 04; Chen 06; Pan 06; Pras 02], while the tracking systems category depends on the correlation of MT positions over time [Kush 06; Ladd 04; Even 05; Wang 08; Paul 08].

The development of location systems has, in part, been favored by the affordable cost of indoor wireless local area network (WLAN) infrastructure. There exist different techniques to position a MT depending on the metrics extracted from the radio frequency signals communicated between base stations (BS_s) and mobile terminals (MT_s). In a perfect environment there are no obstacles between the BS and MT . Measurements taken in non line of sight (NLOS) are unpredictable and lead to highly unreliable measurements compared to measurements taken in line of sight (LOS). Accurate measurements strongly depend on the location of MT . In order to reduce measurement errors, one can employ different techniques, such as mitigation, approximation, prior correction, or filtering. In the last decade, many applications were developed in the research community to position MT . These applications are divided into two main classes: the first uses range-free measurements, like received signal strength (RSS) [Bahl 00b; Vars 07; Yun 09; Swan 08; Guo 08], while the second uses range-based measurements, like angle, distance and time. RADAR [Bahl 00b] is the first positioning system developed by Microsoft to estimate MT location using RSS captured from multiple BS_s . In [Vars 07], the authors make an accurate GSM-based indoor location through the use of wide

signal strength fingerprints. In [Swan 08], the authors use the analysis of the fingerprint structure to identify and eliminate inefficient location fingerprints stored in the fingerprint database. In the second class, many of the location methods and approaches based on geometric calculation depend on time of arrival (TOA). Authors in [Zhen 04] assume that their ranging system is based on estimating TOA transmitted by more than three BS_s and received at MT . In a recent work [Taye 09], the authors developed a hybrid location method by considering the Euclidean distance between the direction of arrival DOA and the RSS, from each unknown position and the information from the fingerprints. A review of wireless indoor positioning methods can be found in [Liu 07]. Most of these approaches suffer from NLOS caused by the existing obstacles in the environment. Particularly, many techniques were developed to mitigate the estimation error due to NLOS. These techniques can be classified into two categories. The first category puts an emphasis on minimizing the effect of NLOS for locating MT , while the second category focuses on the identification of NLOS BS_s and discards them in the process of location. In order to mitigate the NLOS errors during location estimation, an algorithm is proposed in [Chen 99] which is applied when the range measurements, corrupted by NLOS errors, are not identifiable. The authors in [Cong 04] investigated NLOS error identification and correction techniques for mobile user location in wireless cellular systems. They proposed two NLOS mitigation algorithms which work on a prior knowledge of the NLOS error. The simulations depend on a prior information database to achieve good accuracy. The authors in [Mazu 09] added a prior NLOS measurement correction (PNMC) technique to position an MT in a cellular wireless network. In [Bahi 09] the authors considered several indoor environments where the transmitted signals could only reach the receiver through reflected, diffracted, or scattered paths. Since PNMC is based on a statistical processing of a record of measurements taken over a time window, the authors segment the NLOS recorded measurements into segments, and finally the NLOS error correction depends on these segments. An analysis of the location accuracy of TOA/AOA hybrid algorithm with a single BS in LOS scenario is presented in [So 03].

In the following, different measurements and techniques for the static indoor location process will be explored.

1.2 Indoor geo-location: different measurements and techniques

According to measurement techniques utilized to determine the mobile terminals position, location positioning systems can be classified into two basic categories:

- Range-based techniques: This category contains geometric approaches that depend on the propagation time, as Time Of Arrival (TOA), Time Difference Of Arrival (TDOA), or Round Trip Time (RTT) and/or Angle Of Arrival (AOA), to calculate the distance between MT_s and the WLAN access points (APs), then the MT position is estimated by applying triangulation or trilateration method [Zhen 04].
- Range-free techniques: This category of positioning is based on K-nearest neighbor [Bahl 00b], probabilistic [Yous 05], and pattern recognition techniques [Fang 08; Brun 05; Bore 08].

Hybrid approaches using several measurements/techniques attempt to improve the performance of positioning systems when the propagation characteristics vary differently in the environments.

Fig. 1.1 summarizes indoor geo-location measurements, techniques, and technologies.

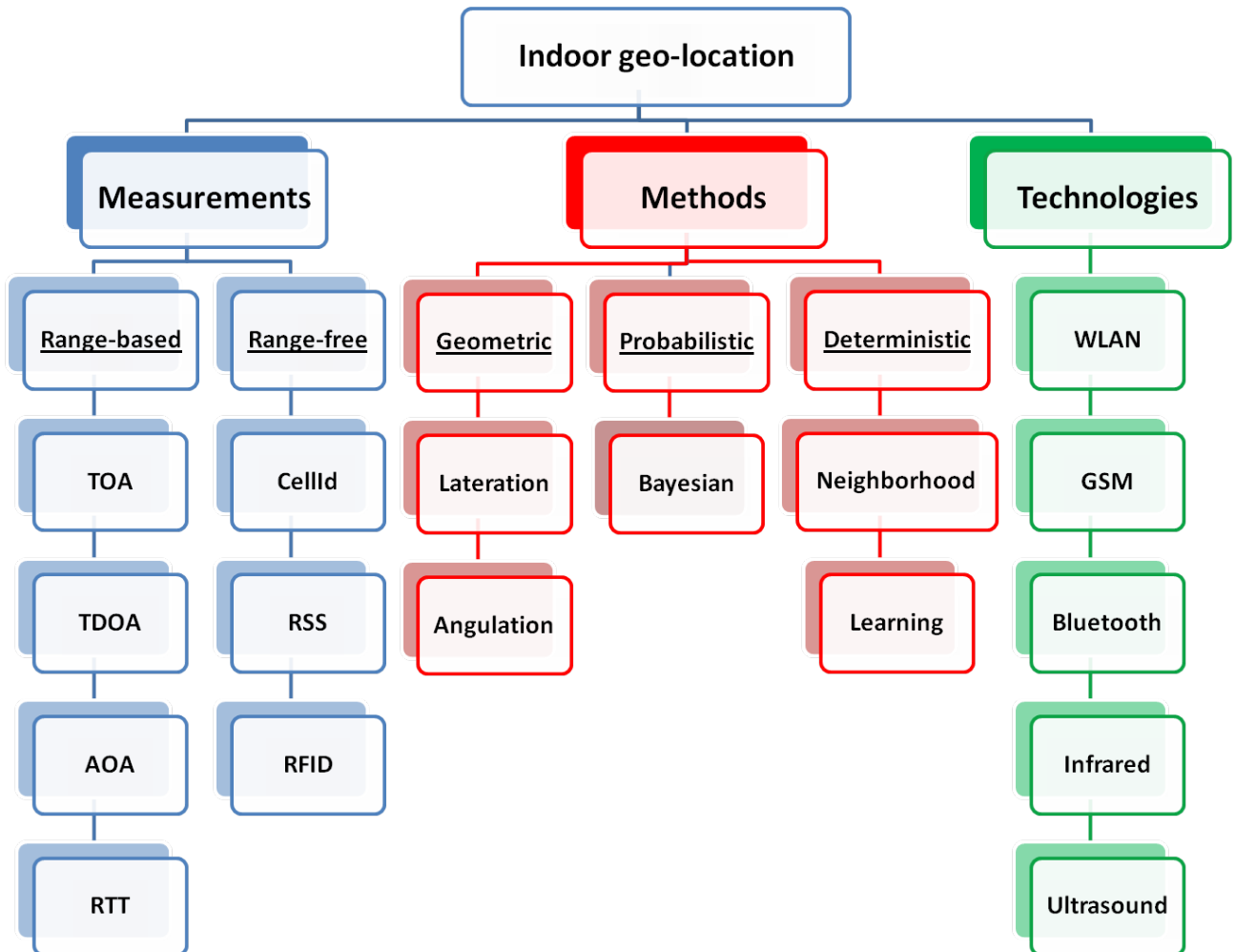


Figure 1.1: Indoor geo-location: measurements, techniques, and technologies.

1.2.1 Range-based techniques

Positioning systems belonging to this category exploit information provided in the wireless LANs to calculate the range (distance/angle) that relates the base stations to the mobile terminal. The knowledge of this basic information is necessary to apply one of lateration/angulation techniques to locate the mobile terminal. In the following, we present a brief description, advantages, and problems related to the use of each technique.

1.2.1.1 Distance-based techniques

Different measurements are used to estimate the distance between the base stations and the mobile terminal, like time of wave propagation, signal phase, and signal strength.

1.2.1.1.a Time Of Arrival (TOA)

Time Of Arrival (TOA), sometimes called Time Of Flight (TOF), techniques are based on the accurate measurement of the arrival time of a signal transmitted from a mobile terminal to several receiving base stations. If we assume that signals travel with the speed of light c , the distance d between the mobile terminal and each receiving base station can be estimated from the elapsed time t of signal propagation: $d = c \times t$. Accurate synchronization is required in the TOA techniques. This synchronization is realized thanks to the knowledge of the transmission date, and all receiving base stations as well as the mobile terminal should be accurately synchronized with a precise time source. In the case of a two dimensional positioning system, TOA measurement must be made with respect to signals from at least three reference base stations. Fig. (1.2) illustrates the location process based on TOA measurements.

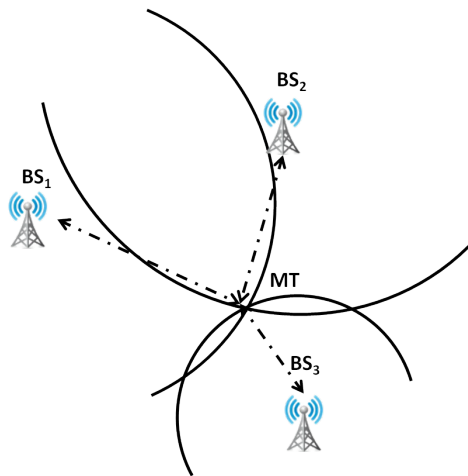


Figure 1.2: TOA/RTT positioning measurement: MT is the mobile terminal to be positioned, BS_1 , BS_2 , and BS_3 are the base stations.

The TOA-based techniques suffer of two problems. The first problem is that all mobile terminals and base stations in the system have to be precisely synchronized. The second one is that the transmitting signal should include a timestamps in order for the base station to calculate the distance traveled by the signal. Finally, TOA can be measured using different signal techniques such as direct sequence spread-spectrum (DSSS) [Pete 98; Li 00] or ultra wide band (UWB) measurements [Corr 03]. A straightforward approach uses a geometric method to compute the intersection points of the circles of TOA. The position of the mobile terminal can also be computed by minimizing the sum of squares of a nonlinear cost function, i.e., least-squares algorithm [Fang 90; Kana 04]. It assumes that the mobile terminal, located at (x_0, y_0) , transmits a signal at time t_0 , the n base stations located at $(x_i, y_i), i \in \{1, 2, \dots, n\}$ receive the signal at time $t_i, i \in \{1, 2, \dots, n\}$. As a performance measure, the cost function can be formed by the equation (1.2.1):

$$F(d) = \sum_{i=1}^n a_i^2 \Delta_i^2(d) \tag{1.2.1}$$

where a_i can be chosen to reflect the reliability of the signal received at the base station i , and $\Delta_i(d)$ is given by the equation (1.2.2):

$$\Delta_i(d) = c \times \delta_t - \sqrt{\delta_x^2 + \delta_y^2} \tag{1.2.2}$$

where c is the speed of light, and the state vector $d = (x, y, t)^T$. This function is formed for each base station, $i \in \{1, \dots, n\}$, and $\Delta_i(d)$ could be minimized with looking to the coordinates x, y , and the time t . Then, the approximate location is determined by minimizing the function $F(d)$ defined in the equation (1.2.1).

There are other algorithms for TOA-based indoor location systems as closest-neighbor (CN) and residual weighting (RWGH) [Kana 04]. The CN algorithm estimates the location of the mobile terminal as the location of the base station or reference point that is located closest to the mobile terminal. The RWGH algorithm can be basically viewed as a form of weighted least-squares algorithm. TOA-based positioning solutions are typically challenged in environments where large amount of multipath (NLOS), interference, or noise exists.

1.2.1.1.b Time Difference Of Arrival (TDOA)

The main idea of Time Difference Of Arrival (TDOA) technique is to use relative time measurements at each receiving base station instead of absolute time measurements. Thus, TDOA does not require the use of a synchronized time source at the mobile terminal in order to resolve timestamps and estimate the position. For each TDOA measurement, the mobile terminal must

lie on a hyperboloid with a constant range difference between the two base stations. The equation of the hyperboloid in two-dimensional (2D) Cartesian coordinates is denoted by (1.2.3):

$$d_{i,j} = \sqrt{(x - x_i)^2 + (y - y_i)^2} - \sqrt{(x - x_j)^2 + (y - y_j)^2} \quad (1.2.3)$$

where (x_i, y_i) and (x_j, y_j) represent the fixed base stations i and j ; and (x, y) represent the coordinates of the mobile terminal [Dran 98]. Except the exact solutions to hyperbolic TDOA equation shown in (1.2.3) through nonlinear regression, an easier solution is to linearize the equations through the use of a Taylor-series expansion and create an iterative algorithm [Torr 84].

A mobile terminal location in a 2D environment can be estimated from the two intersections of two or more TDOA measurements, as shown in Fig. (1.3).

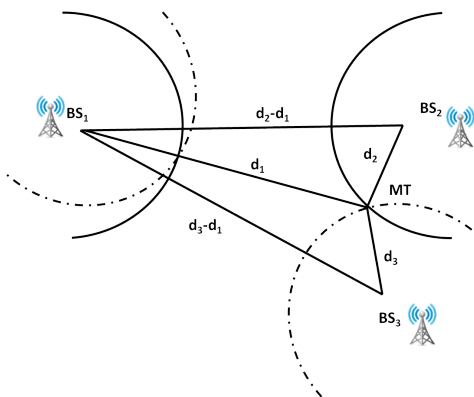


Figure 1.3: TDOA positioning measurement.

Two hyperbolas are formed from TDOA measurements at three base stations (BS_1, BS_2 , and BS_3) to provide an intersection point, which locates the mobile terminal MT .

Conventional methods for computing TDOA estimates are to use correlation techniques. TDOA can be estimated from the cross correlation between the signals received at a pair of base stations. Suppose that, for the transmitted signal $s(t)$, the received signal at base station i is x_i . Assume that $x_i(t)$ is corrupted by the noise $n_i(t)$ and delayed by d_i , then $x_i(t) = s(t - d_i) + n_i(t)$. Similarly, the signal $x_j(t) = s(t - d_j) + n_j(t)$, which arrives at base station j , is delayed by d_j and corrupted by the noise $n_j(t)$. The cross-correlation function of these signals is given by integrating the lag product of two received signals over a time period T , as shown in the equation (1.2.4):

$$\hat{d}_{x_i, x_j}(\tau) = \frac{1}{T} \int_0^T x_i(t) x_j(t - \tau) dt \quad (1.2.4)$$

Except the previous TDOA methods, a delay measurement-based TDOA measuring method was proposed in [Li 00] for 802.11 WLANs, which eliminates the requirement of initial synchro-

nization in the conventional methods.

Geo-location techniques that use TOA and TDOA metrics have several similarities. These techniques have proven to be highly suitable for outdoor geo-location systems. In addition, satisfactory results have been obtained from TOA and TDOA geo-location systems in half-open environments such as theaters, halls, and museums. Indoor, TDOA-based geo-location systems achieve best performance in large environments that are relatively open, with limited amount of obstacles and high ceilings that afford direct LOS between the mobile terminal and the base stations. However, the propagated signals suffer of multiple reflections in obstructed environments, and TOA measurements don't express the real distance between the base station and the mobile terminal, therefore, the performance degrades in terms of accuracy. In general, in these types of environments, TDOA and TOA-based geo-location systems operate efficiently and prove their performance and superiority.

1.2.1.1.c Received Signal Strength (RSS)

The drawbacks in the case of indoor environments of the above mentioned distance-based techniques (TOA and TDOA) using elapsed time to measure distance are the following ones: it is difficult to find direct LOS between the mobile terminal and the base station, the radio wave propagation in obstructed environments would suffer from multipath effects, and the time and angle of arrival signal would be affected by the multipath effect; thus, the accuracy of estimated location will decrease and the performance degrades. An alternative approach consists in estimating the distance of the mobile terminal from the base stations and using the attenuation of received signal strength. The signal attenuation-based methods attempt to calculate the signal path loss due to the wave propagation. Theoretical and empirical models are used to translate the difference between the transmitted signal strength and the received signal strength into a distance estimate. The knowledge of the transmitter output power, cable losses, and antenna gains, as well as the appropriate path loss model, allows an accurate estimation of the distance between two stations. The path loss represents the level of signal attenuation present in the environment, due to the effects of free space propagation, reflection, diffraction, and scattering. An example of a common path loss model used for indoor propagation [Pahl 09] is presented by the equation (1.2.5):

$$P(d) = P(d_0) - 10\alpha \log\left(\frac{d}{d_0}\right) \quad (1.2.5)$$

where d represents the distance between the transmitter and the receiver, $P(d)$ is the received signal strength at distance d measured in dBm , $P(d_0)$ is the referenced signal strength at the

initial distance d_0 , α represents the path loss exponent for the environment that indicates the rate at which the path loss increases with distance. The value of the path loss exponent depends on the signal frequency and the environment, and is highly dependent on the degree of obstruction present in the environment. Table (1.1) summarizes some values of this exponent according to the environment type.

Table 1.1: Different values of the path loss exponent α in different environments.

α	Environment
2	Open free space
3.5	Indoor office
3.7 to 4.0	Commercial or industrial environment
4.5	Dense obstructed environment

To provide a more realistic estimate of the received signal strength, the characteristics of the environment structure should be taken into account. This propagation model can be expressed by the equation (1.2.6) [Even 07]:

$$P(d) = P(d_0) - 10\alpha \log\left(\frac{d}{d_0}\right) + \sum_{i=0}^M n_i R_i + \sum_{i=0}^N n_i T_i \quad (1.2.6)$$

where R_i and T_i are the attenuations introduced during the reflections and transmissions through the material i existing in the environment. In this model, it is considered that we have M different materials on which was at least one reflection, and N different materials through which we have at least one transmission.

The optimal parameters (α , R_i and T_i) that characterize the environment can be found by solving the following minimization problem (1.2.7):

$$[\alpha, R_i, T_i]^{opt} = \arg \min_{\alpha, R_i, T_i} \left[\left(P(d) - P(d_0) + 10\alpha \log\left(\frac{d}{d_0}\right) - \sum_{i=0}^M n_i R_i - \sum_{i=0}^N n_i T_i \right)^2 \right] \quad (1.2.7)$$

Using only RSS-based geo-location systems that do not take into account any additional steps for attenuation and multipath in the environment rarely produces acceptable results except in very controlled situations. This includes those controlled situations where there is always direct LOS between the mobile terminal and the receiving base stations, with little attenuation to be concerned other than free-space path loss and minor impact from multipath. Most of sensor-network-based positioning systems use RSS measurement [Ash 04]. The accuracy of these techniques can be improved by utilizing the pre-measured RSS contours centered

at the receiver [Zhou 05] or multiple measurements at several base stations. A fuzzy logic algorithm shown in [Teub 06] is able to significantly improve the location accuracy using RSS measurement. However, other positioning systems use RSS as range-free measurement. Authors in [Suro 11] proposed a new method of radio frequency (RF) fingerprint-based technique for indoor geo-location. The received signal strength indicator (RSSI) is used as database values which correspond to the location of the sensor nodes. Fuzzy C-Means (FCM) clustering algorithm is applied as the experiment data cluster method. FCM algorithm is deployed to cluster the obtained feature vectors into several classes corresponding to the different amount of RSSI values. Their results show that FCM can cluster the mobile terminals in a group of the fingerprint database. The location of target node is arranged in various forms to validate the accuracy of the clustering technique. Euclidean distance is used as the parameter to compare the similarity between fingerprint database and the mobile terminal location. Their results show that the new method is simple and effective to reduce the complexity, to support the low power and to reduce the time used in the fingerprint-based geo-location technique.

1.2.1.1.d Round-Trip Time (RTT)

As we have mentioned above, TOA measurement requires strong synchronization between base stations. An alternative solution is Round-trip time (RTT) measurement, also called round-trip delay or Round-Time-Of-Flight (RTOF). By definition, RTT is the time required for a signal to travel from a specific base station to a specific destination (mobile terminal) and back again, as shown in Fig. (1.5). The advantage of using RTT is to avoid the time synchronization between base stations; in other words, a more moderate relative clock synchronization requirement replaces the synchronization requirement in TOA. In addition, RTT conserves the same characteristic mentioned for TOA measurement. Therefore, positioning algorithms for TOA can be directly applicable for RTT. In RTT-based positioning systems, the base station plays the role of a common radar. Thus, the mobile terminal will respond to the interrogation signal transmitted by the base station, and the complete round trip propagation time is measured by the base station. However, it is still difficult for the base station to know the exact delay/processing time caused by the responder in this case. If the order of the delay time is relatively small compared with the transmission time, then, it could be ignored and this technique becomes applicable in long-distance or medium-distance systems. However, for short-distance systems, it cannot be ignored. An alternative approach is to use the concept of modulated reflection [Koss 00], which is only suited for short-range systems. An algorithm to measure RTT of WLANs packets is presented in [Gunt 05] with the result of measurement error of a few meters.

1.2.1.1.e Received Signal Phase (RSP)

Received signal phase method, is referred also as phase of arrival (POA) [Pahl 02]. To estimate the distance between the base station and the mobile terminal, the RSP method uses the carrier phase (or phase difference). This technique demands a strong constraint at signal level. All emitted signals from the distributed base stations should be zero offset sinusoidal signals that have the same frequency f . By calculating the propagation delays from the base stations to the mobile terminal, we can determine the phases of received signals at the MT location. Assuming that the base stations BS_1, BS_2, BS_3 , and BS_4 are distributed in a cubic environment, as seen in Fig. (1.4), this delay is expressed as a fraction of the wavelength of the signal, and is denoted by:

$$\phi_i = (2\pi ft_i), t_i = D_i/c \quad (1.2.8)$$

where $i \in \{BS_1, BS_2, BS_3, BS_4\}$, c is the speed of light, and D_i is the distance between the transmitting base station and the mobile terminal to be located. Then, the sinusoidal signal could be written as:

$$S_i(t) = \sin(2\pi ft + \phi_i) \quad (1.2.9)$$

If $0 < \phi_i < 2\pi$, then the transmitted signal's wavelength is longer than the diagonal of the squared environment, therefore, we can calculate the distance estimation by the relation (1.2.10):

$$D_i = (c\phi_i)/(2\pi f) \quad (1.2.10)$$

Then, one of the lateration techniques could be used to locate the mobile terminal. For example, we can use the same positioning algorithms using TOA measurement. Also, the mobile terminal (the receiver) may measure phase differences between two signals transmitted by two base stations, and positioning systems are able to use the TDOA algorithms to locate the mobile terminal [Sall 10].

In the wireless sensor networks domain, the radio-interferometric positioning system (RIPS) [Maro 05] is one representative of the RF phase based techniques.

For a hybrid indoor positioning system, it is possible to use the signal phase method together with TOA/TDOA or RSS method to improve the performance of the location positioning. However, the shortcoming of the RSP method when applied in indoor environments is that it strongly needs a LOS signal path to limit the location errors [Liu 07].

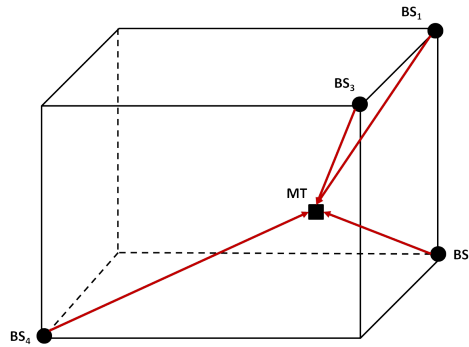


Figure 1.4: RSP positioning measurement: BS_1 , BS_2 , BS_3 , and BS_4 are the transmitter base stations, MT : the mobile terminal to be located.

1.2.1.2 Angle-based techniques: Angle Of Arrival (AOA)

Angle of arrival (AOA) measurement is a method for determining the direction of propagation of a radio-frequency wave incident on an antenna array of the base station. AOA determines the direction by measuring the TDOA and the difference in received phase at individual elements of the array; from these delays, the AOA can be calculated. The Angle Of Arrival (AOA) techniques, called also the direction of arrival (DOA), locates the mobile terminal by determining the angle of incidence at which signals arrive at the base station. Geometric relationships are used to estimate the mobile terminal location from the intersection of two lines of bearing (LOBs) formed by a direct ray tracing to each base station. Fig. (1.5) illustrates AOA positioning measurement.

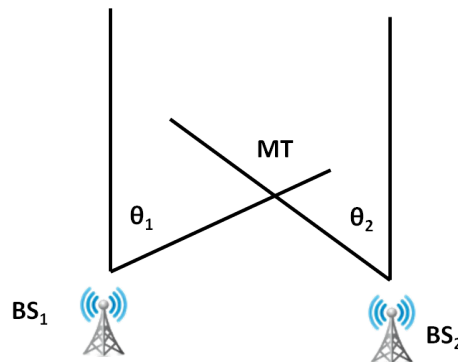


Figure 1.5: AOA positioning measurement: BS_1 and BS_2 are the base stations, MT is the mobile terminal to be positioned, and θ_1 and θ_2 are the angles of arrivals.

In a $2D$ environment, we need at least two base stations for location estimation. To apply the triangulation approach, three or more base stations are required. In its purest form, where direct LOS is evident between the mobile terminal and receiving base stations, mechanically-

agile directional antennas deployed at the receiving base stations are adjusted to the point of the highest signal strength. The positioning of the directional antennas can directly be used to determine the LOBs and measure the angles of incidence θ_1 and θ_2 . In practical commercial and military implementations of AOA, multiple antenna arrays are used to sample the receiving signal, thereby eliminating the need of more complex and maintenance-intensive mechanical antenna systems. The electronic switching can be performed between arrays or portions of each array, and mathematical computations handled by a background computing system used to extract the angles of incidence. This technique actually involves calculating TDOA between elements of the array by measuring the difference in received phase at each element.

AOA techniques have been applied in the cellular industry in early efforts to provide location tracking service for mobile phone users. Multiple tower sites calculate the AOA of the signal of the cellular user, and use this information to perform triangulation. That information is relayed to switching processors that calculate the user location and convert the AOA data to latitude and longitude coordinates, which in turn is provided to emergency responder dispatch systems.

The advantages of AOA are that a position estimate may be determined with as few as three base stations for 3D positioning or two base stations for 2D positioning, and that no time synchronization between base stations is required. A common drawback that AOA shares with some of the other techniques mentioned is its susceptibility to multipath interference. As stated earlier, AOA works well in situations with direct LOS, but suffers from decreased accuracy and precision when conformed with signal reflections from surrounding objects. Unfortunately, in dense urban areas, AOA becomes barely usable because LOS to two or more base stations is seldom present [Wi F 08]. Authors of [Nicu 03] take AOA measurement such ad hoc positioning system (APS). See [Veen 88; Stoi 97; Otte 93] for more details on AOA positioning algorithms and their characteristics and properties.

1.2.2 Range-free techniques

Range-free geo-location systems find the mobile terminal location without calculating either distances or angles. These systems depend on pattern recognition using recorded measurements, called fingerprints, in database or other information indicating the approximate mobile terminal location (for example, the base station identifier).

1.2.2.1 Associated Cell (CellId)

The concept of associated cell, which means the 802.11 access point of the MT, could be considered as one of the simplest and earliest geo-location systems (Fig. (1.6)). This mechanism

of estimating approximates location of the mobile terminal is based on radio frequency (RF), and tracks the cell to which a mobile terminal is attached. This technique does not resolve the position of the mobile terminal beyond indicating the cell with which the mobile terminal is registered. The simplicity, the easy implementation, and low computational cost make such technique favorable.

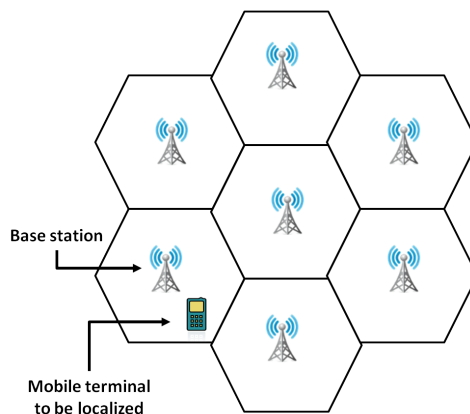


Figure 1.6: Associated cell technique.

Most cell-based WLANs geo-location systems can be adapted to provide associated cell geo-location solution easily and cost-effectively. Since the accuracy is the key issue for geo-location systems, the shortcoming of associated cell positioning approaches for several applications is the unsatisfactory accuracy. Moreover, mobile terminals can be associated to cells that are not in close physical proximity, despite the fact that other nearby cells would have higher signal strength.

To enhance the geo-location of the areas of the cell with the highest probability of containing the mobile terminal, some additional methods of resolving location within the cell is usually required. When receiving cells provide received signal strength indication (RSSI) for mobile terminals, the use of highest signal strength technique can improve location granularity over the cell of origin. In this approach, the location of the mobile terminal is performed based on the cell that detects the mobile terminal with the highest signal strength. Using this technique, the probability of selecting the true nearest cell is increased over that seen with pure associated cell. Depending on the needed accuracy of the application at hand, performance may be more than sufficient for casual location of mobile terminals using the highest signal strength technique. Location-based applications which require high level of accuracy are better served by approaches using the techniques of lateration, angulation, and location patterning that provide better accuracy.

1.2.2.2 Location patterning techniques

This category of geo-location systems is based on the sampling of radio signal fingerprints in a specific indoor environment. It is obvious that the behavior of radio signals depends on the structure of the indoor environment, and on the distributed obstacles as well. The main advantage of positioning techniques belonging to this category is that the location patterning (fingerprinting) technique depends on the infrastructure that is already installed in the test-bed. In other words, a location patterning technique does not require specialized hardware in either the mobile terminal or the base station. In addition, location patterning may be implemented totally algorithmic, which can reduce the complexity and the cost significantly, compared to range-based geo-location techniques.

Location patterning techniques assume:

- in the ideal case, each potential mobile terminal location has a distinctly unique fingerprint. When this fingerprint is close to the real fingerprint, then better performance of the location estimation is achieved;
- each environment or sub-environment has unique signal propagation characteristics. It means that all environments are truly different from the perspective of a pattern recognition geo-location solution.

Most location patterning techniques depend on received signal strength (RSS). Other metrics, including TOA, AOA, or TDOA-based RF fingerprint, could be used to develop location patterning (fingerprinting) solutions as well.

There are two phases for location fingerprinting:

- offline phase (calibration phase): During this stage, a site survey is performed in an environment. The location coordinates/labels and respective signal strengths from nearby base stations are collected.
- online phase (operational phase): During this stage, a geo-location technique uses the currently observed signal strength and previously collected information to figure out an estimated location.

The main challenge of the techniques based on location fingerprinting is that the received signal strength could be affected by diffraction, reflection, and scattering in the propagation indoor environments. As a result, and during the actual collecting process, the calibration stage software typically takes many fingerprints of signal strength for a mobile terminal. Then, we can represent the fingerprint associated with a specific base station as the mean signal strength

of all taken samples of the mobile terminal made by the base station for the fingerprint position coordinates. Therefore, The location vector becomes a vector of mean signal strength: $(x,y) = (\overline{RSS}_{BS_1}, \overline{RSS}_{BS_2}, \dots, \overline{RSS}_{BS_n})$, where (x,y) represent the location coordinates of the fingerprint at hand.

In the operational stage, for example, several base stations provide signal strength measurements concerning a mobile terminal, and forward that information to a geo-location server. The geo-location server executes a positioning algorithm and uses the fingerprint database to estimate the location of the mobile terminal. The geo-location server then transmits the location estimate to the location-based application requesting this information.

There are several fingerprint-based positioning algorithms using pattern recognition technique: probabilistic methods, K-nearest neighbor (KNN), artificial neural networks (ANN), support vector machine (SVM), and smallest M-vertex polygon (SMP). In the following we briefly describe these techniques.

1.2.2.2.a Probabilistic methods

In the probabilistic class of mobile terminal location, the proposed methods use the probability density function instead of simple measurements. The Bayesian inference is used to find the *MT* position depending on the available database. The mobile terminal location is represented by a random variable X , and the observed measurement during the online stage is denoted by s . The conditional probability is given by applying the law of Bayes as follows:

$$P[X|s] = \frac{P[s|X].P[X]}{P[s]} \quad (1.2.11)$$

Where the total probability theorem allows to write:

$$P[s] = \int P[s|X'].P[X'].dX' \quad (1.2.12)$$

It is necessary to know the a priori probability density when the mobile terminal is at position X_i . In the case of discrete system, we assume that there are n location candidates X_1, X_2, \dots, X_n , in the database. Thus the discrete form of the equation (1.2.12) is given by the equation (1.2.13):

$$\int P[s|X'].P[X'].dX' \approx \sum_{i=1}^n P[s|X_i].P[X_i] \quad (1.2.13)$$

Then, the equation (1.2.11) of the conditional probability of the mobile terminal position given the observation s is given by (1.2.14):

$$P[X|s] = \frac{P[s|X].P[X]}{\sum_{i=1}^n P[s|X_i].P[X_i]} \quad (1.2.14)$$

A probability of presence is associated with each of the positions of the database. The distribution a posteriori defined above allows to determine the most probable position of the mobile terminal and the following decision rule can be obtained:

$$\text{Choose } X_i \text{ if } P(X_i|s) > P(X_j|s), \text{ for } i, j \in \{1, 2, \dots, n\}, i \neq j \quad (1.2.15)$$

Using Bayes law, and assuming that $P(X_i) = P(X_j)$ for $i, j \in \{1, 2, \dots, n\}$ we have the following decision rule based on the likelihood that ($P(s|X_i)$ is the probability that the observation s is measured, given that the mobile terminal is located in location X_i):

$$\text{Choose } X_i \text{ if } P(s|X_i) > P(s|X_j), \text{ for } i, j \in \{1, 2, \dots, n\}, i \neq j \quad (1.2.16)$$

In addition to the histogram approach, authors in [Roos 02] propose the kernel approach, that considers a theoretical probability density to calculate likelihood. Assuming that the likelihood of each location candidate is a Gaussian distribution, the statistical properties (mean and standard deviation) of each location candidate can be calculated. Basing on the fact that the base stations in the environment are independent, the overall likelihood of one location candidate is calculated by directly multiplying the likelihoods of all base stations. Therefore, the likelihood of each location candidate can be calculated from observed measurements during the online stage, and the estimated location is to be decided by the previous decision rule. However, this is applicable only for discrete location candidates. Mobile terminals could be located at any position. The estimated 2D location (\hat{x}, \hat{y}) given by the equation (1.2.17) may interpolate the position coordinates and give more accurate results. It is a weighted average of the coordinates of all sampling locations:

$$(\hat{x}, \hat{y}) = \sum_{i=1}^n (P(X_i|s)(x_{X_i}, y_{X_i})) \quad (1.2.17)$$

Other probabilistic modeling techniques for location-based applications and services in WLANs may involve pragmatically important issues like calibration, active learning, error estimation, and tracking with history. So Bayesian network based and/or tracking-assisted positioning have been proposed [Kont 04].

1.2.2.2.b K-nearest neighbors (KNN)

Depending on the fingerprint map, constructed in the offline stage, of the indoor environment, the KNN technique estimates the mobile terminal location. Using the current value of RSS transmitted by the mobile terminal, the KNN technique searched for K-nearest matches in the built fingerprint database as shown in Fig (1.7).

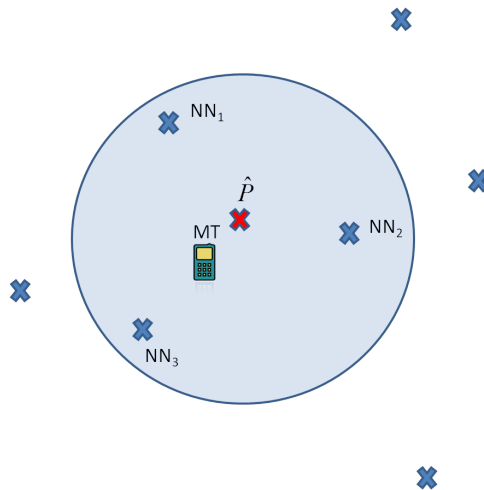


Figure 1.7: KNN positioning technique: NN_i are the nearest neighbors, MT is the mobile terminal to be located, and \hat{P} is the estimated location.

Neighbors are defined according to a chosen metric or distance function in the RSS space. To optimize the location process, least mean square (LMS) principle is usually applied. Then, the estimated location of the *MT* is obtained by simple/weighted averaging of the location candidates. Choosing an appropriate value of the parameter K affects the performance of this technique. If $K = 1$, then the *MT* location is simply assigned to the location candidate of its nearest neighbor. KNN technique was used in RADAR [Bahl 00b] and [Hoss 07]. Authors of RADAR positioning system create the fingerprint database by collecting RSS, location coordinates, and orientation information in 70 different places in their test-bed from three active base stations (access points). In addition to the already existing obstacles in the indoor environment, the human body of the person who collects the fingerprints is considered as an obstruction between the base stations and the mobile terminal. For that reason, redundant fingerprint samples have been taken for different (north, sud, west, and east) orientations; therefore, the captured fingerprint $(x,y,Orientation,RSS_1,RSS_2,RSS_3)$ forms one of four fingerprint candidates for each distinct location. To reduce the database size, authors of RADAR introduced an orientation independent method called OINNSS, which analyzes each *BS* in the fingerprint vector across the four orientations and proposes to calculate the mean of these oriented fingerprint candidates, then to register only the maximum for each base station. In [Dawe 11],

authors have designed an improvement that estimates physical positions independently of orientation. Instead of treating each orientation separately, authors sum the distance across all four orientations for each physical location as follows. Denote by (O, RSS_1, RSS_2, RSS_3) a given fingerprint, and an observed fingerprint by $(O, RSS'_1, RSS'_2, RSS'_3)$ at the orientation O , the geo-location process aims at locating the mobile terminal by comparing the observed fingerprint to those in the fingerprint database using Euclidean distance metric defined by equation (1.2.18):

$$Dist = \sum_{O=1}^4 \left(\sum_{i=1}^n (RSS_{O,i} - RSS'_i)^2 \right)^{1/2} \quad (1.2.18)$$

where $RSS_{O,i}$ corresponds to the fingerprint value from BS_i at orientation O . The algorithm then returns the mobile terminal location by choosing the nearest neighbor who minimizes this distance:

$$(x,y,z) = \underset{(O_i, RSS_{i,1}, RSS_{i,2}, RSS_{i,3})}{\arg \min} (Dist) \quad (1.2.19)$$

1.2.2.2.c Artificial neural networks (ANN)

Neural-network-based positioning systems depend on multi-layer perceptron networks (MLP). MLP networks consist at least of three layers: input, output, and one (or more) hidden layers. MLP used in positioning systems often restricts to one hidden layer with a transfer function. Received signal strengths (RSSs) represent the input of MLP, while the location coordinates (x,y) in 2D environment, or (x,y,z) in 3D environment, form the targets for the training step. The aim of the training step is to construct the appropriate input matrix of weights. To transfer the input data of RSS to the hidden layer, it should be multiplied by the input weight matrix, and then added to the chosen input layer bias. The output of this transfer function is multiplied by the trained hidden layer weight matrix, and then added to the hidden layer bias if it is chosen. The goal of the hidden layer is to receive the input data and put it in the transfer function. Then, the output result of this function has to be multiplied by the trained hidden layer weight matrix and then added to the hidden layer bias if it is chosen. The output layer contains 2 or 3 neurons in 2D or 3D environments. Each neuron represents one of the coordinates of the estimated location of the mobile terminal (see Fig. (1.8)).

The back-propagation neural network (BPNN) is currently the most representative learning algorithm in ANN [Rume 86], and has been successfully applied to a wide range of scientific areas, especially in applications involving forecasting, image processing, pattern recognition and signal processing. A study discussed the use of artificial neural network (ANN) for indoor

positioning system (IPS) using RSS in indoor wireless facility which has varying human activity, material of walls and type of wireless access points (WAP), hence simulating a heterogeneous environment [Hami 10]. The major drawback of the traditional BPNN is their slow learning process. Resilient back-propagation (Rprop) is the best algorithm in terms of convergence speed, accuracy as well as robustness with respect to the training parameters [Ried 93]. Comparing to the back-propagation algorithm, the Rprop converges faster and needs less training. Authors in [Chen 11] proposed a novel algorithm that combines both time of arrival (TOA) and angle of arrival (AOA) measurements to estimate the *MT* in NLOS environments using the intersections of two circles and two lines, based on the most resilient back-propagation (Rprop) neural network learning technique. Therefore, integrating all available heterogeneous measurements increases the location accuracy.

ANN different topologies, learning approaches, and applications will be discussed in (3.2).

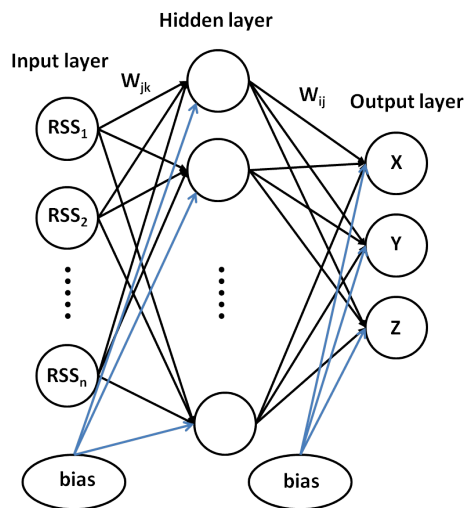


Figure 1.8: MLP-based geo-location system with one hidden layer.

1.2.2.2.d Support vector machine (SVM)

A support vector machine (SVM) is a concept in statistics and computer science for a set of related supervised learning methods that analyze data and recognize patterns, used for classification and regression analysis. SVMs achieved excellent empirical performance in lot of engineering, medicine, and science applications [Cris 00; Liu 05]. More details about the theory of SVM can be found in [Kecm 01; Vapn 99]. Concerning location fingerprinting, support vector regression (SVR) has been used successfully. A new location discovery technique based on support vector machines has been introduced along with the underlying statistical learning

theory concepts. This technique can be used in its regression version to estimate the location of a mobile user, and as a classification engine (SVC) to decide the area, for example the room, the user is currently in [Brun 05; Wu 04]

1.2.2.2.e Smallest M-vertex polygon (SMP)

To locate a mobile terminal, SMP depends on the location candidates (x_i, y_i, z_i) estimated by every base station (using RSS values). These position candidates (including at least one candidate location from each base station) form M-vertex polygon, where M represents the number of base stations replying to the request of the mobile terminal. Repeating the same process gives several M-vertex polygons. Choosing the smallest polygon that has the shortest perimeter, then, averaging its vertices coordinates give the location estimate of the mobile terminal. SMP has been used in MultiLoc [Para 02]

In the following paragraphs, we will review the different types of tracking systems and the filtering approaches to improve the location estimates.

1.3 Tracking systems and prediction filters

1.3.1 Tracking systems

A local positioning system (LPS) is a tracking (navigation) system that provides location information within the coverage of the network access points. Unlike GPS or other global navigation satellite systems (GNSS), local positioning systems don't provide global coverage. Nowadays, local positioning systems are often used as complementary or alternative positioning technology to GPS, especially in indoor environments where GPS technology is not available, for example, inside buildings, or urban canyons. LPS are classified in the following main categories:

- **Network-based LPS:** Systems belonging to this category rely on some existing networks to determine the position of the mobile terminal by measuring its signal metrics (such as the AOA, TOA, TDOA, RTT, RSP) when received at the network base stations. In this technology, the base stations measure the signal transmitted from the mobile terminal and relay them to the central unit for further processing and data fusion to provide an estimate of the mobile terminal location. The major advantage of network-based LPS is that the mobile terminal is not involved in the location process; thus the technology does not require modifications to existing mobile terminals (handsets). One of the key challenges of network-based techniques is the requirement to work closely with the service provider, as it entails the installation of hardware and software within the operator's infrastructure.

- **Terminal-based LPS:** In this category, the MT determines its location from signals received from some base stations. Still, embedding LPS receiver into mobile terminals leads to increased cost, size, and battery consumption. It also requires the replacement of large quantity of mobile terminals (handsets) that are already on the market.
- **Hybrid LPS:** Hybrid positioning systems use a combination of network-based and terminal-based technologies for location determination. One example would be some modes of assisted GPS (A-GPS), which can both use GPS and network information to compute the location. Both types of data are thus used by the mobile terminal to make the location more accurate. Alternatively tracking with both systems can also occur by having the phone attaining its GPS-location directly from the satellites, and then having the information sent via the network to the person that is trying to locate the mobile terminal. Services allowing such mobile terminals (typically, smartphones) tracking are Souguide, Mologogo, instaMapper, Buddyway, Vismo and Google Latitude.

In the lack of information measurement or in its absence, all LPS fail to locate the mobile terminal, therefore, the prediction process gives a probable next location of the mobile terminal depending on the previous location and on the movement characteristics. The following paragraph will detail soft approaches that are most used in tracking process.

1.3.2 Prediction filters

1.3.2.1 Kalman filter

Kalman filter is a powerful mathematical tool and easy to be implemented. According to the previous state of a linear dynamic system, the applied commands and measurement noise, Kalman filter allows to estimate the current state of this system. Kalman filter has numerous applications in technology fields. A common application is for guidance, navigation and control of vehicles, particularly aircraft and spacecraft. Furthermore, Kalman filter is a widely applied concept in time series analysis used in fields such as signal processing, economics, navigations, tracking objects, and many computer vision applications (feature tracking, cluster tracking, and fusion data). In this paragraph, we will present the classical Kalman filter, that on which all other Kalman filter derivatives are based. Typical example of Kalman filter application is tracking a mobile terminal where its position and speed depend on the position and speed at the preceding instant, including random noise; such system is called noisy dynamic system.

Kalman filter processes all the available information and weights them according to their precision to obtain the best estimate of the system state, taking into account:

- the knowledge of the laws of the system evolution and measurements;
- the statistical properties of the system noise, measurement and model uncertainties;
- the information about the system parameters initial conditions.

Fig. (1.9) shows the schema of functionality principle of Kalman filter.

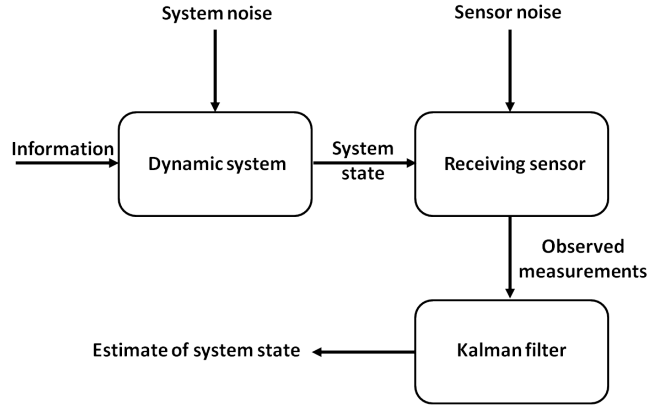


Figure 1.9: Functionality principle of Kalman filter.

1.3.2.1.a Kalman filter modeling

The aim of any dynamic system is to estimate its parameters. To do so, the state of this dynamic system is denoted by a vector X . Then, the key point of predicting the next state vector is to determine the evolution law of the system state as a recurrence equation. This means that only the estimated state from the previous time step k and the current measurement at the time step $k + 1$ are needed to compute the estimate for the current state vector. The following equation (1.3.1) represents the evolution law of the state vector of the dynamic system:

$$X_{k+1} = F_k X_k + W_k \quad (1.3.1)$$

where F_k is the state transition model which is applied to the previous state k , W_k is the process noise which is assumed to be drawn from a zero mean Gaussian white noise with covariance Q_k :

$$W_k \sim N(0, Q_k) \quad (1.3.2)$$

To complete the dynamic system modeling, at time k , a measurement Y_k of the true state vector X_k is given by equation (1.3.3):

$$Y_k = H_k X_k + V_k \quad (1.3.3)$$

where H_k is the observation model which maps the true state vector into the observed vector, and V_k is the observation noise which is assumed to be zero mean Gaussian white noise with covariance R_k :

$$V_k \sim N(0, R_k) \quad (1.3.4)$$

The initial state, and the noise vectors at each step $\{X_0, W_1, \dots, W_k, V_1 \dots V_k\}$ are all assumed to be mutually independent:

$$\begin{cases} \forall i, j, W_i \perp V_j \\ \forall i \neq j, V_i \perp V_j \\ \forall i \neq j, W_i \perp W_j \end{cases} \quad (1.3.5)$$

According to the modeling assumptions, the Kalman filter is the optimal filter to estimate the state vector of a dynamic system in terms of minimizing the estimation error. It ensures that the error in the estimate is zero mean and it minimizes the uncertainty on this error. Mathematically speaking, $E[\tilde{X}_k] = 0$, thus $\tilde{X}_k = \hat{X}_k - X_k$ is a zero mean Gaussian with covariance matrix P_k , where, \tilde{X}_k is the prediction error and \hat{X}_k is the predicted state vector.

- **Initialization:** at the first iteration $k = 0$, if the initial state of the system is perfectly known $\hat{X}_0 = X_0$, then P_0 is null:

$$P_0 = E[(X_0 - \hat{X}_0)(X_0 - \hat{X}_0)^T] \quad (1.3.6)$$

However, at the iteration k , the output of Kalman filter is the state vector X which minimizes the covariance matrix P_k :

$$P_k = E[(X_k - \hat{X}_k)(X_k - \hat{X}_k)^T] = cov(X_k - \hat{X}_k, X_k - \hat{X}_k) \quad (1.3.7)$$

Two steps are necessary to achieve this output. Firstly, an a priori estimate, denoted by X_k^- , will be calculated without taking into account the current measurement Y_k . Then, using the current measurement $Y_k = H_k X_k + V_k$, this estimate will be updated to obtain the posteriori estimate X_{k+1}^+ .

- **Dynamic system evolution:** knowing that $\hat{X}_k^- = E[X_k]$, using the equation (1.3.1) we can write:

$$\hat{X}_k^- = F_{k-1} \hat{X}_{k-1} \quad (1.3.8)$$

The covariance matrix of the estimate error using the same equation (1.3.1) is given by the equation (1.3.9):

$$P_k^- = cov(X_k - X_k^-, X_k - X_k^-) = F_{k-1} P_{k-1} F_{k-1}^T + Q_{k-1} \quad (1.3.9)$$

- Measurement update:** after having the a priori estimate \hat{X}_k^- , Kalman filter uses the current measurement Y_{k+1} to correct this estimate and to obtain the a posteriori estimate denoted by \hat{X}_k^+ . Fig (1.10) shows the main functionality steps, prediction process and correction process, of Kalman filter. The prediction process consists of two steps, the first one is to estimate a priori the new position \hat{X}_k^- , while the second step calculates the covariance matrix of the a priori estimate error P_k^- . The correction process calculates at first the filter gain K_k which minimizes the estimate error covariance, then it updates the position \hat{X}_k , and finally, it updates the error covariance matrix P_k .

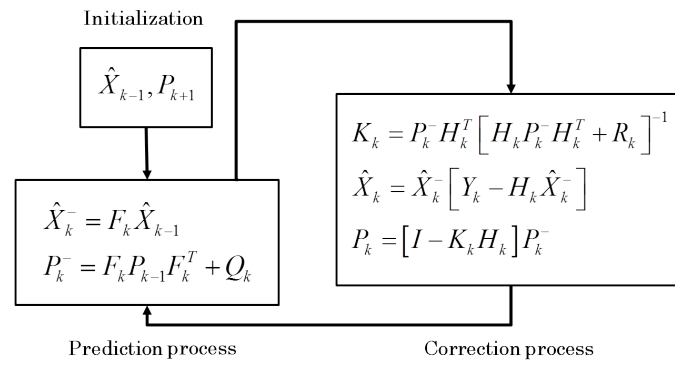


Figure 1.10: Functionality processes of Kalman filter.

This type of filtering is very interesting for the applications that estimate the state vector of the dynamic system with no need to have large computing capacity, such as a mobile terminal having limited computing resources. Kalman filter allows taking into account the measurement history over the time. Nowadays, this filter is integrated in many tracking applications, because it smooths the trajectory of the mobile terminal by reducing the degrading effect of noise measurements. However, it does not cover all situations, including those in which the dynamic system equations are nonlinear. To overcome the nonlinearity limits, extensions of Kalman filter can respond to non-optimal estimation problems offering this type of constraints. The approaches proposed in extended Kalman filter [Welc 01] and the unscented Kalman filter [Juli 97; Merw 00] aim to linearize the dynamic equation system with a limited development.

1.3.2.2 Particle filter

In the case of non-linear dynamic systems, the assumptions and the restrictions that related to Kalman filter and its derivatives limit their performance. Even the additive noise is not always assumed to be zero mean Gaussian noise. Therefore, modeling the behavior of non-

linear dynamic systems and non-Gaussian noises by Kalman filter or one of its derivatives will give non-optimal estimate of the system state vector. The need of novel approach which overcomes the limitation of Kalman filters leads to exploit the Sequential Monte-Carlo (SMC) methods to determine the probability density function (PDF) a posteriori [Gust 02]. Thanks to their flexibility and low-complexity, these methods are used effectively in many estimation problems. The particle filters may be a serious alternative for real-time applications classically approached by model-based Kalman filter techniques [Kail 00; Gust 00].

1.3.2.2.a Particle filter modeling

In addition to linear dynamic systems modeled using Kalman filter, the non-linear dynamic systems will be modeled basing on the SMC method exploited by the particle filters. Kalman filter and its derivatives propose to model the a priori evolution law of the non-linear dynamic system which estimates the state vector at the step k , and the correction process of the estimate values depending on the current measurement. However, the hypothesis on the system linearity and the Gaussian noise constraints are not necessary any more in particle filters. The equation system (1.3.10) models the estimation problem of any dynamic system:

$$\begin{cases} X_k = f_k(X_{k-1}, V_{k-1}) \\ Y_k = h_k(X_k, N_k) \end{cases} \quad (1.3.10)$$

where, X_k is the estimate state vector at time k , V_{k-1} is the dynamic system noise applied to the prediction process, Y_k is the current measurement used to correct the estimate state vector obtained by the prediction step, and N_k represents the measurement noise applied to the measurement equation. Contrarily to the Kalman filter model, the noises presented in particle filter model are not necessarily Gaussian. To improve the state vector estimation, the particle filter seeks the best probability density $P[X_k|Y_{0:k}]$. That means that by using Bayesian estimation, the particle filter aims to find the optimal estimation of the state vector of the dynamic system taking into account the up-to-date measurements $\{Y_0, Y_1, \dots, Y_k\}$.

To simulate the non-linear, non-Gaussian Markovian models, some notations will be cited in the table (1.2):

To simulate non-linear, non-Gaussian Markovian models, we suppose the hidden state vector X_k . The set of the system state vectors is presented by a Markovian process where $p(X_0)$ is its initial distribution. The set of measurements Y_k are supposed to be independent of that of the estimate state vectors. The particle filter aims to estimate the a posteriori distribution $p(X_{0:k}|Y_{1:k})$ and its statistical characteristics as well (1.3.11):

$$I(f_k) = E_{p(X_{0:k}|Y_{1:k})} [f_k(X_{0:k})] \triangleq \int f_k(X_{0:k}) p(X_{0:k}|Y_{1:k}) dX_{0:k} \quad (1.3.11)$$

Table 1.2: Particle filter notations.

Symbol	Meaning
X_k	Hidden state vector
$p(x_0)$	Initial distribution
$p(X_k X_{k-1})$	Transition probabilities
Y_k	Measurement used to correct the estimated state vector
$p(Y_k X_k)$	Marginal probability density
$p(X_{0:k} Y_{1:k})$	A posteriori distribution
f_k	Integrable interest function

At the time step k , the a posteriori distribution is given by Bayes theorem presented in equation (1.3.12):

$$p(X_{0:k}|Y_{1:k}) = \frac{p(Y_{1:k}|X_{0:k})p(X_{0:k})}{\int p(Y_{1:k}|X_{0:k})p(X_{0:k})dX_{0:k}} \quad (1.3.12)$$

Then, the recursive equation to calculate the conjoint probability density $p(X_{0:k}|Y_{1:k})$ is obtained directly as show in equation (1.3.13):

$$p(X_{0:k+1}|Y_{1:k+1}) = p(X_{0:k}|Y_{1:k}) \frac{p(Y_{k+1}|X_{k+1})p(X_{k+1}|X_k)}{p(Y_{k+1}|Y_{1:k})} \quad (1.3.13)$$

By the same, the prediction process of the marginal distribution $p(X_k|Y_{1:k-1})$ is given by the recursive equation (1.3.14):

$$p(X_k|Y_{1:k-1}) = \int p(X_k|X_{k-1})p(X_{k-1}|Y_{1:k-1})dX_{k-1} \quad (1.3.14)$$

While the correction process is presented by equation (1.3.15):

$$p(X_k|Y_{1:k}) = \frac{p(Z_k|X_k)p(X_k|Y_{1:k-1})}{\int p(Z_k|X_k)p(X_k|Y_{1:k-1})dX_k} \quad (1.3.15)$$

Therefore, $p(Y_{1:k})$, the marginal probability density $p(X_{0:k}|Y_{1:k})$, and $I(f)$ are necessary to apply this estimation.

Finally, although various models have been proposed in the literature, they often require the use of very large collections of data in order to fit them and display great sensitivity to changes in the radio propagation environment. A multi-model particle filtering algorithm for indoor tracking of mobile terminals, using RSS data using the methodology, called interacting multiple models (IMM), has been used for modeling the motion of maneuvering targets. The extension of IMM application to handle also the uncertainty in the RSS observations is referred to the resulting state-space model as a generalized IMM (GIMM) system [Achu 09]. In their

work [Achu 12], authors use switching multiple models (SMM) that account for different classes of target dynamics and propagation environments and propose a flexible probabilistic switching scheme. The resulting state-space structure is termed as a generalized switching multiple model (GSMM) system and investigates two types of models for the RSS data: polynomial models and classical logarithmic path-loss representation.

1.4 Location systems: architectures and requirements

Available location systems on the market reply almost demands of location-based applications (LBA) and services (LBS). Those systems vary in accordance to their architectures and requirements. Location system architectures could be classified into four groups. Table (1.3) summarizes the main positioning system architectures:

Table 1.3: Location system: different architectures.

Concept		Definition
Remote positioning system	Passive	Measurements are made by the base station without the cooperation of the mobile terminal
	Active	The mobile terminal is active and cooperates in the process of positioning
Auto positioning system		Measurements are made by the mobile terminal with/without sending the position to the base station

Remote positioning system (RPS) allows to locate mobile terminals using the measurements available at the base station. The essential advantage of RPS is the capability of treating large sets of information that are available in the base station using its powerful central processing units. RPS category is also divided in two subcategories, active remote positioning system (ARPS) and passive remote positioning system (PRPS). In the first subcategory, the mobile terminal is active and cooperates in the process of the positioning process.

In addition to the offered services, the domination of one positioning system on the other positioning systems is related to its requirements. A compromise of the requirement package characterizes each positioning system. However, neither of the positioning systems available in the market is optimal in all requirements nor reply to all demands. Therefore, choosing the suitable system depends on requirements and demands.

Location system main requirements could be classified into five groups, as shown in table (1.4).

The existing location systems using WiFi technology are shown in table (1.5), and those using other technologies are cited in table (1.6) [Kolo 06].

Table 1.4: Location system requirements.

Requirements	Definition
Flexibility	The ability to be installed in all WLAN infrastructures available on the market.
Low cost	Using of a software-based solution avoiding the need of specialized hardware.
Scalability	The independence of the number of mobile terminals and of the location scenario target.
Generalization	Providing the location information in places where an insufficient calibration was performed.
Accuracy	The capability of providing accurate locations.

Table 1.5: Location systems using WiFi: specification and properties.

Property	Ekahau	Intel Place Lab	Skyhook WPS	RADAR	AeroScout
Deployment range	Building/local area	Metropolitan area	Metropolitan area	Building/local area	Building/local area
Position calculation	Server (Ekahau positioning engine)	Mobile device	Mobile device	Server	Server (AeroScout positioning server/engine)
Position method	Location fingerprinting using RSS	Map-based pinpointing and triangulation	Map-based pinpointing and triangulation	Location fingerprinting and triangulation (lateration)	TOF triangulation (TDOA for absolute location; RSSI for symbolic location)
Transmitter	WiFi nodes	WiFi nodes	WiFi nodes	WiFi devices	Active RFID tags or WiFi devices
Receiver	Ekahau client	Place Lab client	Skyhook client	Standard WiFi	AeroScout Location receiver (TDOA), AeroScout exciter (choke-point); standard WiFi AP (RSSI)
Accuracy	1-3 m	20+ m	20+ m	2-4.3 m	1-5 m

Table 1.6: Location systems using different technologies: specification and properties.

Property	MIT Cricket	Rosum TV	BlipNet	GPS
Deployment range	Building	Metropolitan area	Building	Global (not indoors)
Position calculation	Mobile device	Rosum location server or mobile device	Blip server positioning engine	Device
Position method	TOF lateration and proximity (with one beacon)	Multi-lateration	Inquires and pagings	TOF lateration
RF signal used	RF (418 MHz) + ultrasound	Terrestrial broadcast TV	Bluetooth	GPS
Transmitter	Beacon	TV towers	Mobile device	28 satellites
Receiver	Listener	Rosum RTMM chipset	Blip node (Bluetooth AP)	Commodity receivers
Accuracy	1-3 m	30-50 m indoor; 5 m outdoor	10 cm - 10 m	3-20 m outdoor

1.5 Conclusion

In this chapter, we defined the problem of the mobile terminal location and its applications. Then we explored the different measurements and techniques used in the research community to position mobile terminals. Advantages and drawbacks of these techniques were mentioned depending on the elements of the positioning system at hand. The major challenge in indoor location research field is the NLOS limitations. For tracking systems and filtering approaches, we explored the different types of tracking systems and their properties. The models of conventional predictors, such as Kalman filter and particle filter, were described. Different architectures and requirements of positioning systems were mentioned.

One of our objectives in this thesis is to overcome the NLOS problem without prior knowledge of the environment and without applying prior measurement correction approaches. Another objective is to enhance the performance of local positioning systems, and achieve satisfactory accuracy in both static and dynamic location (tracking) of mobile terminal.

Chapter 2 will present a new hybrid method to position a static mobile terminal without

any prior knowledge of the environment structure and without applying prior measurement correction approaches. A comparison of deterministic and learning range-free techniques is presented in chapter 3. Finally, chapter 4 is dedicated to enhance the performance of the dynamic location (tracking) systems by, integrating fractional integration (derivation) to conventional predictors.

OUR INDOOR LOCATION BASED ON TOA AND AOA USING COORDINATES CLUSTERING

2.1 Introduction

Hybrid approaches are realized by combining more than one measurement and/or more than one positioning technique. The aim of hybrid methods is to improve the accuracy of estimated location, therefore, to enhance the performance of positioning systems.

This chapter addresses the proposal of a new clustering method for indoor location, based on both time of arrival (TOA) and angle of arrival (AOA) measurements. A new type of clustering will be introduced to classify the location estimates, called coordinate clustering. The results are obtained in a variety of locations in $2D$ and $3D$ simulated environments, with LOS and NLOS multipath ray tracings. Within a few centimeters, the proposed method is able to locate the MT either without prior knowledge of the environment or without applying prior measurement correction approaches [Dakk 11a; Dakk 11b].

2.2 Clustering and problem formulation

The location-based applications (LBA) for indoor environments becomes a substantial need in terms of people guidance, security and goods tracking. Numerous techniques were developed for location purpose in indoor environments, where GPS is not applicable because of the coverage limitation and its low precision. Museums, hospitals, and theaters are typical examples of indoor environments in which wireless networks present an alternative solution for traditional geo-location techniques of mobile terminals. Nevertheless, existing walls, furniture, moving people, and open/closed doors are the main obstacles to realize reliable location systems with satisfactory accuracy. Our objective in this work is to locate mobile terminals in indoor environments without applying any mitigation, approximation, prior correction, or filtering approaches.

2.2.1 Cluster analysis

Gathering data into groups, or data clusters, allows one to have a more structured approach to process the data. Those groups are necessary in terms of data sets size and algorithm efficiency. To build clusters, objects that have common characteristics are assigned to the class that captures the similar aspect of candidates. Each cluster is represented by a cluster prototype in terms of minimizing the distance between the cluster prototype and the other objects in the same cluster. Applying algorithms to cluster prototypes instead of using all data set reduces its complexity, especially for the algorithms that are not practical for large amount of data set. However, other cooperative strategies for constructing clusters could be applied to improve the quality of the estimation of the distance between the mobile terminal and the base station [Serg 09]. Usually, clustering data is the first step to achieve other objectives like data summarization, compression, or finding the nearest neighbor. In the research community, clustering analysis is a very useful utility applied to several fields, such as statistics, machine learning, information retrieval, and pattern recognition.

2.2.2 Measurements choice

As we have seen in the previous chapter, a lot of metrics could be used in different positioning systems. Our hybrid approach depends on two range-based metrics, time of arrival (TOA), which helps to calculate the traveled distance from the mobile terminal to the base station, and angle of arrival (AOA), which determines the direction of arrival (DOA) and locates the mobile terminal by determining the angle of incidence at which signals arrive at the base station.

2.2.3 Problem formulation

Our proposed method for indoor location allows overcoming the limitations of NLOS methods. This method relies on a new approach to clustering the locations estimated by different BS_s distributed around the immediate MT 's environment. As revealed earlier, in the cluster analysis section, estimates of clustering location is a useful approach. Processing these clusters will improve the efficiency of the proposed algorithm, and enhance the accuracy of the final location of the mobile terminal to be located. For example, Fig. (2.1)(a) shows the simulated case study in $2D$, while Fig. (2.1)(b) portrays it in $3D$ with the Euclidean coordinates system.

Here, we assume that MT can move to different locations in the environment and we use ray tracings between BS_s and the target MT to estimate the target location. The location is performed when the MT is relatively static in its environment. However, tracking mobile terminals will be discussed in more detail in the following chapter. One can notice that only

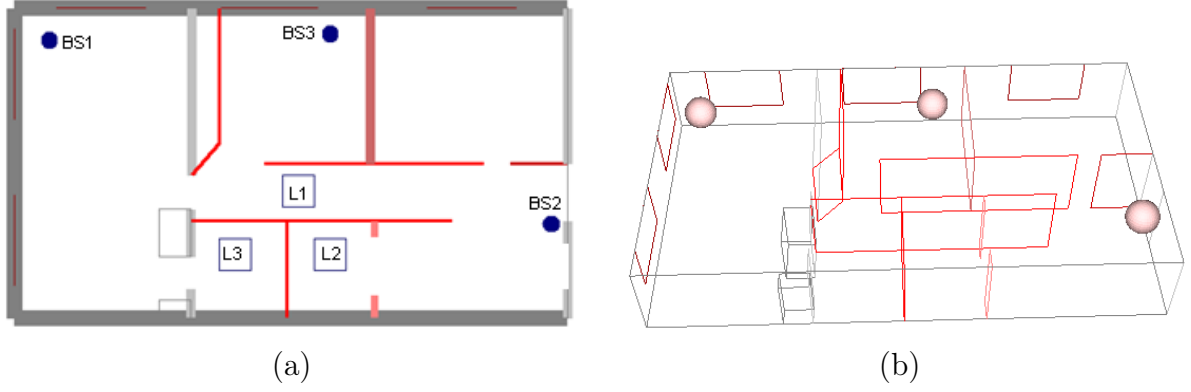


Figure 2.1: Case study equipped with three BS_s , (a) 2D environment, (b) 3D environment.

a few ray tracings have direct sight to the target, and that there are ray tracings with one or more reflections, due to the existing obstacles in the environment. Besides walls and furniture in the case of 2D environments, we have the floor and the ceiling reflections, just like in the case of 3D environments. The crossed distance from BS to MT is calculated by equation (2.2.1):

$$d = c \times t \quad (2.2.1)$$

d is the distance crossed by the ray tracing from BS to MT , t is the traveling time from BS to MT , and c is the speed of light.

The Euclidean coordinates are calculated using the polar coordinates for 2D and spherical coordinates for 3D.

For a 2D direct ray tracing (LOS) the coordinates (x,y) of an estimated location \hat{P} of a MT are calculated by equation (2.2.2):

$$\begin{cases} x = x_0 + d \times \cos \varphi, \\ y = y_0 + d \times \sin \varphi \end{cases} \quad (2.2.2)$$

and for a 3D direct ray tracing (LOS) the coordinates (x,y, z) are calculated by the equation (2.2.3):

$$\begin{cases} x = x_0 + d \times \sin \theta \times \cos \varphi, \\ y = y_0 + d \times \sin \theta \times \sin \varphi, \\ z = z_0 + d \times \cos \theta \end{cases} \quad (2.2.3)$$

where:

(x,y,z) : MT location.

(x_0,y_0,z_0) : BS location.

φ : angle of arrival.

θ : angle of elevation.

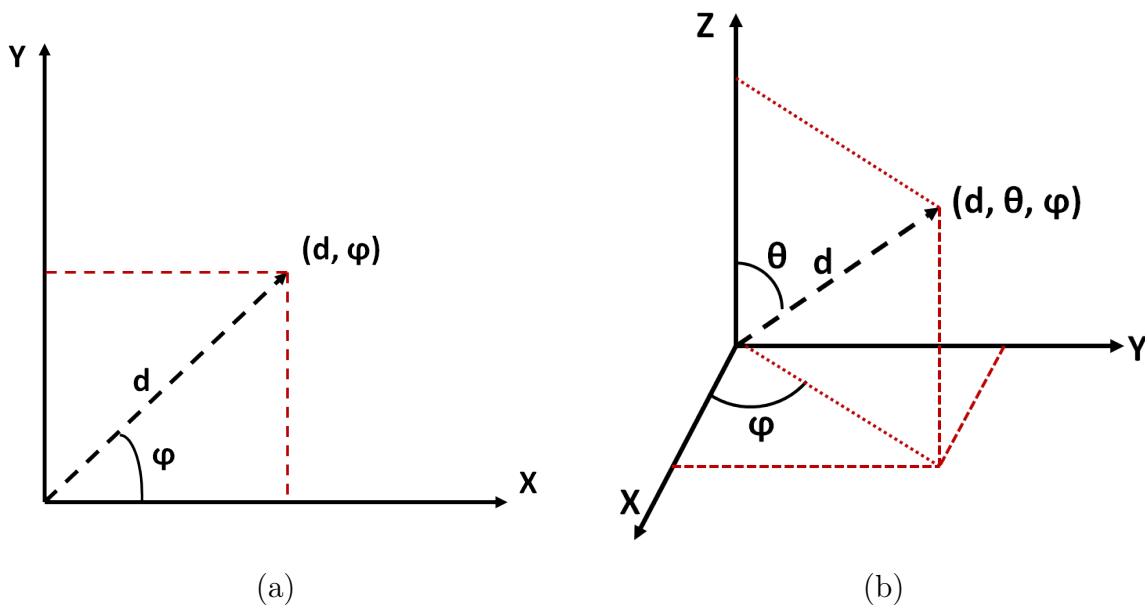


Figure 2.2: (d, θ, φ) radial distance d , angle of elevation θ , and angle of arrival φ : (a) Polar coordinates, (b) Spherical coordinates.

2.3 Proposed method

In this section, we present the details of the proposed method in two dimensional environment. Then, we generalize our approach to the three dimensional environment case.

2.3.1 Two dimensional environment case

For each ray from BS to MT , the estimated location depends on d and φ , as shown in the equation (2.2.2). If the experience was performed in a place which is free of obstacles (LOS), we could estimate the right MT location with a high accuracy. Unfortunately, this is not the case for indoor environments. Obstacles reflect the transmitted rays of BS , therefore MT receives the reflected rays without any knowledge about the number of obstacles scattering the ray tracings. The proposed method considers all ray tracings as in LOS, Fig. (2.3) shows the estimate locations using direct ray tracing and reflected ray tracing by one obstacle.

As we assumed that we do not have any prior information about the environment, almost all the estimated locations are far from the real MT location, due to the NLOS multipath caused by the obstacles (walls, furniture, persons, etc.). Fig. (2.4) illustrates the calculated observations of the MT location using the three BS_s .

In the literature, some methods solve quadratic equation systems to extract the intersections of circles, or solve linear equation systems to find the intersecting radical axis of circles [Bahi 09]. Here, we introduce the clustering concept to determine the location of MT . The clustering

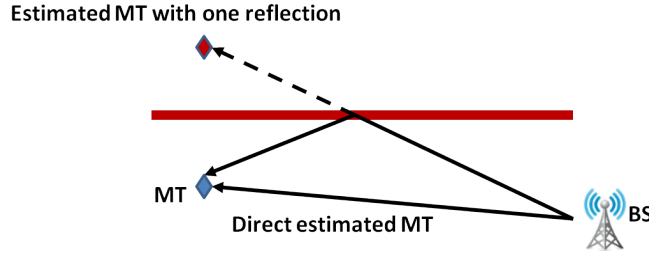


Figure 2.3: Estimated locations of the MT in a $2D$ environment, BS : the location of the base stations, MT : the location of the mobile terminal.

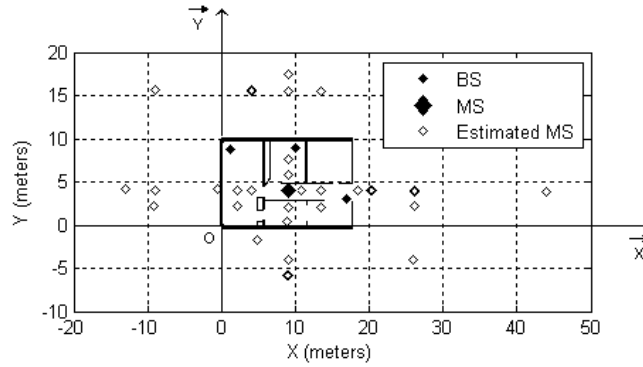


Figure 2.4: Estimated locations of the MT in a $2D$ environment, BS : the location of the base stations, MT : the location of the mobile terminal, estimated MT : the location estimated as in LOS condition.

procedure comprises two steps, one at the abscissa axis, \overrightarrow{OX} and the other at the ordinate axis \overrightarrow{OY} . The location process will depend on the clusters which have the highest number of observations of the MT location coordinates. We scan the estimated locations and gather the neighbors according to the axis \overrightarrow{OX} and then according to the axis \overrightarrow{OY} . We denote $P_i^{(x)}$ and $P_j^{(x)}$ the neighbors at \overrightarrow{OX} axis if $|P_i^{(x)} - P_j^{(x)}| \leq \delta_x$, Fig. (2.5)(a). Similarly, we call $P_i^{(y)}$ and $P_j^{(y)}$ the neighbors at \overrightarrow{OY} axis if $|P_i^{(y)} - P_j^{(y)}| \leq \delta_y$, Fig. (2.5)(b). At the end of this process, two lists have been created, $X_Neighbor_List$ and $Y_Neighbor_List$, for each estimated location, $\hat{P}_i(P_i^{(x)}, P_i^{(y)})$ as shown in Fig. (2.5).

From these coordinate neighbor lists, we choose the major coordinate lists which are the ones having the highest number of coordinate neighbors. If the coordinate clusters with the same maximum number of neighbors exist, then we change the thresholds δ_x, δ_y till we have one coordinate cluster with a higher number of neighbors. Changing the thresholds implies rebuilding the coordinate neighbor lists. To avoid this process, we calculate the Euclidean distance between the coordinate neighbors. Final location of MT is estimated by that coordinate cluster which has the smallest differences between its members.

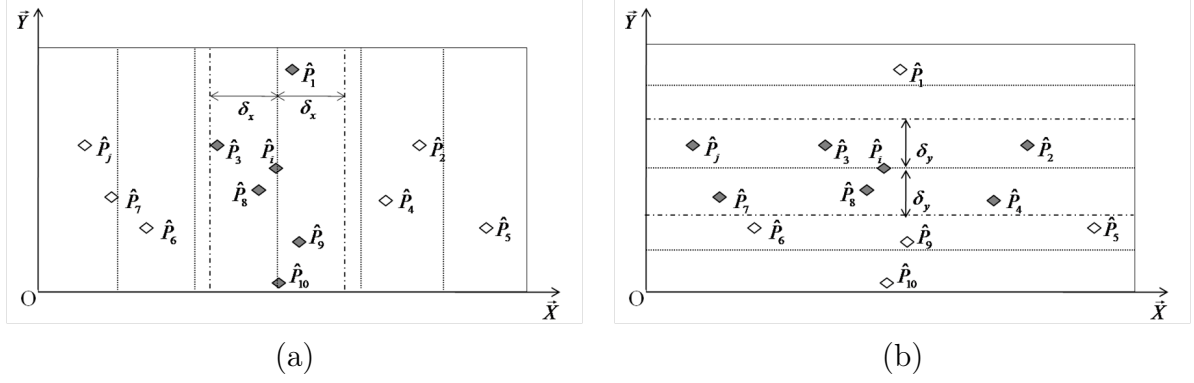


Figure 2.5: Estimated locations of the coordinate neighbors, (a) the neighbors to \hat{P}_i according to the axis $O\vec{X}$, (b) the neighbors to \hat{P}_i according to the axis $O\vec{Y}$.

In the first step, the MT location $\hat{P}(P^{(x)}, P^{(y)})$ is estimated by calculating the average of the list which has most neighbors according to the axis $O\vec{X}$, and similarly for the axis $O\vec{Y}$. This step is expressed by equation (2.3.1):

$$\begin{cases} P^{(x)} = \frac{1}{k} \sum_{i=1}^k x_i \\ P^{(y)} = \frac{1}{l} \sum_{i=1}^l y_i \end{cases} \quad (2.3.1)$$

It is obvious that in LOS, the smallest trajectory corresponds to the smallest traveling time. Therefore, the accuracy is inversely correlated with time, and the distance crossed by the ray tracing. For this reason, we will use the weighted average (WA) [Seow 08] method to improve the final estimation of MT location, which is given as (2.3.2):

$$\begin{cases} P^{(x)} = \frac{\sum_{i=1}^k w_i x_i}{\sum_{i=1}^k w_i} \\ P^{(y)} = \frac{\sum_{j=1}^l w_j y_j}{\sum_{j=1}^l w_j} \end{cases} \quad (2.3.2)$$

Algorithm (2.3.1) summarizes the different steps of the proposed location method based on the coordinate clustering.

The notations used in Algorithm (2.3.1) are defined in Table (2.1).

The complexity of the proposed algorithm is $O(n)$ for the initialization step, and $O(n^2)$ for the setting-up of neighbor lists, where n is the size of candidate locations. Building the neighbor lists is the most important step in the algorithm, which takes $O(n^2)$ iterations. The complexity of the proposed algorithm depends on three parameters: the number of BS_s distributed in the environment and the thresholds δ_x , δ_y . If we increase the number of BS_s distributed in the environment, then the number of estimated locations n will be increased, thus the complexity of the proposed algorithm will be higher, but the accuracy will be better. By the same, if

 Different steps of the proposed method.

```

1 (1) Initialization
2 for each  $r_i \in R(B)$  do
3     Input  $(\tau_i, \varphi_i)$ 
4     Calculate  $(d_i, w_i, \hat{P}_i(\hat{x}_i, \hat{y}_i))$ 
5      $L(MT) = L(MT) \cup \hat{P}_i(\hat{x}_i, \hat{y}_i)$ 
6 end
7 (2) Creating neighbor lists
8 for each  $\hat{P}_i(\hat{x}_i, \hat{y}_i) \in L(MT)$  do
9     for each  $\hat{P}_{j \neq i}(\hat{x}_j, \hat{y}_j) \in L(MT)$  do
10        if  $|\hat{x}_i - \hat{x}_j| \leq \delta_x$  then
11            Update  $(\Omega_x, I_x) // \{(\hat{x}_i) \text{ and } (\hat{x}_j) \text{ are neighbors at } \overrightarrow{OX}\}$ 
12        end
13        if  $|\hat{y}_i - \hat{y}_j| \leq \delta_y$  then
14            Update  $(\Omega_y, I_y) // \{(\hat{y}_i) \text{ and } (\hat{y}_j) \text{ are neighbors at } \overrightarrow{OY}\}$ 
15        end
16    end
17 end
18 (3) Locating  $MT$ 
19  $\alpha = \frac{\sum_{i=1}^k w_i \hat{x}_i}{\sum_{i=1}^k w_i} // \{\hat{x}_i \in \Omega_x(I_x)\}$ 
20  $\beta = \frac{\sum_{j=1}^l w_j \hat{y}_j}{\sum_{j=1}^l w_j} // \{\hat{y}_j \in \Omega_y(I_y)\}$ 
21 return  $(\alpha, \beta) //$  Final location of mobile terminal
    
```

Table 2.1: Notations.

Symbol	Meaning
B	Set of BS_s distributed in the environment
$R(B)$	Set of ray tracings emitted by B
$L(MT)$	Set of MT estimated locations
Ω_x	Set of $x_neighbor$ lists
I_x	Index of $max_n \{\Omega_x : n \text{ number of } x \text{ neighbors}\}$
Ω_y	Set of $y_neighbor$ lists
I_y	Index of $max_n \{\Omega_y : n \text{ number of } y \text{ neighbors}\}$
(α, β)	Final MT estimated location

we change the threshold values, n will change also, which impacts the proposed algorithm complexity.

The following steps determine the weight vector. We start by analyzing the performance of TOA/AOA hybrid mobile location [So 03]. The time and angle measurements at BS are given by equation (2.3.3):

$$\begin{cases} \hat{\tau} = \tau + \varepsilon_\tau \\ \hat{\varphi} = \varphi + \varepsilon_\varphi \end{cases} \quad (2.3.3)$$

where τ is the true TOA, φ is the true AOA, ε_τ and ε_φ are the corresponding measurement errors and the assumed uncorrelated zero-mean Gaussian noise, respectively. The variance of the distance error, denoted by σ_d^2 , is given by equation (2.3.4):

$$\sigma_d^2 \approx c^2 (\sigma_\tau^2 + \tau^2 \sigma_\varphi^2) = c^2 \sigma_\tau^2 + d^2 \sigma_\varphi^2 \quad (2.3.4)$$

where σ_τ , σ_φ are the variance of the time and the angle, respectively. Since the accuracy depends inversely on the distance, the used weight [Seow 08], denoted by w_i , is defined by equation (2.3.5):

$$w = \frac{1}{d^2} \times e^{-(c\sigma_\tau + d\sigma_\varphi)} \quad (2.3.5)$$

The derivatives of (2.3.5) according to its parameters (σ_τ , σ_φ) are given by equation (2.3.6):

$$\begin{cases} \frac{dw}{d\sigma_\tau} = -\frac{c}{d^2} \times e^{-(\sigma'_\tau + d\sigma_\varphi)} \\ \frac{dw}{d\sigma_\varphi} = -\frac{1}{d} \times e^{-(\sigma'_\tau + d\sigma_\varphi)} \end{cases} \quad (2.3.6)$$

where $\sigma'_\tau = c\sigma_\tau$.

From (2.3.6), one can notice that higher $(\sigma'_\tau, \sigma_\varphi)$ gives smaller weight. Experimentally, we choose $(\sigma'_\tau, \sigma_\varphi)$ that minimizes the Euclidean distance between the real and estimated locations of MT . One can use recursive least squares (RLS) to find optimal values. We denote by $P(x, y)$ and $\hat{P}(\hat{x}, \hat{y})$ two locations of MT in the environment. The squared Euclidean distance between the locations (P, \hat{P}) is given by equation (2.3.7):

$$D(P, \hat{P}) = (x - \hat{x})^2 + (y - \hat{y})^2 \quad (2.3.7)$$

Using the weights determined in (2.3.5), we can write equation (2.3.7) as follows (2.3.8):

$$D_w(P, \hat{P}_w) = (x - w \times \hat{x})^2 + (y - w \times \hat{y})^2 \quad (2.3.8)$$

In the process of positioning the MT , we have different estimated locations of the MT . The sum of the squared Euclidean distances between those estimated locations and the exact MT location is given by equation (2.3.9):

$$\sum_{i=1}^n D_{w_i}(P, \hat{P}_{w_i}) = \sum_{i=1}^n ((x - w_i \times \hat{x}_i)^2 + (y - w_i \times \hat{y}_i)^2) \quad (2.3.9)$$

Finally we aim at finding $(\sigma'_\tau, \sigma_\varphi)$ to minimize the objective function denoted by $f(\sigma'_\tau, \sigma_\varphi)$, as follows (2.3.10):

$$\min f(w_i) = \min \sum_{i=1}^n D_{w_i}(P, \hat{P}_{w_i}) \quad (2.3.10)$$

We have estimated the location of *MT* based on the coordinate clustering method and the use of above parameters both in LOS and NLOS. However, the WA of all estimated locations (without coordinate clustering) computes the location of *MT* accurately in LOS, while this accuracy is unsatisfactory in NLOS.

2.3.2 Extension to three dimensional environment case

To generalize our method for three dimensional environments, we introduce the *z* coordinate in all the above equations. In a 3*D* environment, besides the two sub-clusters created at \overrightarrow{OX} and \overrightarrow{OY} levels, a third sub-cluster needs to be created at the axis \overrightarrow{OZ} level. We call $P_i^{(z)}$ and $P_j^{(z)}$ the neighbors according to the axis \overrightarrow{OZ} if $|P_i^{(z)} - P_j^{(z)}| \leq \delta_z$. Fig. (2.6) shows the estimated locations in a 3*D* environment.

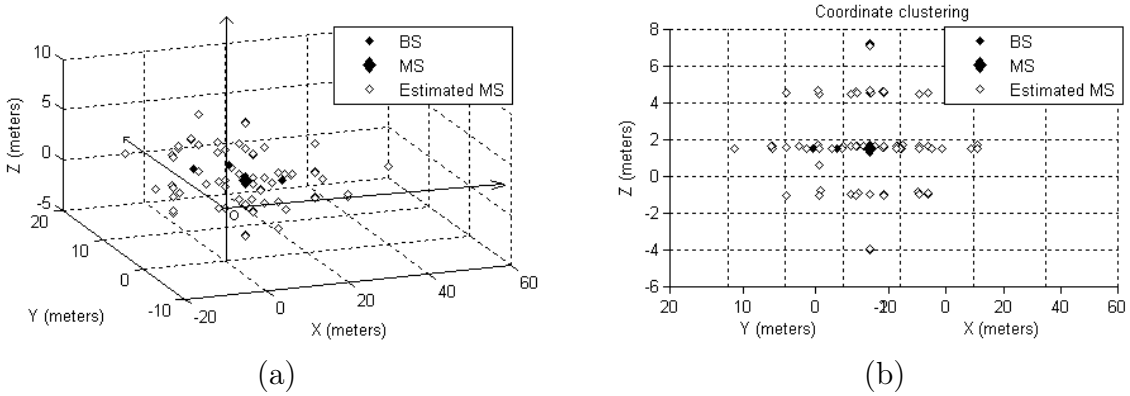


Figure 2.6: Estimated locations in a 3*D* environment, (a) general view, (b) *xy* projection.

We extend the estimated location $\hat{P}(\hat{x}, \hat{y}, \hat{z})$ of *MT* and the average calculation now be-

comes (2.3.11):

$$\begin{cases} P(x) = \frac{1}{k} \sum_{i=1}^k x_i \\ P(y) = \frac{1}{l} \sum_{j=1}^l y_j \\ P(z) = \frac{1}{m} \sum_{q=1}^m z_q \end{cases} \quad (2.3.11)$$

By adding the third coordinate to the WA, the new coordinates of the *MT* become (2.3.12):

$$\begin{cases} P(x) = \frac{\sum_{i=1}^k w_i x_i}{\sum_{i=1}^k w_i} \\ P(y) = \frac{\sum_{j=1}^l w_j y_j}{\sum_{j=1}^l w_j} \\ P(z) = \frac{\sum_{q=1}^m w_q z_q}{\sum_{q=1}^m w_q} \end{cases} \quad (2.3.12)$$

To complete the generalization, we introduce the angle of elevation θ at the *BS*. The error in measuring θ is given by the following expression (2.3.13):

$$\hat{\theta} = \theta + \varepsilon_\theta \quad (2.3.13)$$

Based on the noise assumption, ε_θ is zero-mean Gaussian noise with variance. The variance of the distance error, denoted by σ_d^2 , is then defined as (2.3.14):

$$\sigma_d^2 \approx c^2 (\sigma_\tau^2 [1 + \sin^2(\theta)] + \tau^2 [\sigma_\varphi^2 + \sigma_\theta^2 \cos^2(\theta)]) \quad (2.3.14)$$

Assuming that $\sigma_\theta = \sigma_\varphi = \sigma_{AOA}$, the equation (2.3.14) can be re-defined as (2.3.15):

$$\sigma_d^2 \approx c^2 (\sigma_\tau^2 [1 + \sin^2(\theta)] + \tau^2 \sigma_{AOA}^2 [1 + \cos^2(\theta)]) \quad (2.3.15)$$

From (2.3.15), one can notice that, if $\theta = 0$, then the effect of σ_{AOA} is multiplied by 2. On the other hand, if $(\theta = \frac{\pi}{2}$ or $-\frac{\pi}{2})$, then the time impact is multiplied by 2.

2.4 Experimental results and discussion

2.4.1 Case study

Our case study is a simulated environment with an area of $(17 \times 10) m^2$ created by Radiowave Propagation Simulator (RPSim) software [GmbH 08]. Multiple rooms with different sizes and

a big hall connected by a long corridor have been designed. Walls and furniture scatter the ray tracings as does the floor and the ceiling. It is a typical example of an indoor environment. Complex indoor environments could be designed by joining multiple simple indoor environments. In [Baal 09b; Baal 09a] the authors give more insights for environment parameters: the impact of BS_s placement and the obstacles in the location error.

Our case study gives an idea of indoor positioning system behavior using one or more BS_s to locate MT in different LOS/NLOS locations. Fig. (2.1)(a) illustrates the design of our case study in a 2D environment equipped with three BS_s .

By running Algorithm (2.3.1) for different locations, as mentioned in the case study, the combination of $(\sigma'_\tau, \sigma_\varphi)$ is determined by varying σ'_τ in the range $[0,1]$ meter and σ_φ in the range $[1,10]$ degrees to minimize the Euclidean distance defined by (2.3.10). The other parameters used in the experiments, which depend on the environment dimensions, were fitted by running the Algorithm 1 for positioning the MT situated in L_1 using BS_1 . We changed the threshold δ_x and δ_y in the same way, then we estimated the distance error. Fig. (2.7) depicts the parameters fitting.

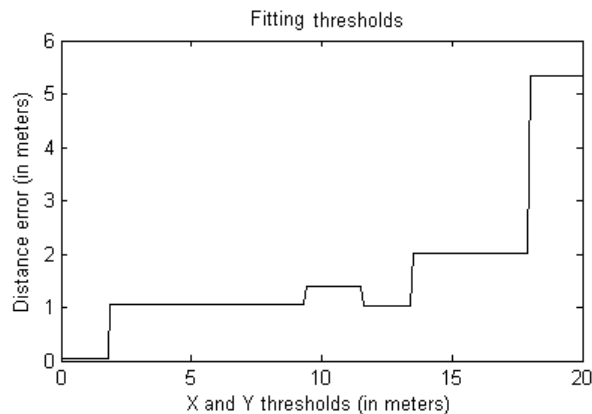


Figure 2.7: Fitting the parameters δ_x and δ_y .

One can notice that when δ_x and δ_y vary from 0.01 m to 1.8 m, the achieved accuracy is good, because only LOS and one bound scattering NLOS multipath ray tracings are used to estimate the MT location. Whereas when δ_x and δ_y vary between 1.9 m and 9.3 m, other observations contribute in the final estimation process, thus LOS, one and two bounds scattering NLOS multipath ray tracings are taken into consideration to locate the MT , and so on.

For all experiments, the values of the parameters of the proposed method are summarized in Table (2.2).

Table 2.2: Values of the parameters.

Parameter	Value
σ'_τ	1 m
σ_φ	5°
δ_x	0.5 m
δ_y	0.5 m
δ_z	0.1 m

2.4.2 Two dimensional case

In this section, we present the performance of the coordinate clustering-based approach for the case study described earlier. Experiments have been performed by applying superposition to three BS_s (BS_1 , BS_2 , BS_3) and detecting the MT in different locations (L_1 , L_2 , L_3) in the environment shown in Fig. (2.1)(a). Table (2.3) assumes the distance error in different experiences with $\sigma_{AOA} = 5^\circ$ and $\sigma'_\tau = 1$ m.

Table 2.3: 2D coordinate clustering method: distance error in meters.

$2D$	$L_1(m)$	$L_2(m)$	$L_3(m)$
BS_1	0.053209	19.545694	0.010110
BS_2	0.035887	0.014778	0.052184
BS_3	0.028520	15.562191	0.027819
BS_{12}	0.018971	0.014778	0.009948
BS_{13}	0.028520	0.001525	0.027803
BS_{23}	0.028520	0.006097	0.027819
BS_{123}	0.028520	0.006097	0.027803

A region is called a blind zone or a dead zone if a few ray tracings reach it while most of these rays are affected by multiple reflections. It can be noticed in Table (2.3) that the achieved accuracy is reasonable in most cases, except for the location L_2 seen by BS_1 or BS_3 . L_2 is located in a dead zone for BS_1 and BS_2 . On the other hand, when combining BS_1 with BS_2 , the error is reduced, due to the visibility between BS_2 and MT at location L_2 . Building coordinate neighbor lists from the ray tracings issued by multiple BS_s improves the location accuracy to the extent that the accuracy achieved by estimating the location of MT using a single BS is unacceptable. This case is presented in Table (2.3) for L_2 seen by BS_1 and BS_3 . Fig. (2.8) depicts the histogram of the distance error shown in Table (2.3). The strange values of the distance error in L_2 have not been taken into account.

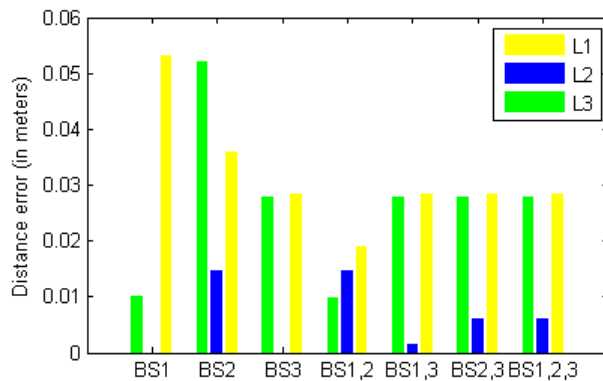


Figure 2.8: 2D coordinate clustering method (distance error in meters).

We notice that the distance errors depend on the number of BS_s , the distance between BS and MT , the visibility and the number of ray tracings reaching the MT .

2.4.3 Thresholds impact

δ_x and δ_y are important parameters which improve (or degrade) the performance. The results in Table (2.3) are obtained when $\delta_x = 0.5 m$. We observed that a large error (distance error is 15.562191 m) occurred during the location of MT in L_2 using BS_3 . The thresholds sensitivity plays a vital role in error reduction because if $\delta_y = 0.01 m$, then a good estimation is achieved. Changing the values of δ_x and δ_y implies regenerating the coordinate neighbor lists. To avoid this process, we compared the Euclidean distance measured between the coordinates in those lists which have the same maximum number of neighbors. To calculate the final location of MT , we considered the most coherent list, i.e. the list with the least differences between its members. The minimal values of the thresholds are the values that allow finding at least one coordinate cluster with one neighbor. The maximum values of the thresholds allow building one coordinate cluster containing all the estimated locations. Since the complexity of the proposed algorithm depends on the size of the candidate locations, we must choose threshold values that allow locating the MT accurately by using a limited size of estimated locations.

2.4.4 Three dimensional case

The robustness of the proposed method for 3D environments was tested using the same simulator (RPSim) [GmbH 08]. The obtained results are reported in Table (2.4).

The first observation, from Table (2.4), is the small value of the distance error estimated by BS_3 in L_2 , which was not sufficient in 2D. The reason is straightforward: unlike the location L_2 , which is still in a blind or a dead zone for BS_1 , some of BS_3 new ray tracings arrived to

Table 2.4: 3D coordinate clustering method: distance error in meters.

3D	$L_1(m)$	$L_2(m)$	$L_3(m)$
BS_1	0.100078	19.547120	0.100078
BS_2	0.105673	0.100257	0.101188
BS_3	0.099729	0.103069	0.100419
BS_{12}	0.100419	0.100257	0.100082
BS_{13}	0.099729	0.103069	0.100419
BS_{23}	0.099729	0.101903	0.100419
BS_{123}	0.099729	0.101903	0.100419

L_2 after reflecting from the floor or the ceiling in the 3D environment. These new ray tracings are adjacent to the neighbor lists used in the proposed method, which results in an improved accuracy.

2.5 Comparison

To confirm the performance of the proposed method, we compared its results with the results obtained from WA method in the same 2D environment. Table (2.5) presents the experimental results of WA without clustering.

Table 2.5: 2D WA: distance error in meters.

2D	$L_1(m)$	$L_2(m)$	$L_3(m)$
BS_1	5.332696	19.545694	0.013505
BS_2	0.197128	0.065494	0.107475
BS_3	0.048442	0.236093	0.035520
BS_{12}	0.196842	0.065494	0.013591
BS_{13}	0.048442	0.236093	0.035500
BS_{23}	0.048442	0.169734	0.035520
BS_{123}	0.048442	0.169734	0.035500

Firstly we found an unexpected and unusual distance error value for the location L_2 viewed by BS_1 . But the distance error for the location L_2 viewed by BS_3 is smaller than the error calculated by the proposed method. In this case, only a few ray tracings delivered by BS_3 could reach the MT in the location L_2 after multiple reflections. The proposed method builds the neighbor lists where the largest list had false coordinates among these few ray tracings. However, the WA used all the estimated values, including the false and true ones, thus the accuracy achieved is better. The same logic could explain the major distance error for the

location L_1 viewed by BS_1 . The WA uses all estimated values, including the false and true ones, whereas the proposed method restricts the estimation to the largest coordinate lists, which have the most true coordinate values. On the other hand, the combination of estimated values from more than one BS improves the accuracy by weighting the values according to the traveled distance. The comparison of the results, in Tables (2.3) and (2.5), shows the performance of the proposed method. Fig. (2.9) presents the histogram of the distance error shown in Table (2.5); the strange values of L_1 and L_2 seen by BS_1 have not been taken into account.

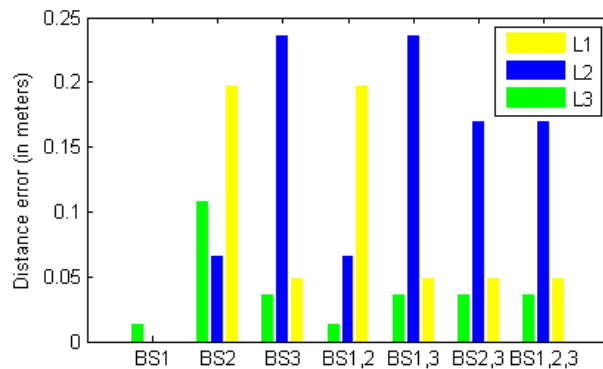


Figure 2.9: 2D WA method: distance error in meters.

Aiming to compare the proposed method with other location methods, it is necessary to expose the performance and location accuracy achieved in two different approaches. In [Boue 09] the illustrated method is based on range-free location of RFID. In a 2D environment with separate distances between RFID-readers, if free space propagation occurs, then the error ranges from 0.15 m to 1.26 m, whereas if obstructed space propagation occurs, then the error ranges from 0.41 m to 1.26 m. In [Zhou 05] the authors merged two sets of data gathered from WiFi and GSM networks, to enlarge the data source. This way, they could improve the accuracy tremendously and reach centimeter-level accuracy. Our proposed method reaches the same level with two features: a single data source WiFi and no overhead of mathematical complexity.

The comparison between the proposed method and the WA method, in L_1 , L_2 and L_3 , is presented in Fig. (2.10), (2.11), and (2.12) respectively.

One can remark that the proposed method outperforms the WA method. To show the stability of the proposed method, multiple experiments have been performed in different locations in the designed environment. These locations are presented in Fig. (2.13), and the obtained results are presented in Table (2.6).

One can remark that the proposed method provides a good accuracy in different locations of MT , except for those locations situated in blind zones. For example, L_4 and L_5 are in the

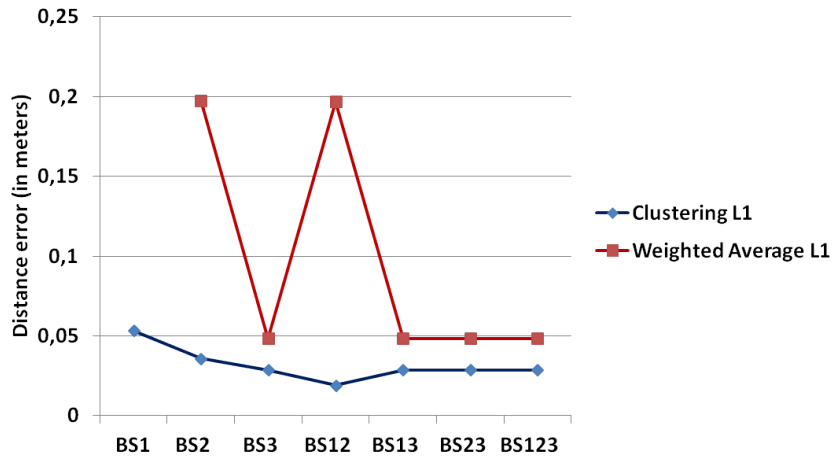


Figure 2.10: Comparison between the proposed method and WA method in L_1 .

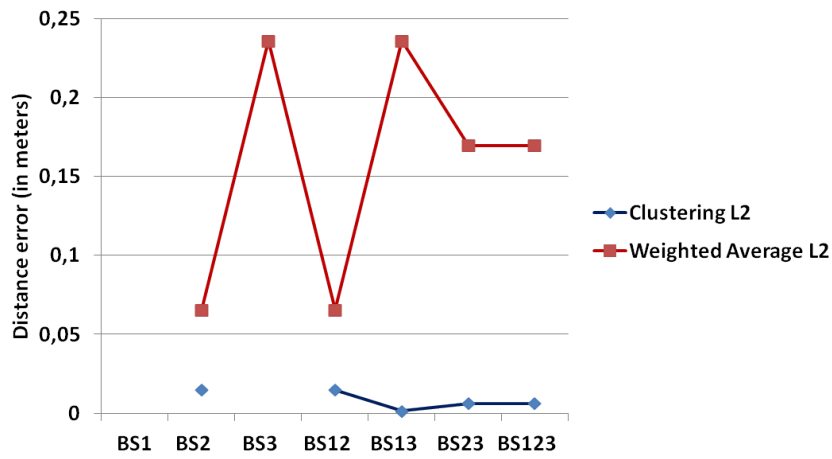


Figure 2.11: Comparison between the proposed method and WA method in L_2 .

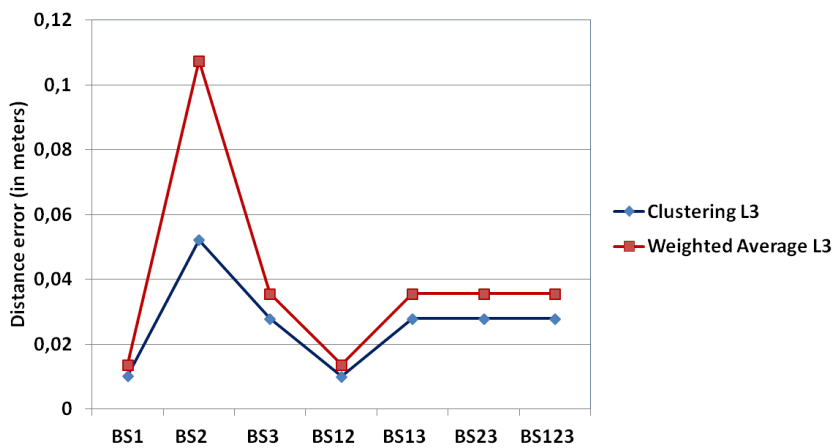


Figure 2.12: Comparison between the proposed method and WA method in L_3 .

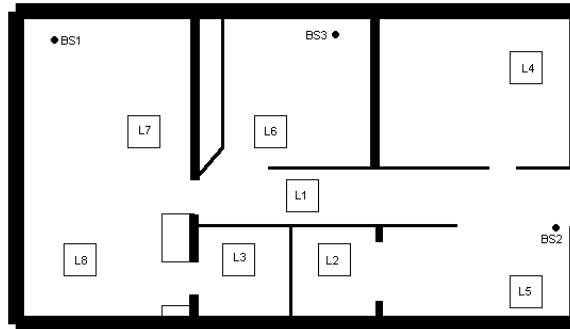


Figure 2.13: More supporting locations: different locations in the designed environment.

blind zone of BS_1 , and L_8 also is difficult to be seen by BS_2

Table 2.6: More supporting results: different locations in the designed environment.

$2D$	$L_4(m)$	$L_5(m)$	$L_6(m)$	$L_7(m)$	$L_8(m)$
BS_1	13.515645	11.153003	0.021322	0.014925	0.040842
BS_2	0.015372	0.014054	0.016398	0.053043	5.809635
BS_3	0.032351	0.011373	0.019069	0.017969	0.030936
BS_{12}	0.015075	0.013539	0.017576	0.017012	0.031742
BS_{13}	0.031852	0.014836	0.018587	0.016683	0.037163
BS_{23}	0.010419	0.012229	0.016178	0.014161	0.023327
BS_{123}	0.009836	0.011736	0.016341	0.015729	0.034137

2.6 Conclusion

A new hybrid coordinate clustering approach for indoor location, which depends on TOA/AOA in multipath environment, has been presented. The proposed method does not need any prior knowledge or prior mitigation technique to correct the error caused by the multipath ray tracings. In most cases, the proposed method has been proved efficient. The achieved accuracy showed the robustness of the proposed method, in two dimensional and in three dimensional environments, taking into consideration the floor and the ceiling reflections. In real world conditions, many blind or dead zones exist, because of the small number or distorted distribution of the BS_s , and the continually changing indoor environments (open/close doors, prefabricated walls, rearrangement of furniture, and moving people). There are many location methods which are based on geometric calculation, depending on TOA and AOA. Other methods, based on probabilistic calculation, depend on RSS [Bahl 00b; Vars 07; Yun 09; Swan 08; Guo 08]. A combination of TOA/AOA/RSS information could be useful to develop a two phase, geometric

and probabilistic hybrid method, thus overcoming the limitations in blind or dead zones of the environment.

In the next chapter, we discuss two range-free indoor location techniques, K-nearest neighbor and artificial neural network. However, the performances of those methods are not as accurate as our range-based method proposed in this chapter, but they utilize the available heterogeneous information RTT and RSS to overcome the limitation of blind or dead zones.

A COMPARISON OF LEARNING AND DETERMINISTIC RANGE-FREE TECHNIQUES FOR INDOOR GEO-LOCATION

3.1 Introduction

A direct consequence of our range-based coordinate clustering method for indoor location presented in the previous chapter is the need of a positioning system, that stems the limitation drawn from blind or dead zone where the mobile terminal cannot be positioned. Authors in [ZYou 10] attempt to answer the following question: how to deploy a WLAN in order to guarantee the requested Quality of Service (QoS), while reducing the location error? The authors propose a new approach, where WLAN planning and positioning error reduction are modeled as an optimization problem and tackled together during WLAN planning process.

Range-free techniques provide an alternative solution to locate the mobile terminal in critical blind areas because most of range-free techniques use fingerprint-based methods: for example, RSS-based location technique exploits the signal propagation of WLAN. This class of systems is based on two principle phases, offline phase and online phase. During the offline phase, a fingerprint database is built by collecting data over all the considered indoor environment. Then, to retrieve a position we look for the nearest fingerprint. Fig (3.1) illustrates the two phases, offline and online, of a fingerprint-based location system.

A list of fingerprint-based location systems is presented in Table (3.1). Bayesian-based approaches use probabilistic methods, while the other approaches, K-nearest neighbor, use deterministic methods. Probabilistic methods take into account a higher number of fingerprint samples at each position, therefore, they achieve a good accuracy. However, they are more complex from a computational point of view. The main drawback of the Bayesian system is that it needs more access points, and long training time. As shown in Table (3.1), the accuracy varies from 1.5 *m* at 77 % of the time, when using 5 APs for [Ladd 02] to 2.5 *m* at 90 % of the time, when using 10 APs for [Roos 02]. While the best performance, given only 3 APs, is achieved by [Saha 03], and the worst accuracy, given the same number of APs, is achieved by [Bahl 00b]: 2.1 *m*, at 38 % of the time. Nevertheless, the performance of each

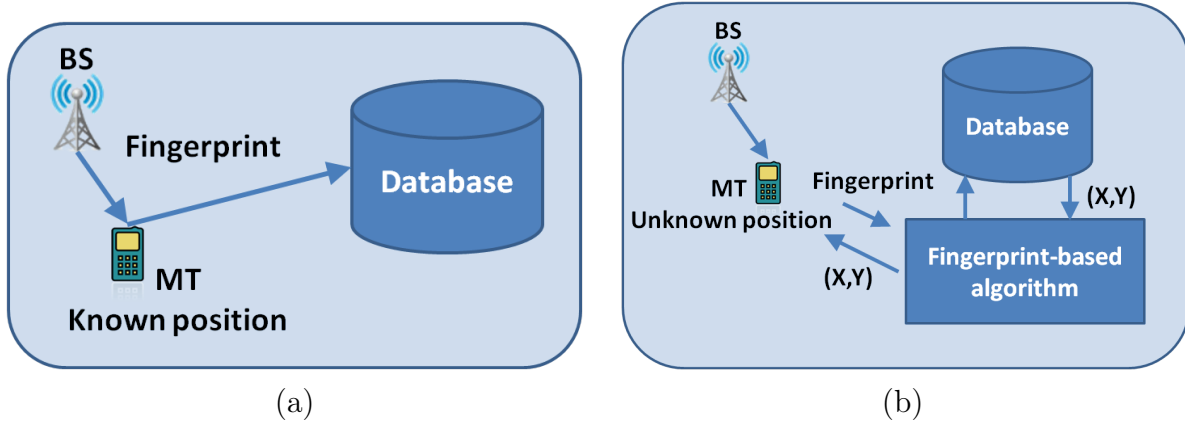


Figure 3.1: Fingerprint-based system phases: (a) Offline phase and (b) Online phase.

system strongly depends on the adjusted implementation parameters, the fingerprint database resolution, the number and the distribution of the APs, and the structure of the considered indoor environment. Our objective is to study the fingerprint-based positioning systems and to compare their performance on a common test-bed using identical databases.

Table 3.1: Comparison of existing positioning systems based on RSS measurement [Kaem 05].

System	Technique	Number of APs	Precision and % of the time attained
[Brun 05]	neural network and Weighted K-nearest neighbor	6	4.9 m to 5.2 m at 95 %
[Haeb 04]	Bayesian	15 to 33	3 m at 97 %
[Zhe 04]	Bayesian with RSS distribution model	5	1.8 m at 90 %
[Yous 03]	Bayesian	4	2.1 m at 90 %
[Saha 03]	Nearest neighbor and neural network	3	2 m at 90 %
[Para 02]	Weighted K-nearest neighbor	2 to 7	7.2 m at 75%, 12.2 m at 95 %
[Ladd 02]	Bayesian	5	1.5 m at 77 %
[Roos 02]	Bayesian	10	2.5 m at 90 %
RADAR enhancements [Bahl 00a]	Nearest neighbor with environment profiling	5	3.16 m at 90 %
RADAR [Bahl 00b]	Nearest neighbor	3	2.1 m at 38 %

We can summarize the objectives of this work in these points:

- a comparison of two range-free positioning techniques: artificial neural network (ANN) technique and K-nearest neighbor (KNN) technique, on the same test-bed;
- a study of the impact of various parameters that affect the performance of those techniques, as the number of BSs (APs), the number of hidden layers, and the fingerprint database resolution;
- a proposal of a new metric for the nearest neighbor technique, called δ -nearest neighbor;
- a study of heterogeneous fingerprint database influence on the performance of the location method.

3.2 Artificial neural networks (ANN)

3.2.1 Definition

An artificial neural network (ANN) is a computational model based on the structure and functions of biological neural networks. Each artificial neuron consists of three components: the weighted connections, the combination function and the activation (transfer) function. The most used combination function is the addition. The summed information, (a), is transferred to the output through a transfer function f . This function can be linear: $p = f(a) = a$, or nonlinear: $p = f(a) = \frac{1}{1+e^{-a}}$, referred as Log-Sigmoid, and $p = f(a) = \frac{1}{1+e^{-2a}} - 1$, called Tan-Sigmoid. This activation function produces the neuron output. Fig. (3.2) represents the components of an artificial neuron.

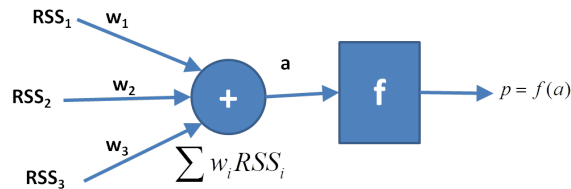


Figure 3.2: Components of an artificial neuron.

Neural networks are organized into layers of neurons: all neurons in a layer have the same inputs and the same transfer function. The number of layers and the number of neurons in each layer depend on the complexity of the considered problem and the desired accuracy. Information that is processed through the network affects the structure of the ANN because the weight of a neural network changes, based on the inputs and the output.

The advantages of using ANN can be summarized as:

- a neural network can perform tasks that a linear program cannot do;
- due to its parallel nature, a neural network provides a solution even if one of its element fails;
- a neural network does not need to be reprogrammed, because of its learning procedure.

The disadvantages of using ANN are:

- the training phase is necessary for a neural network to be efficient. This procedure may be very slow for large sets of fingerprints;
- it requires high processing time (for large neural networks).

3.2.2 Neural network topologies

Another aspect of the artificial neural networks is that there are different topologies, which consequently require different types of algorithms. Depending on the existence of feedback, two main categories of neural network topologies can be distinguished, feedforward networks and recurrent networks. Hybrid topologies of these categories can be useful for several applications [Parl 94].

3.2.2.1 Feedforward neural networks

A common structure of feedforward neural networks is multi-layer perceptron (MLP) [Sidd 12]. MLP networks consist of at least three layers, an input layer, one or more hidden layers, and an output layer. In fully connected neural networks, each neuron is connected to each neuron in the following layer. The role of the input layer is to distribute the input fingerprints to subsequent layers. Input neurons have linear activation function and no thresholds (bias). Each hidden unit node and each output node have thresholds associated with them in addition to the weights. The hidden neurons have nonlinear activation function, that gives the MLP the ability to emulate nonlinear mapping properties, and it makes the network suitable for many applications, without the limitations of pure linear networks. Hence, each fingerprint sample feeding into a node in a subsequent layer has the original input fingerprint, multiplied by a weight with a threshold added, and then is passed through an activation function that may be linear or nonlinear (hidden units). Furthermore, it is proved (Kolmogorov's Theorem) [Kruer 92] that a two neuron-layer perceptron network with nonlinear function can generate any function as output with the desired approximation. An example of MLP network with two hidden layers is shown in Fig. (3.3).

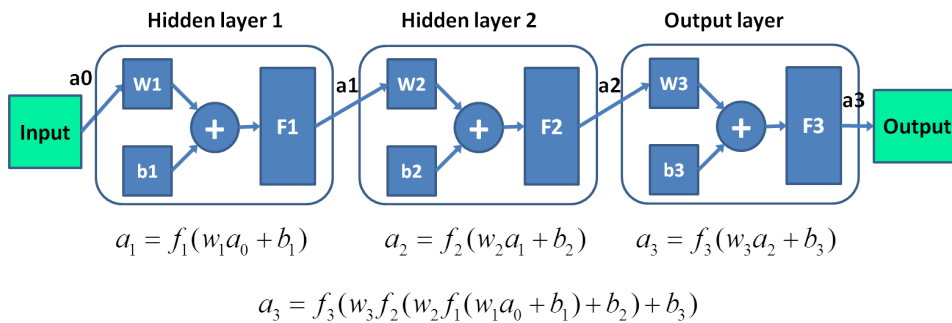


Figure 3.3: Two hidden layer MLP networks. F_i are the activation functions, W_i the adjusted weights, and b_i are the thresholds

The activation functions are tan-sigmoid with values in the interval $[-1, 1]$ or log-sigmoid with values in the interval $[0, 1]$ for the hidden layer, and linear function for the output layer.

The applied learning algorithm is the *Backpropagation*.

With regard to linear parameterized networks, the advantage of MLP is the reduced number of parameters. It is clear that this number depends on the dimension of the input, nevertheless this dependence is not exponential. The shortcomings of these types of networks resides in their nonlinear parameterization [Chen 91].

3.2.2.2 Recurrent neural networks

In this class of neural networks the interconnections of the neurons make possible feedback of the data flow between layers. This topology of neural networks consists of two neuron layers and has internal feedback from the outputs of the hidden layer to the input layer. So these fingerprints are again introduced as inputs for the neurons of the hidden layer. To do so, a "short-term memory" is achieved, because the information introduced into the network temporarily influences the future response of its neurons. The employed activation functions are in both layers, as in the case of the MLP already described. Backpropagation is one of learning algorithms for the training of these networks. The Elman, Jordan, Kohonen or Hopfield networks belong to this category [Simp 95]. Fig. (3.4) represents Elman recurrent neural network.

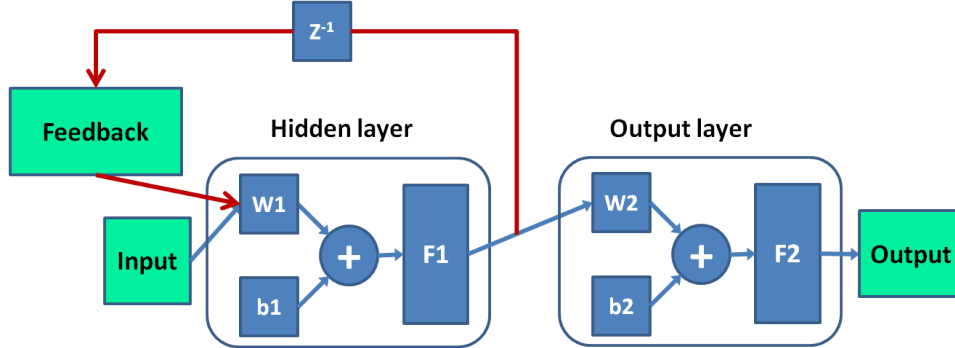


Figure 3.4: Elman recurrent network. F_i are the activation functions, W_i the adjusted weights, and b_i are the thresholds

3.2.2.3 Hybrid neural networks

In this topology, the input layer to the neural network is a time delayed series of input fingerprints. The first input unit receives the instantaneous fingerprint, sequentially introduced. The other input units have the delayed values of the input fingerprint. Fig (3.5) presents the schema of dynamic MLP network.

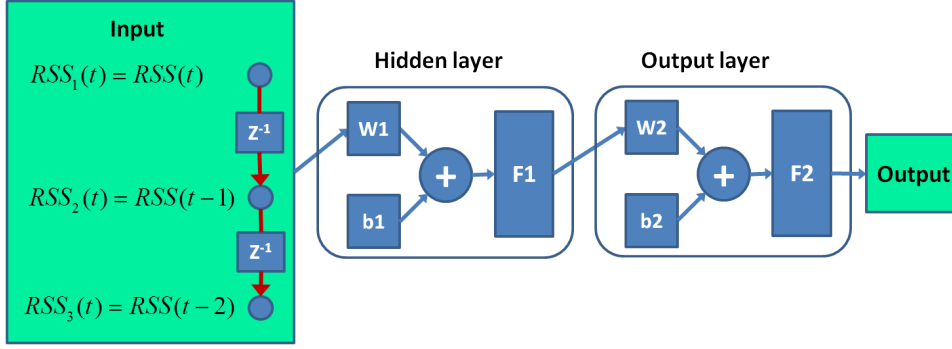


Figure 3.5: Dynamic MLP network. t is the time delay, F_i are the activation functions, W_i the adjusted weights, and b_i are the thresholds

3.2.3 Neural network training (learning)

The steepest descent algorithm, also known as the *error backpropagation* (EBP) algorithm [Rume 86; Werb 88], could be considered as one of the most significant breakthroughs for training neural networks. However, the drawback of EBP is its slow convergence. The Levenberg-Marquardt algorithm [Leve 44; Marq 63] solves the problems existing in both gradient descent method and the Gauss-Newton method for neural-networks training, by the combination of those two algorithms. It is regarded as one of the most efficient training algorithms [Haga 94]. For small-sized networks training, the computation is efficient, but for large-sized networks, such as in image recognition problems, the Levenberg-Marquardt algorithm may be even slower than the steepest descent algorithm [Yu 10]. Another problem for large-sized training fingerprints is that the memory cost tends to be not feasible.

At the beginning, the initial weights are chosen randomly, then the training (learning) process begins. To do so, three different learning approaches could be applied, supervised learning, unsupervised learning (or adaptive learning), and reinforcement learning.

3.2.3.1 Supervised learning

In supervised learning, both of the input fingerprints and the desired outputs are provided. Then, to adjust the network weights, MLP network starts processing the input fingerprints and compares the obtained outputs to the desired ones. The overall performance of the MLP is measured by the mean square error (MSE) given by equation (3.2.1):

$$\begin{cases} e = \frac{1}{N} \sum_{i=1}^N e_i \\ e_i = \sum_j^M (y_i(j) - y'_i(j))^2 \end{cases} \quad (3.2.1)$$

where e_i corresponds to the error for the i^{th} fingerprint, y_i is the desired output, y'_i is the output vector from the trained network for the i^{th} fingerprint, N is the dimension of the input fingerprint vector, and M is the dimension of the output vector. For mobile terminal location: $M = 2$ in $2D$ environments and $M = 3$ in the case of $3D$ environments.

Errors are then propagated back through the MLP network to adjust the weights which control the network performance. Using the same training set, this process occurs repeatedly to adjust the network weights.

3.2.3.2 Unsupervised (adaptive) learning

Contrarily to supervised learning, the desired outputs are not provided in unsupervised (adaptive) learning approach, only the input fingerprints are provided, the MLP network itself must then decide what features it will use to group the input fingerprints. In other words, in this learning paradigm, the network is expected to discover statistically salient features of the input fingerprints. This is often referred to as self-organization or adaption [Grau 07].

3.2.3.3 Reinforcement learning

Finally, an intermediate approach between supervised and unsupervised learning approaches is the reinforcement learning approach. In this type of learning, the network does some action on the environment and gets a feedback response from the environment. The learning system grades its action good (rewarding) or bad (punishable) based on the environmental response and accordingly adjusts its weights. Generally, weights adjustment is continued until an equilibrium state occurs. The self-organizing neural learning may be categorized under this type of learning.

3.2.4 Neural network applications

In the last decade, many researches contributed to develop and to adopt the artificial neural network concepts to practical applications. Recurrent neural networks are used to model a sensor node, the node's dynamics, and interconnections with other sensor network node. Then, this modeling approach is used for sensor node identification and fault detection in wireless sensor networks [Mous 08]. A new controller approach applied to redundant robot manipulators constrained by mobile obstacles, and all unknown functions in the robot dynamical model, written in extended Cartesian space, are carried out using multilayer perceptron (MLP) neural networks [Daac 12]. Actually ANNs have proved their efficiency and robustness in many research fields and they can be applied to a wide variety of problems, such as breast cancer detection [Jung 05], classification of satellite imagery [Stat 06], pattern recognition [Bish 95],

image compression [Mish 12], stock market prediction [Gure 11], etc.

Artificial neural networks have been introduced in the indoor location field. The results indicate that ANN-based positioning systems can provide accuracy and precision which is quite adequate for the development of indoor location systems (ILS), while using the already available WLAN infrastructure. The reason for selecting ANN is because of its robustness against noise and interference, which are among the major factors affecting the accuracy of ILS [Hami 10].

3.3 Proposed ANN approach for indoor location

Our approach consists of two phases: fingerprint collection (offline phase) and locating the mobile terminal (online phase). In the following, we present the case study and our algorithm to build the fingerprint database. Then, we explain the ANN-based algorithm to perform the indoor location.

3.3.1 Case study and fingerprint collection

3.3.1.1 Case study

Hospitals, museums, libraries, or any closed environment where GPS signal is not available anymore, could be considered as a case study for indoor location process. Several base stations or WLAN access points are distributed to cover the area of the case study at hand. Unfortunately, WLAN signals are scattered, diffracted, or reflected by existing obstacles, walls, furniture, and even by moving people. Therefore, fingerprint values vary significantly from day to day and also from hour to hour. Hence, the offline step of the fingerprint-based location system demands major efforts to construct a reliable fingerprint database. Afterwards, regular updates should be performed on this fingerprint cartography, particularly, in the case of adding (activating) or removing (deactivating) WLAN access points. The same result can be expected in the case of changing of the inner structure of the case study.

Several studies in the literature of indoor location proposed different test-beds to realize their experiments (see Table 3.2). Each test-bed has different total area, different number of base stations (or WLAN access points), and different number of fingerprint locations and orientations. Therefore, the fingerprint density is calculated as the total area divided by the number of locations; it represents the area covered by a single fingerprint. Obtained results strongly depend on the fingerprint density, so, high fingerprint density implies high accuracy and good performance. For example, a fingerprint density of 39 *m* gives an average distance

between fingerprints of 6.2 m while a fingerprint density of 9 m yields a distance of 3 m . An error distance of 6.2 m represents at worst the location of the nearest base station to the actual location. Table (3.2) lists some test-beds presented in previous researches and compares their total area, number of fingerprints, and fingerprint density [Dawe 11].

Table 3.2: Location test-bed and fingerprint density.

Study	Area (m^2)	Number of locations	Fingerprint density	fingerprint spacing (m)
UoW-Testbed [Dawe 11]	2160	56	1:39	6.2
[Hoss 07]	540	62	1:9	3
[Yous 03]	1768	110	1:16	4
RADAR enhancements [Bahl 00a]	940	49	1:19	4.4
RADAR [Bahl 00b]	980	70	1:14	3.7

To realize our experiments for ANN technique (and later for KNN technique), and to compare the achieved results and performances, we have to choose a test-bed that simulates the real indoor environment. However, comparing KNN and ANN performances to the performance that is obtained in our previous study (coordinate clustering) imposes a strong constraint and limits our choices of this test-bed (see 3.3.3).

3.3.1.2 Fingerprint collection

The step of fingerprint collection involves scanning all channels in the WLAN spectrum to identify all available base stations (access points APs). Fingerprint collection also requires the time correlated sampling of the WLAN band in order to build a robust image of the signal strength characteristics of APs. Some programs were developed, called *RSSI Loggers*, to handle the fingerprint collection process [Dawe 11]. Two main methods enable obtaining a fingerprint in a specific place. The first method is simple and manual. We go to the specific location and capture WLAN signals during a period of time until the acquiring fingerprint becomes stable. Different orientations (north, south, east, and west) result in registering different fingerprints for the same location [Dawe 11]. The second method consists of applying a path loss model used for indoor propagation, taking into account the existing obstacles (see (1.2.6) [Even 07]). The advantage of the first method is to collect real fingerprints but in limited physical locations, while the second method can generate more theoretical fingerprints and calibration to quickly build the database [Paol 09].

Our strategy to build the fingerprint database is divided into four steps:

- for each base station, collecting the available measurements, such as RSS and RTT;

- correction process, for the blind and dead zones in the test-bed;
- normalization procedure, to have fingerprint values in the interval $[0, 1]$;
- the fusion step, to build heterogeneous fingerprints (RSS, RTT).

Fig (3.6) illustrates our approach to collect fingerprints and to build the fingerprint database.

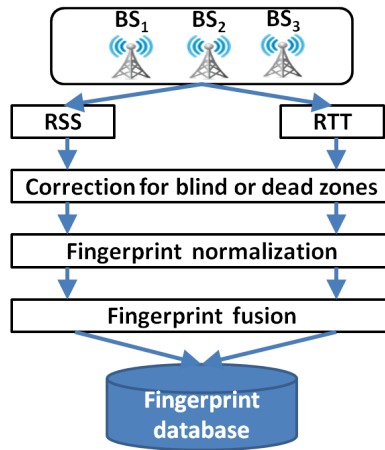


Figure 3.6: Procedure of building fingerprint database.

3.3.2 ANN-based proposed algorithm for indoor location

Once the fingerprint database has been constructed (offline phase), a new fingerprint database with Gaussian additive noise is constructed to evaluate the performance of our ANN-based algorithm. Then, the MLP network is ready to be figured with optimal parameters, such as the number of hidden layers, the number of hidden units in each hidden layer, the activation function, the training iterations, etc. To do so, we take the pre-built fingerprint database as input to the MLP network and desired outputs are provided. Using a supervised training method, we launch the learning procedure with specific MLP parameters. At the end of the learning procedure, we test the obtained MLP against the noisy fingerprint database. Depending on the achieved performance, modifications to MLP network parameters occur. The adjustment procedure carries on until no improvement to the algorithm performance. Therefore, the MLP network parameters are fixed. Fig (3.7) illustrates our ANN-based algorithm to solve the indoor location problem.

3.3.3 ANN experimental results

To compare the results that were obtained in our previous study (coordinates clustering), we have to choose the same indoor environment designed in 2.4. As we have mentioned previously,

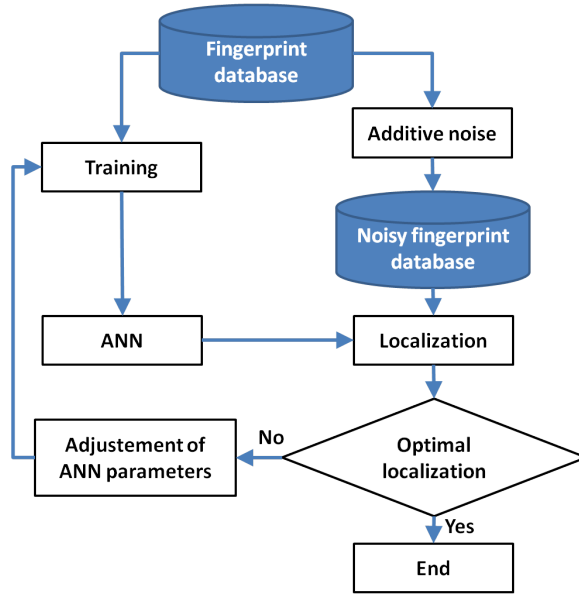


Figure 3.7: ANN indoor location algorithm.

our case study is a simulated environment with an area of $(17 \times 10) m^2$ created by Radiowave Propagation Simulator (RPSim) software [GmbH 08]. RPSim software allows the production of fingerprint cartography with different densities, and provides different useful measurements for indoor location process as RSS (in dBm) and RTT (in nsec). Fig. (2.1)(a) illustrates the design of our case study in a 2D environment equipped with three BS_s .

Our fingerprint database was constructed based on the fingerprint pattern shown in Fig. (3.8)

(X, Y)	BS1	BS2	BS3
RSS (dBm)	-79.2	-56.8	-100
RTT (nsec)	7.12	3.91	0

Figure 3.8: Fingerprint pattern database.

The couple $(RSS = -100 dBm, RTT = 0 nsec)$ describes the dead or blind zones, while the couple $(RSS \neq -100 dBm, RTT = 0 nsec)$ describes the very close zone to the active BS . For this reason, the delay spread is considered as null. Fig. (3.9) (a) illustrates the RSS covered area in our test-bed for BS_1 , and Fig. (3.9) (b) illustrates the delay spread for the same base station BS_1 .

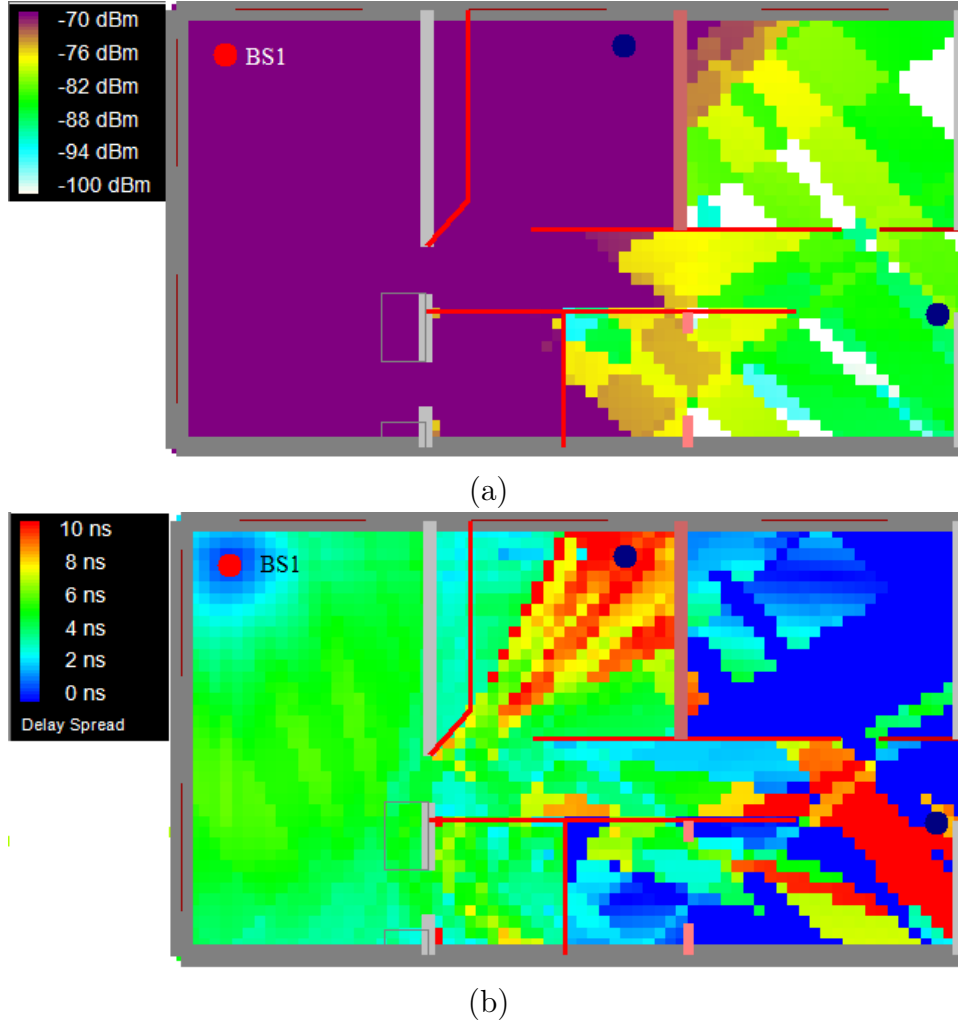


Figure 3.9: Covered area in our test-bed for BS_1 : (a) RSS coverage and (b) RTT spread.

Two fingerprint databases with different resolutions were built using RPSim. The first database contains 153 physical location fingerprints, with a resolution of $1 m^2$, while the second database is built by using 2448 physical location fingerprints with a resolution of $25 cm^2$.

Experiments have been performed by applying superposition to three BS_s (BS_1, BS_2, BS_3), and using a feed-forward neural network model (MLP) with the syntax:
 $net = \text{newff}(\text{Input}, \text{Output}, [S_1 S_2 \dots S_n], \{TF_1 TF_2 \dots TF_n\}, \text{BTF}, \text{BLF}, \text{PF})$.

Table (3.3) summarizes the different characteristics of the used MLP model.

3.3.3.1 Impact of hidden layers number

Initially, experiments were done using a feed forward neural network model with one hidden layer. The obtained results are shown in Table (3.4). It is clear that the best performance is achieved when all the base stations are active. On the other hand, the worst performance is

Table 3.3: Principle elements of feed-forward neural network model.

Element	Description	Default value
Input	The fingerprint database	(RSS_1, RSS_2, RSS_3)
Output	The real physical positions	(x, y, z)
S_i	Size of i^{th} layer (number of neurons)	40 if $n = 1$ and 20 if $n = 2$
TF_i	The transfer function of i^{th} layer	'tansig'
BTF	Backprop network training function	'trainlm'
BLF	Backprop weight/bias learning function	'learngdm'
PF	Performance function	'mse'

registered to RSS_3 fingerprints that come from BS_3 . One can see that the combination of more than one RSS value allows to have distinguishable fingerprints, and then better performance. The best performance is around 70 % within 1 m distance error using RSS_{123} fingerprints of the three active BS_s . It means that 70 % of the tested fingerprints are located within a circle centered by the real position of the fingerprint, and the rayon of this circle is 1 m .

Table 3.4: The performance of ANN technique using one hidden layer.

Accuracy	RSS_1	RSS_2	RSS_3	RSS_{12}	RSS_{13}	RSS_{23}	RSS_{123}
$Acc \leq 25 \text{ cm}$	1.44 %	0.39 %	0.11 %	3.91 %	4.36 %	3.66 %	9.79 %
$Acc \leq 50 \text{ cm}$	4.96 %	2.04 %	1.02 %	13.69 %	14.11 %	13.34 %	29.81 %
$Acc \leq 75 \text{ cm}$	11.37 %	5.28 %	2.89 %	24.39 %	27.81 %	26.33 %	52.13 %
$Acc \leq 1 \text{ m}$	18.3 %	9.47 %	5.88 %	35.48 %	42.98 %	39.53 %	70.29 %

To study the impact of the number of hidden layers, we choose MLP network with two and four hidden layers with respect of the total number of hidden neurons. This means that 40 neurons in all MLP models were used in these experiments. In Table (3.5), we notice that the significant improvement in performance takes place only in combination of two RSS values RSS_{12} , RSS_{13} , and RSS_{23} fingerprints. Comparing to the obtained results using MLP with only one hidden layer, the performance for RSS_{12} fingerprints attains 35.48 % within 1 m distance error, while the performance using MLP with two hidden layers attains 43.05 % within the same distance error. Idem for RSS_{13} and RSS_{23} where the achieved performance is 42.98 % and 39.53% using one hidden layer, and the achieved performance is 58.08% and 48.61% using two hidden layers respectively, with the same distance error 1 m . Fig 3.10(a) illustrates the performance of MLP with one hidden layer, while Fig (3.10(b)) shows the better performance of MLP with two hidden layers.

Table 3.5: The performance of ANN technique using two hidden layers.

Accuracy	RSS_1	RSS_2	RSS_3	RSS_{12}	RSS_{13}	RSS_{23}	RSS_{123}
$Acc \leq 25\text{ cm}$	1.51 %	0.74 %	0.28 %	5.14 %	7.43 %	6.48 %	11.33 %
$Acc \leq 50\text{ cm}$	4.72 %	2.53 %	1.09 %	16.83 %	24.78 %	20.27 %	35.2 %
$Acc \leq 75\text{ cm}$	10.84 %	6.2 %	3.56 %	31.5 %	42.59 %	35.73 %	56.88 %
$Acc \leq 1\text{ m}$	18.34 %	10.52 %	6.62 %	43.05 %	58.08 %	48.61 %	71.28 %

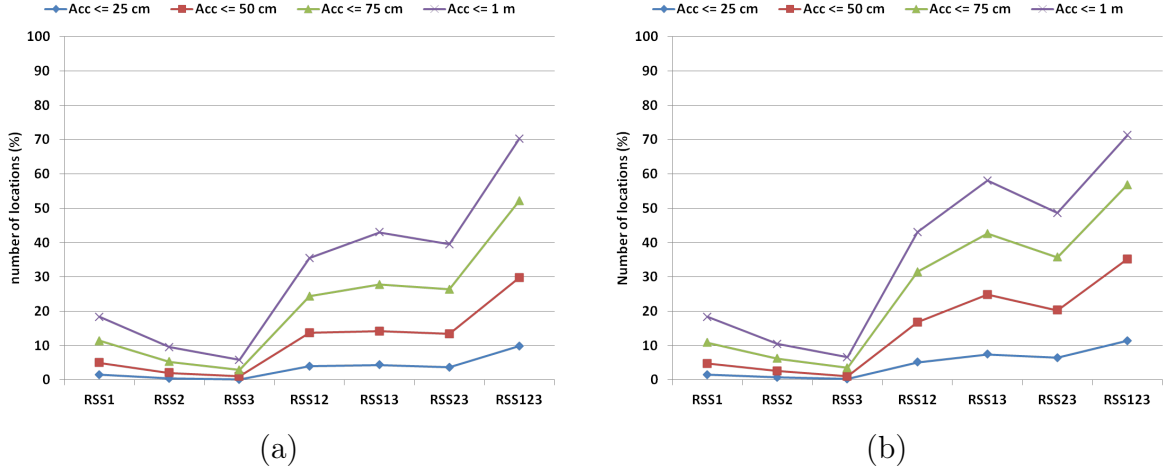


Figure 3.10: Illustration of the performance of ANN: (a) using one hidden layer and (b) using two hidden layers.

3.3.3.2 Impact of heterogeneous fingerprints

Received signal strength is not the only available information on the base station side. Other information as RTT could be useful for location process. Although RTT values are very different from those of RSS, the couple (RSS, RTT) is a more distinguishable fingerprint. The input layer contains two, four, or six neurons according to the active base stations, while the hidden and the output layers remain as described in Table (3.3). Table (3.6) summarizes the obtained results of MLP with one hidden layer, and Fig. 3.11 illustrates the good performance of the heterogeneous (RSS, RTT) fingerprints. As expected, the best result of 85.41 % within 1 m distance error, is obtained for three active base stations.

3.3.3.3 Impact of fingerprint database resolution

To this end, the impact of ANN variants has been studied using the same fingerprint database with 2448 samples (resolution of 25 cm^2). To complete our study, we have to test the database resolution effect.

Table 3.6: The performance of ANN technique using (RSS, RTT) heterogeneous fingerprints and one hidden layer.

Accuracy	RSS_1RTT_1	RSS_2RTT_2	RSS_3RTT_3	$RSS_{12}RTT_{12}$	$RSS_{13}RTT_{13}$	$RSS_{23}RTT_{23}$	$RSS_{123}RTT_{123}$
$Acc \leq 25\text{ cm}$	1.51 %	1.09 %	0.99 %	3.31 %	5.46 %	5.17 %	11.66 %
$Acc \leq 50\text{ cm}$	5.21 %	4.26 %	3.7 %	12.88 %	19.18 %	16.3 %	34.26 %
$Acc \leq 75\text{ cm}$	11.47 %	8.87 %	8.1 %	25.94 %	34.78 %	30.1 %	59.34 %
$Acc \leq 1\text{ m}$	19.39 %	15.38 %	13.62 %	36.61 %	49.63 %	44.03 %	85.41 %

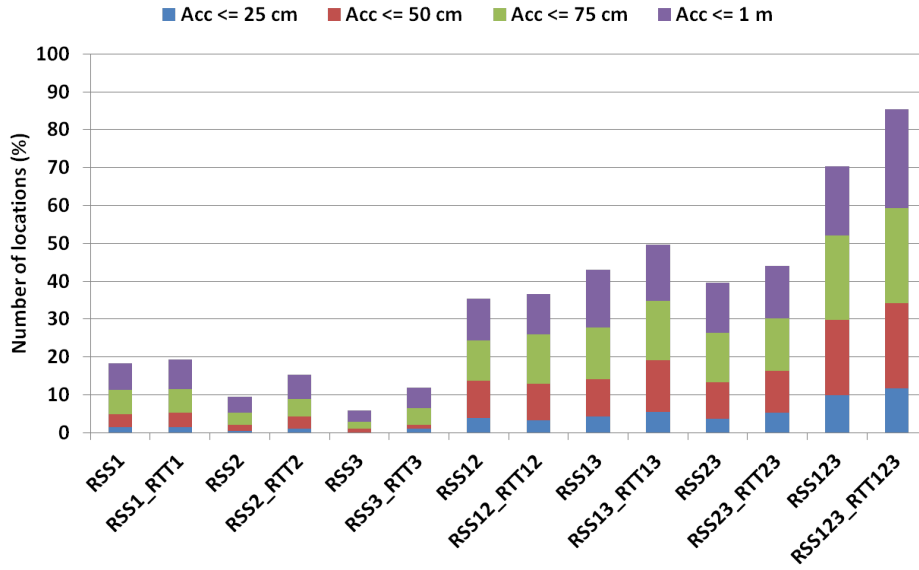


Figure 3.11: Illustration of the performance of ANN using heterogeneous (RSS, RTT) fingerprints and one hidden layer.

To show the impact of the database resolution, another fingerprint database with 153 samples (resolution of $1m^2$) was built. The experiments have been made by applying ANN technique with one hidden layer using homogeneous fingerprints (RSS_1, RSS_2, RSS_3). Fig (3.12) illustrates the obtained results and proves the superiority of large-sized fingerprint database. The graph clearly highlights the significant improvement to the performance of ANN technique.

3.4 K-nearest neighbor (KNN)

KNN technique estimates the mobile terminal location in indoor environments, depending on the fingerprint database that is constructed in the offline phase of fingerprint-based system. Using the current fingerprint transmitted by the mobile terminal, the KNN technique searched for the K nearest matches in the pre-built fingerprint database. Neighbors are defined according to a chosen metric or a distance function in the fingerprint space. Table (3.7) summarizes the

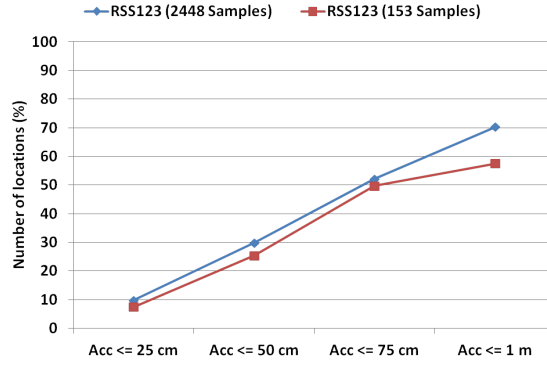


Figure 3.12: Illustration of the ANN performance with one hidden layer, using different database resolutions (2448 samples with resolution of 25 cm^2 , and 153 samples with resolution of 1 m^2).

distance functions between two fingerprints $(RSS_1, RSS_2, \dots, RSS_n)$ and $(RSS'_1, RSS'_2, \dots, RSS'_n)$ where n is the number of base stations.

Table 3.7: Distance functions between two fingerprints: (RSS_i) and (RSS'_i) , $1 \leq i \leq n$.

Distance	Parameter	Function
Manhattan	1-norm distance	$\sum_{i=1}^n RSS_i - RSS'_i $
Euclidean	2-norm distance	$\left(\sum_{i=1}^n (RSS_i - RSS'_i)^2 \right)^{1/2}$
Minkowski	p-norm distance	$\left(\sum_{i=1}^n (RSS_i - RSS'_i)^p \right)^{1/p}$
Tchebychev	∞ -norm distance	$\lim_{p \rightarrow \infty} \left(\sum_{i=1}^n (RSS_i - RSS'_i)^p \right)^{1/p} = \sup_{1 \leq i \leq n} RSS_i - RSS'_i $
Mahalanobis	σ -norm distance	$\left(\sum_{i=1}^n \frac{(RSS_i - RSS'_i)^2}{\sigma^2} \right)^{1/2}$

To optimize the location process, least mean square (LMS) principle is usually applied. Then, the estimated location of the MT is obtained by simple/weighted averaging of the location candidates. Choosing an appropriate value of the parameter K affects the performance of this technique. If $K = 1$, then the MT location is simply assigned to the location candidate of its nearest neighbor, referred also by closest neighbor (CN). RADAR [Bahl 00b] is the first positioning system developed by Microsoft to estimate MT location using RSS captured from multiple BS_s . In [Swan 08], the authors use the analysis of the fingerprint structure to identify and eliminate inefficient location fingerprints stored in the fingerprint database. For more details, see 1.2.2.2.b.

3.4.1 Proposed KNN-based algorithm for indoor location

The same constructed fingerprint database for ANN technique (see 3.3.1.2) is used to perform the indoor location process based on KNN algorithm. However, to evaluate the algorithm performance, a noisy fingerprint database is derived from the original one by adding Gaussian noise. Multi-output procedures have been developed to obtain experimental results for all variants of KNN algorithm, such as the number of neighbors K , the chosen metric δ , the heterogeneous fingerprints, and the database resolution. Fig (3.13) illustrates our KNN algorithm to perform the indoor location process.

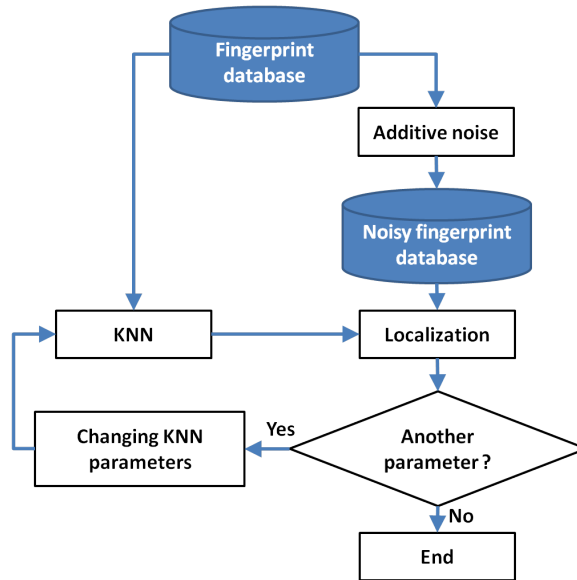


Figure 3.13: KNN indoor location algorithm.

3.4.2 KNN-based experimental results

To illustrate the performance of the KNN-based indoor location technique, we show the results on different fingerprints. Experiments have been performed by applying superposition to three BS_s (BS_1, BS_2, BS_3). In the following, we discuss the impact of the nearest neighbor number K , the chosen metric δ -nearest neighbor, the heterogeneous fingerprints, and the database resolution. In all KNN tests, we consider the Euclidean distance defined in Table (3.7) to denote neighbors of the fingerprint at hand.

3.4.2.1 Impact of nearest neighbor number K

It is obvious that $K = 1$ is an easy choice of the critical parameter K of the nearest neighbor technique, called also the closest neighbor (CN). Obtained results are shown in Table (3.8). For

different lengths of the fingerprints in our database, the 1-NN proves its good performance, in particular, for the triplet fingerprints (RSS_1, RSS_2, RSS_3), 1-KK attains 57.16 % within 25 cm distance error, and 87.68 % within 1 m distance error. However, the worst performance, 16.33 % within 1 m distance error, is obtained from the fingerprints of BS_3 . Upon analysis of these RSS_3 fingerprints, we noticed slight differences between them, due to the uniform coverage of RSS over all the test-bed when BS_3 is active.

Table 3.8: The performance of KNN technique using Euclidean distance metric and ($K = 1$).

Accuracy	RSS_1	RSS_2	RSS_3	RSS_{12}	RSS_{13}	RSS_{23}	RSS_{123}
$Acc \leq 25\text{ cm}$	6.12 %	4.82 %	4.58 %	30.41 %	28.16 %	29.88 %	57.16 %
$Acc \leq 50\text{ cm}$	10.14 %	8.34 %	7.81 %	41.85 %	42.59 %	41.64 %	71.56 %
$Acc \leq 75\text{ cm}$	15.8 %	14.36 %	12.57 %	52.41 %	55.16 %	53.22 %	81.91 %
$Acc \leq 1\text{ m}$	21.72 %	19.18 %	16.33 %	59.52 %	65.26 %	61.77 %	87.68 %

For $K = 3$, the experimental results are presented in Table (3.9). Due to the high fingerprint density in our database, the results obtained for $K = 1$ and $K = 3$ are too close. For lower fingerprint density, the better performance has been achieved for $K > 1$.

Fig. (3.14)(a) and (b) depict the illustration of the performance of KNN for $K = 1$ and $K = 3$ respectively.

Table 3.9: The performance of KNN technique using Euclidean distance metric and ($K = 3$).

Accuracy	RSS_1	RSS_2	RSS_3	RSS_{12}	RSS_{13}	RSS_{23}	RSS_{123}
$Acc \leq 25\text{ cm}$	1.94 %	1.16 %	0.67 %	20.49 %	17.74 %	19.25 %	44.63 %
$Acc \leq 50\text{ cm}$	6.62 %	4.61 %	3.03 %	38.01 %	37.56 %	37.91 %	71.35 %
$Acc \leq 75\text{ cm}$	11.83 %	8.59 %	6.09 %	49.95 %	53.71 %	50.65 %	82.75 %
$Acc \leq 1\text{ m}$	18.09 %	13.23 %	9.86 %	58.68 %	65.75 %	61 %	89.41 %

3.4.2.2 Impact of the chosen metric: δ -nearest neighbor (δ -NN)

In this experiment, we denote by δ_{RSS} the rayon of the circle whose center is the fingerprint at hand RSS. δ_{RSS} is a percentage of a fingerprint value, for example $\delta_{RSS} = 3$ represents 3 % of the actual fingerprint value RSS. δ -nearest neighbor is every fingerprint situated within this circle. However, δ_{RSS} heavily depends on the fingerprint density. In the worst case, whereas no neighbors are found in the δ_{RSS} -circle, the mobile terminal is not localizable.

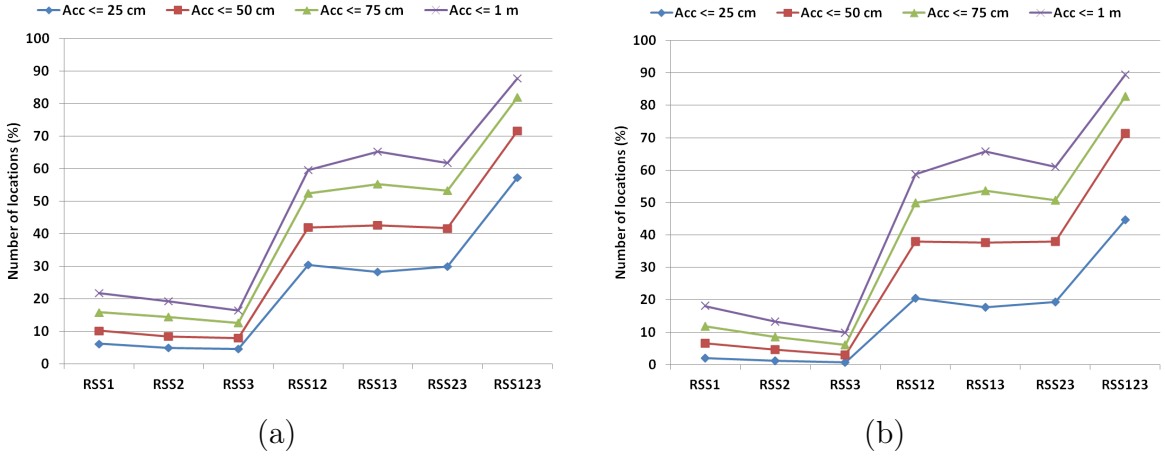


Figure 3.14: Illustration of the performance of KNN using Euclidean distance metric: (a) $K = 1$ and (b) $K = 3$.

The obtained results for $\delta_{RSS} = 3$ and $\delta_{RSS} = 10$ are presented in Tables (3.10) and (3.11) respectively. From these results, one can notice that smaller δ_{RSS} values imply better performance, because only close fingerprints participate in the location process. Fig (3.15(a) and (b)) illustrate the performance of δ -NN for $\delta_{RSS} = 3$ and $\delta_{RSS} = 10$ respectively.

Table 3.10: The performance of δ NN technique using $\delta_{RSS} = 3\%$ Euclidean metric.

Accuracy	RSS_1	RSS_2	RSS_3	RSS_{12}	RSS_{13}	RSS_{23}	RSS_{123}
$Acc \leq 25\text{ cm}$	0.92 %	0.74 %	0.42 %	7.99 %	7.95 %	8.98 %	20.73 %
$Acc \leq 50\text{ cm}$	4.29 %	2.18 %	1.34 %	22 %	23.83 %	24.01 %	51 %
$Acc \leq 75\text{ cm}$	10.38 %	5.56 %	2.96 %	36.25 %	42.1 %	39.85 %	73.64 %
$Acc \leq 1\text{ m}$	16.83 %	9.68 %	6.16 %	47.03 %	57.51 %	52.69 %	85.04 %

Table 3.11: The performance of δ NN technique using $\delta_{RSS} = 10\%$ Euclidean metric.

Accuracy	RSS_1	RSS_2	RSS_3	RSS_{12}	RSS_{13}	RSS_{23}	RSS_{123}
$Acc \leq 25\text{ cm}$	1.44 %	0.53 %	0.42 %	3.24 %	3.48 %	4.82 %	8.38 %
$Acc \leq 50\text{ cm}$	4.12 %	1.9 %	1.3 %	11.44 %	12.53 %	14.33 %	26.43 %
$Acc \leq 75\text{ cm}$	9.19 %	4.68 %	2.96 %	21.93 %	25.94 %	25.98	45.23 %
$Acc \leq 1\text{ m}$	15.95 %	8.76 %	5.95 %	33.37 %	41.43 %	37.63	62.48 %

3.4.2.3 Impact of heterogeneous fingerprints

As seen in (3.4.2.3), we use the available information RSS and RTT to form one heterogeneous fingerprint. For each active base station, a couple of information (RSS_i, RTT_i) $i \in \{1, 2, 3\}$

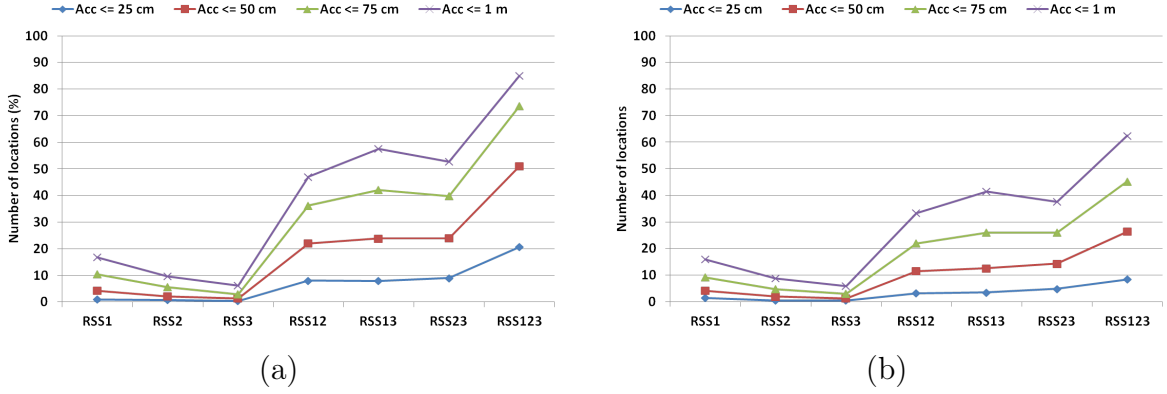


Figure 3.15: Illustration of the performance of δNN : (a) $\delta_{RSS} = 3\%$ and (b) $\delta_{RSS} = 10\%$.

represents a fingerprint. Experimental results in Table (3.12) show the best performance for the heterogeneous fingerprint database. Within 1 m distance error, the performance attains 95 % (see Fig (3.16)).

Table 3.12: The performance of KNN technique using RSS and RTT measurements, Euclidean distance metric, and ($K = 1$).

Accuracy	$RSS_1 RTT_1$	$RSS_2 RTT_2$	$RSS_3 RTT_3$	$RSS_{12} RTT_{12}$	$RSS_{13} RTT_{13}$	$RSS_{23} RTT_{23}$	$RSS_{123} RTT_{123}$
$Acc \leq 25 cm$	16.26 %	20.49 %	17.18 %	58.04 %	56.42 %	55.76 %	76.24 %
$Acc \leq 50 cm$	22.81 %	28.05 %	23.86 %	70.22 %	68.85 %	66.81 %	87.05 %
$Acc \leq 75 cm$	31.33 %	35.52 %	31.01 %	80.22 %	79.27 %	76.7 %	92.57 %
$Acc \leq 1 m$	37.52 %	41.68 %	36.54 %	84.79 %	84.62 %	82.61 %	94.9 %

3.4.2.4 Impact of fingerprint database resolution

To this end, the impact of KNN variants has been studied using the same fingerprint database with 2448 samples (resolution of $25 cm^2$). To complete our comparative study, we have to test the database resolution effect.

To show the impact of the database resolution, another fingerprint database with 153 samples (resolution of $1 m^2$) was built. The experiments have been made by applying KNN technique with $K = 3$, using homogeneous fingerprints (RSS_1, RSS_2, RSS_3). Fig (3.17) illustrates the obtained results and proves the superiority of large-sized fingerprint databases. A clear observation is the significant improvement to the performance of KNN technique.

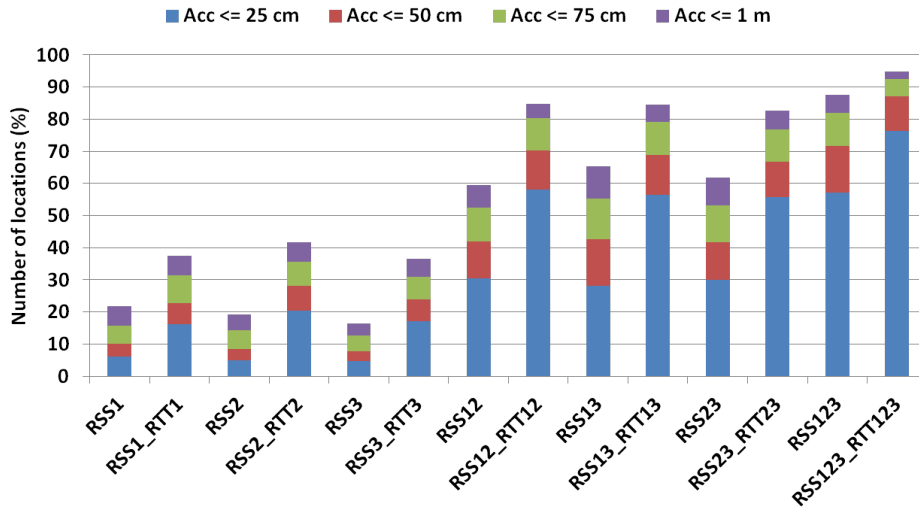


Figure 3.16: Illustration of the performance of KNN using heterogeneous (RSS, RTT) fingerprints and $K = 1$.

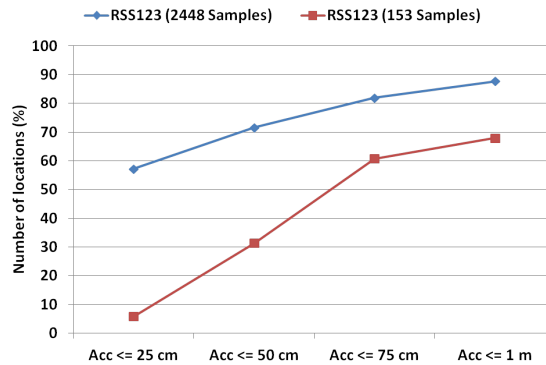


Figure 3.17: Illustration of the KNN performance with $K = 3$, using different database resolutions (2448 samples with resolution of 25 cm^2 , and 153 samples with resolution of 1 m^2).

3.5 ANN vs KNN: comparison and discussion

As we have seen previously, the performance of any fingerprint-based indoor positioning technique heavily depends on the chosen test-bed, the database characteristics, and the different variants of each technique. For ANN and KNN presented in this comparative study, the obtained results proved their capability and efficiency to locate a MT in an indoor environment with satisfactory accuracy (according to the application). To evaluate, objectively, which technique is better, we have to compare the best performance of ANN technique with the corresponding KNN performance using the same fingerprint database, in terms of homogeneous or heterogeneous fingerprints and database resolution. Fig. (3.18) illustrates this comparison.

Both ANN and KNN indoor positioning techniques proved their performance and robustness

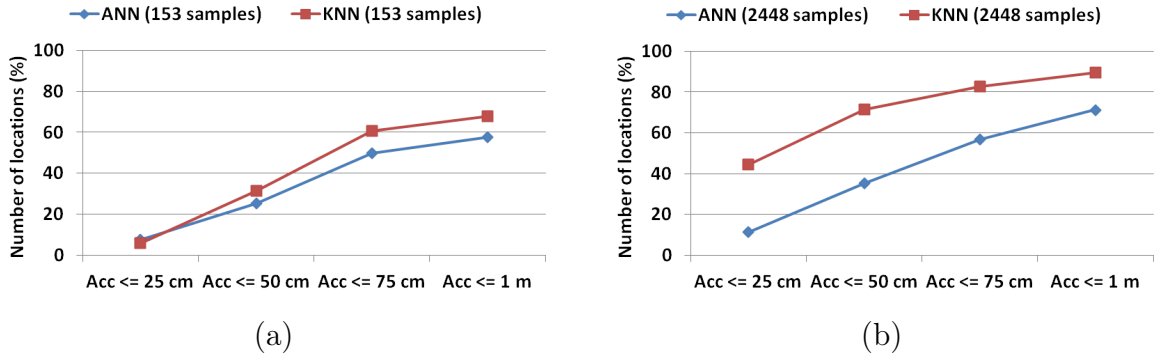


Figure 3.18: ANN and KNN best performance comparison: (a) Homogeneous fingerprint database with 1 m² resolution and (b) Homogeneous fingerprint database with 25 cm² resolution.

for indoor location process. From the obtained results, KNN positioning technique proves its superiority and robustness for higher fingerprint database resolution. As shown in Fig. (3.18)(a), no significant difference between ANN and KNN technique for low resolution fingerprint database was observed. However, KNN technique outperforms ANN technique for high resolution fingerprint database (see (3.18)(b)). To this end, the construction of the fingerprint database has a major impact in the behavior of fingerprint-based indoor positioning systems, and remains a key issue.

Finally, the complexity of the KNN-based algorithm restricts to compute the distance from the target fingerprint to every other fingerprint in the database. This algorithm has a running time of $O(N \times D)$, where N is the cardinality of fingerprint samples and D is the search space dimension. Since the search space dimension is equal to the fingerprint dimension (6 in the case of three BSs: 3 RSS values and 3 RTT values in extreme cases), the KNN algorithm has no complexity beyond the storage of the database. However, for MLP networks, the computational complexity will be increased drastically by increasing the number of hidden neurons. The MLP has complexity $O(M^2)$, where M is the greatest number of nodes in the hidden layers.

3.6 Conclusion

In this chapter, two range-free techniques for indoor location (ANN and KNN) were presented. Experimental results for homogeneous and heterogeneous fingerprints showed the good performance of those techniques. Nevertheless, KNN deterministic method overcomes the ANN learning technique for most cases. Algorithms based on nearest neighbors, that calculate location estimation based on RSS fingerprint observation vector, offer greater efficiency in terms of accuracy versus computational cost. In addition to its simplicity and effectiveness, KNN tech-

nique offers significant performance enhancement in highly variable environments and proves to increase location accuracy [Dakk 12a].

Using the infrastructure that is already installed in the indoor environment and without any extra requirements made these methods favorable. Although their performance is not as good as our coordinate clustering method, presented in the previous chapter, these techniques prove their superiority when presented with a lack of information in blind or dead zone.

In the next chapter, we discuss the dynamic location (tracking) systems. The mobile terminal is supposed to be in movement, and this movement is modeled by linear dynamic system laws. Lack of information or even its absence is problematic to determine the location of the mobile terminal accurately. However, the history of the mobile terminal trajectory could be useful to predict the next location.

MOBILE TRACKING BASED ON FRACTIONAL INTEGRATION

4.1 Introduction

Static indoor location of a mobile terminal (MT) has been intensively studied during the last decade and several applications were developed in the research community to localize MT. All the applications show the need of a technical solution for accurate wireless geolocation [Dakk 11a; Khan 11; Khan 10; Fisc 10; Ebli 10; Bria 10]. The integration of the physical location of a mobile terminal (MT) with the user contexts forms a useful information for many commercial applications [Abhi 07; Mike 04]. Indeed, application of tracking systems (TSs) is a substantial basis for individual navigation, social networking, asset management, traffic management, or mobile resource management, etc. Indoor positioning systems need the current measurements to locate a stationary mobile terminal. These measurements often suffer from several noise types, such as the ambient noise, equipment sensibility, interferences, etc. However, mobile location tracking systems depend not only on the current measurements, but also on the history of the MT trajectory, and the MT movement characteristics. While the Global Positioning System (GPS) works quite well outside of buildings and in urban canyons, locating an indoor mobile terminal in a real-world environment is much more problematic; therefore, the prediction problem remains an essential obstacle to construct reliable indoor TSs. Particularly, in lack of information cases, the prediction step is unavoidable. Different approaches were proposed in the literature to improve the location estimate or to predict the next position in the case of noisy measurements or even in its absence. The most used is that based on prediction filters, such as linear filters (LF), Kalman filters (KF), and particle filters (PF).

In this chapter, we propose to use the properties of digital fractional integration (DFI) to enhance the performance of the classical predictors (linear predictors and Kalman filters). Here, we focus on the dynamic indoor location of a mobile terminal (MT) or mobile terminal tracking. To illustrate the obtained results, two indoor trajectory scenarios inspired from real daily promenades are simulated (museum visit and hospital doctor walk), and to confirm the robustness of our method, two other scenarios, spiral and sinusoidal trajectories, are simulated.

Experimental results show a significant improvement of the performance of the classical predictors, particularly in noisy cases. Then, we propose to apply the short-archive principle to reduce the influence of the accumulated rounding error during long-time tracking. As a result, the goal of this work is to present a new method that allows classical predictors (with/without short-archive principle) to solve the tracking problem efficiently, especially, under noisy conditions. A mathematical proof and intensive study of short-archive principle using 5, 10, and 15 previous estimates, prove the superiority of DFI predictors using only last few locations of MT [Dakk 12c].

In the following paragraph, the digital fractional differentiation/integration (DFD/DFI) notion and its properties will be presented. Then we will mention in detail our contribution to enhance the performance of conventional predictors in the indoor location tracking process.

4.2 Digital fractional integration: characteristics and applications

The fractional integration (or differentiation) dates back to the exchange of letters between Leibniz and l'Hopital in 1695 [Oldh 74]: in a letter dated on September 30th, 1695 L'Hopital wrote to Leibniz asking him about a particular notation he had used in his publications for the n^{th} -derivative of the linear function $f(x) = x$, $D^n x / D x^n$. L'Hopital posed to Leibniz the question: what would be the result if $n = 1/2$? The answer from Leibniz was: "An apparent paradox, from which one day useful consequences will be drawn". By these words the fractional differentiation was born. A remarkable merit of fractional differentiation operators is that they may still be applied to functions that are not differentiable in the classical sense. Unlike the integer order derivative, the fractional order derivative at point x is not determined by an arbitrary small neighborhood of x . In other words, the fractional derivative is not a local property of the function. There are several well-known approaches to unification of differentiation and integration notions, and their extension to non-integer orders [Prod 02]. A general survey on the different approaches is given in [Mill 93].

The theory of fractional derivatives was primarily developed as a theoretical field of mathematics. More recently, fractional integration has found applications in various areas: in control theory it is used to determinate a robust command control [Oust 96]; it is also used to solve the inverse heat conduction problem [Batt 01]; other applications are reported for instance in neuronal modeling [Ramu 02], in image processing for edge detection [Math 03], and in biomedical

signal processing [Ferd 00].

4.2.1 Fractional integration

We consider a fractional integral operator that has the function $y(t)$ as output and $x(t)$ as the input function. Then, the equation defining this operator is :

$$y(t) = J^\alpha x(t) \tag{4.2.1}$$

where J is the fractional integration operator and α is the fractional integration order. α can be integer, real or complex number. In the case of fractional integration, the real part of α is negative.

We denote the α^{th} integral operator by J^α .

In this chapter, we consider one of the numerous definitions of the operator in (4.2.1) proposed by Riemann-Liouville for fractional differentiation, it is defined by the formula:

$$J^\alpha x(t) = \frac{1}{\Gamma(\alpha)} \int_c^t (t - \xi)^{\alpha-1} x(\xi) d\xi \tag{4.2.2}$$

where: $x(t)$ is a real function, $x > 0$, $Re(\alpha) > 0$, c the integral reference and Γ the Euler-gamma function. Whereas the fractional differentiation D^α (the left sided fractional integration or the inverse operation) can be computed by:

$$J^\alpha(D^\alpha f(t)) = f(t) \tag{4.2.3}$$

where, $J^\alpha = D^{-\alpha}$, which generalized an analogous property of integer derivatives and integrals.

The discrete operator \hat{J} of fractional integration of order α proposed by Grünwald is given by:

$$\hat{J}^\alpha x(n) = \frac{1}{h^\alpha} \sum_{k=0}^N \omega_k^{(\alpha)} x(n - kh) \tag{4.2.4}$$

where h is the sampling step (the smaller the sampling step h is, the better the approximation is), n is an integer and indicates the index of the current sample, N is the total number of samples and $\omega_k^{(\alpha)}$ are the binomial coefficients. For implementing the fractional integration

method devoted to the computation of fractional integrals, it is necessary to compute these coefficients and one of the possible approaches is to use the recurrence relationships defined by the following recurrent relation:

$$\begin{cases} \omega_0^{(\alpha)} = 1 \\ \omega_{k+1}^{(\alpha)} = \frac{(k+1)+\alpha-1}{(k+1)}\omega_k^{(\alpha)}, \quad k = 0, 1, 2, \dots, N-1 \end{cases} \quad (4.2.5)$$

This approach is suitable for a fixed value of α . It allows the creation of an array of coefficients, which can be used for fractional differentiation of various functions, and other similar repeated operations. However, for some problems (e.g. in system identification), the most appropriate value of α , must be found; this means that various values of α are considered, and for each particular value of α the coefficients $\omega_{k+1}^{(\alpha)}$ must be computed separately. In such a case, the recurrence relationships (4.2.5) are not very suitable. Instead, the fast Fourier transform method [Henr 78] can be used [Mill 93].

From the expression (4.2.3), the function $y(n) = \hat{J}^\alpha x(n)$ is the output function of a discrete fractional filter, where $x(n)$ is the input function (as said before). The equation (4.2.4) may be implemented taking advantage of the recurrent relation (4.2.5) which avoids explicit computation of coefficients $\omega_{k+1}^{(\alpha)}$ and their storage in memory. This system only includes one parameter, the order of differentiation α , and this is a solid argument in favor of the use of this discrete system for mobile tracking.

A positive real part for fractional integration of order α is chosen for (4.2.4), so the fractional integral (4.2.2) can be computed. Definition (4.2.4) shows that the fractional integral of a function takes into account the past of the function $x(n)$. For more details about the definition of the fractional integration, we suggest to the reader to see [Oldh 74; Prod 02]. The computation of the α^{th} integral at all points of the interval $[a, b]$ produces $N+1$ formulas, that can be written in the following matrix form:

$$\begin{bmatrix} J^\alpha x(n_0) \\ J^\alpha x(n_1) \\ \vdots \\ J^\alpha x(n_{N-1}) \\ J^\alpha x(n_N) \end{bmatrix} = \frac{1}{h^\alpha} \begin{bmatrix} w_0^{(\alpha)} & 0 & 0 & \dots & 0 \\ w_1^{(\alpha)} & w_0^{(\alpha)} & 0 & \dots & 0 \\ \vdots & \ddots & \ddots & \dots & \vdots \\ w_{N-1}^{(\alpha)} & \ddots & w_1^{(\alpha)} & w_0^{(\alpha)} & 0 \\ w_N^{(\alpha)} & w_{N-1}^{(\alpha)} & \ddots & w_1^{(\alpha)} & w_0^{(\alpha)} \end{bmatrix} \begin{bmatrix} x(0) \\ x(1) \\ \vdots \\ x(N-1) \\ x(N) \end{bmatrix} \quad (4.2.6)$$

4.2.2 Properties of the fractionally integrated trajectory

In this section, the properties of the fractionally integrated path are studied. We start by the geometric properties, in terms of regularity, thereafter the statistical properties are presented.

4.2.2.1 Regularity

To illustrate the modifications on regularity at the application of the fractional integration on a positive function with negative or positive order α , a non-negative and causal function (f) is considered. We consider an example of a museum visit path (Fig. (4.1)(a)), where the different coordinates are positive. As the path is a two dimensional function, we decided to treat every dimension separately (two separated functions): the X coordinates function called $X(n)$ and the Y coordinates function, called $Y(n)$.

Then, the DFI is applied to each function separately. The whole result of applying the digital fractional integration (DFI) to the considered path with $\alpha = 0.5$ is presented in Fig. (4.1)(b). Now let us see what happens when we integrate fractionally the different coordinates. We take for example the $X(n)$ function and we integrate it with different orders: 0.1, 0.3, and 0.5. The corresponding results are presented in Fig. (4.2)(b), (c), and (d), respectively.

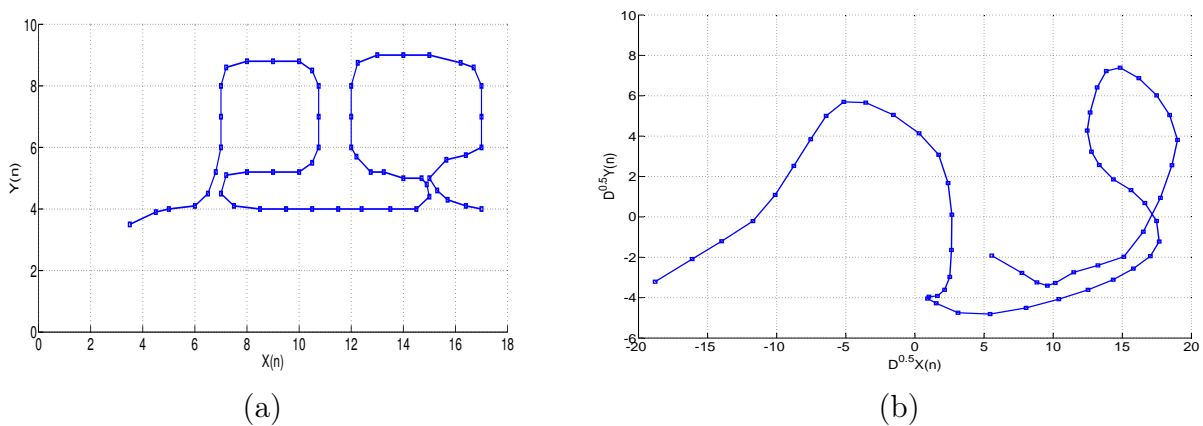


Figure 4.1: Illustration of the application of the DFI to a path. (a): original museum visit path, (b) DFI of the museum path with $\alpha = -0.5$. Where, n is the number of samples and the distance between the points is expressed in meter.

The application of the fractional integration provides a compressed path, where the amplitude range is decreasing with the increase of α positive. On the contrary, it can be derived from the property of the differentiated path given in expression (4.2.4) that, when α is negative, the amplitude range of the integrated function increases. This property can be explained by the frequency properties of the fractional differentiation filter.

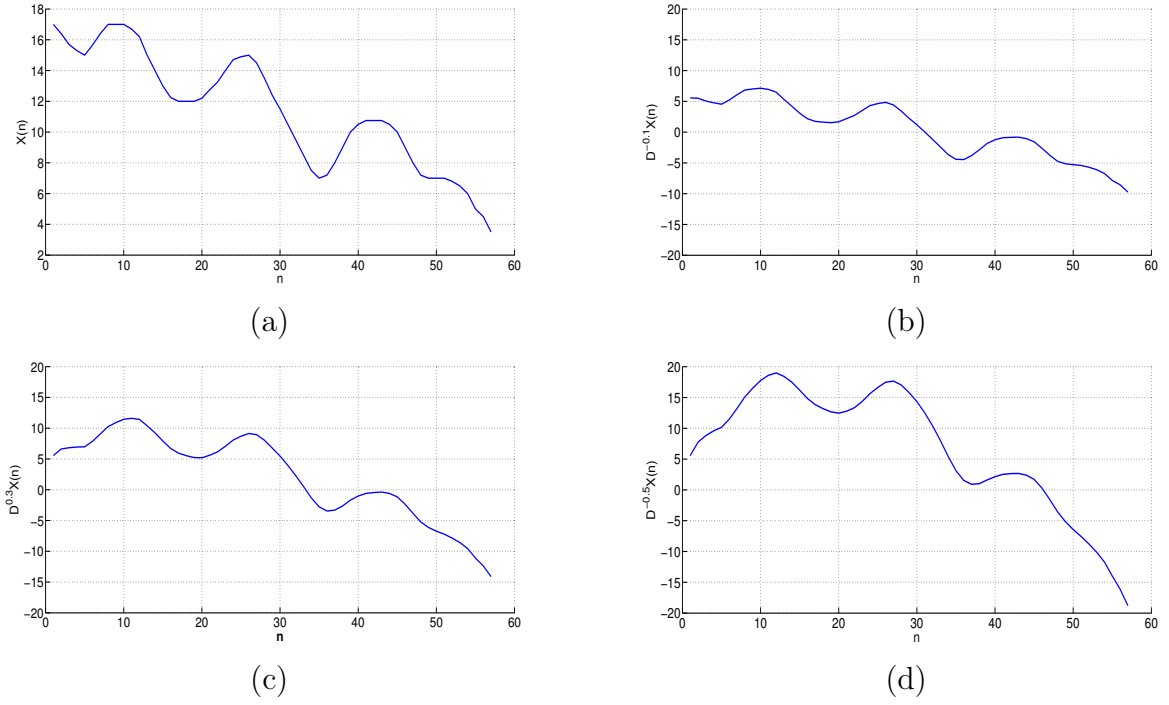


Figure 4.2: Illustration of the application of the DFI to X coordinates of the museum path. (a): original X coordinates $X(n)$, (b) DFI of $X(n)$ path with $\alpha = 0.1$, (c) DFI of $X(n)$ path with $\alpha = 0.3$, (d) DFI of $X(n)$ path with $\alpha = 0.5$. Where, n is the number of the samples and the distance between the points is expressed in meter.

4.2.2.2 Statistical analysis of the fractionally integrated path

In this subsection, we propose to see the statistical effect of the application of the fractional integration on a given path. The interpretation of the application of DFI to a one dimensional coordinate path is given as an example for illustration. We were interested by two statistical properties of the integrated function: average value and autocorrelation function. To do so, we introduced a path and we fractionally integrated it with different integration orders in the interval $[0, 1]$.

4.2.2.2.a Average value of the differentiated function

The Z - transform function of the discrete filter given in (4.2.4) can be written as:

$$H(z) = \frac{G(z)}{F(z)} = (1 - z^{-1})^\alpha \quad (4.2.7)$$

From (4.2.7), we can easily show that the average value of the output path, i.e. the integrated function, is given by:

$$\mu_g = H(0) \times \mu_f \quad (4.2.8)$$

where μ_f is the average value of the function f . The value of μ_g is infinite when the DFI order is positive. Then, in order to keep constant the average value of the path, the original trajectory is centered before applying the DFI.

4.2.2.2.b Autocorrelation

The cross-correlation expression of two functions (signals) is given by:

$$R_{xy}(m) = E \{f(n+m) g(n)\} = E \{f(n) g(n-m)\} \quad (4.2.9)$$

where $E \{\cdot\}$ is expected value operator.

Autocorrelation corresponds to the special case $f(n) = g(n)$, $-\infty < n < +\infty$

$$R_{xx}(m) = E \{f(n+m) \cdot f(n)\} \quad (4.2.10)$$

The estimation of the raw autocorrelations is given by:

$$\hat{R}_{xx}(m) = \begin{cases} \sum_{n=0}^{N-m-1} f(n+m) \cdot f(n) & m \geq 0 \\ \hat{R}_{xx}(-m) & m < 0 \end{cases} \quad (4.2.11)$$

where N is the length of the sequence f and m is the lag: $m = 0, 1, \dots, N-1$

In the case of zero mean white noise signal, the normalized autocorrelation coefficient of the differentiated function is given by:

$$\rho(m) = \frac{R_{xx}(m)}{R_{xx}(0)} = \frac{\Gamma(1+n)\Gamma(m-n)}{\Gamma(-n)\Gamma(m+n+1)} \quad (4.2.12)$$

Proposition: *The application to a function of the DFI with a positive order decreases the autocorrelation of a function and consequently reduces the prediction error. The opposite case happens when a DFI with a negative order is applied to this function [Ferd 00; Ferd 11].*

Proof: In order to prove this proposition we consider the case of a linear predictor of order N that we use to predict the position of a MT. We define the predictor at hand by:

$$\hat{X}(k) = \sum_{i=1}^N a_i X(k-i) \quad (4.2.13)$$

where a_i are predictor coefficients, $X(i)$ is the position at the time i of the MT, and $\hat{X}(i)$ is the estimated position.

To predict the position $X(k)$, the predictor uses a linear combination of the N previous positions. The parameters a_i are called the prediction coefficients and $1 \leq i \leq N$.

Then, the prediction error is defined by:

$$e(k) = X(k) - \widehat{X}(k) \quad (4.2.14)$$

The variance of the prediction error $e(k)$ is defined by:

$$\sigma_e^2 = \sum_{i,j=0}^N a_i a_j \Phi_X(i-j) + \sum_{i=1}^N a_i \sigma_X^2 \quad (4.2.15)$$

where $\Phi_X(k)$ is the autocorrelation function of the path $X(k)$. It is obvious that if the original path $X(k)$ is not totally random and the coefficients a_i are correctly chosen, the variance of the error $e(k)$ is lower than that of the original trajectory.

The coefficients a_i minimizing the mean square error $\sigma_e^2 = E \left\{ (X - \widehat{X})^2 \right\}$, are given by the equation system:

$$\frac{\delta \sigma_e^2}{\delta a_i} = \sum_{j=0}^N a_j \Phi_X(i-j) + \sigma_X^2 = 0 \quad (4.2.16)$$

where $i = 1, 2, \dots, N$ and the variance σ_X^2 is unknown at the beginning, because it depends on the prediction error variance σ_e^2 . In practice, this equation system will be solved by successive approximations. Using (4.2.16) in (4.2.15), the minimal value of the residual variance σ_e^2 , denoted by $\sigma_{e,\min}^2$, is given by the following equation:

$$\sigma_{e,\min}^2 = \sigma_X^2 - \sum_{i=1}^N a_i \Phi_X(i) \quad (4.2.17)$$

Then, it is easy to find the following expression (4.2.18):

$$\sigma_{e,\min}^2 = \sigma_X^2 \left[1 - \sum_{i=1}^N a_i \rho_X(i) \right] \quad (4.2.18)$$

where σ_X^2 is the variance of the path $X(n)$ and $\rho_X(i)$ are its autocorrelation coefficients. The ratio of the variances is expressed by the relation:

$$G_X = \frac{\sigma_X^2}{\sigma_{e,\min}^2} = \left[1 - \sum_{i=1}^N a_i \rho_X(i) \right]^{-1} \quad (4.2.19)$$

The prediction gain expresses the achieved variance reduction by linear prediction of order N . Then, to prove that the DFI of the path $X(n)$ is more correlated than the original path, one must prove that the prediction gain $G_{D^\alpha X}$ of DFI of $X(n)$ is greater than G_X . To do so, it

is sufficient to demonstrate that the autocorrelation coefficients of the fractionally integrated path are greater than those of $X(n)$. We define the DFI of $X(n)$ by:

$$D^\alpha X(k) = \sum_{j=0}^N \omega_j^\alpha X(k-j) \quad (4.2.20)$$

and its autocorrelation coefficients by:

$$\rho_{D^\alpha X(k)} = \sum_k D^\alpha X(k) \times D_{k+j}^\alpha X(k+j) \quad (4.2.21)$$

From (4.2.20) it is obvious that:

$$X(k) + \sum_{l=1}^N \omega_l^\alpha X(k-l) \geq X(k) \quad (4.2.22)$$

and for $k+l$:

$$D^\alpha X(k+l) = X(k+l) + \sum_{j=1}^N \omega_j^\alpha X(k+l-j) \geq X(k+l) \quad (4.2.23)$$

From (4.2.22) and (4.2.23), and as $X(k)$ is a positive function, we can write the following relation:

$$D^\alpha X(k) \times D^\alpha X(k+l) \geq X(k) \times X(k+l) \quad (4.2.24)$$

Then,

$$\sum_k D^\alpha X(k) \times D^\alpha X(k+l) \geq \sum_k X(k) \times X(k+l) \quad (4.2.25)$$

Finally, we have:

$$\rho_{D^\alpha X(k)} \geq \rho_{X(k)} \Rightarrow G_{D^\alpha X} \geq G_X \quad (4.2.26)$$

The autocorrelation increase of the differentiated function, with negative order α , in the interval $]-1, 0]$, applied to a zero mean white noise, is illustrated in Fig. (4.3)(a). The increase of the autocorrelation can be seen through the increase of the autocorrelation coefficients values that correspond to the lag values. When the lag is equal to zero, the autocorrelation is equal to 1 and it decreases when the lag increases. However, when α varies from 0 to -1, this decrease is more and more smooth, thus indicating the increase of the dependency between the different samples. Fig. (4.3)(b) illustrates the opposite event, the decrease of the autocorrelation through the application of the DFI, when α varies from 0 to 1.

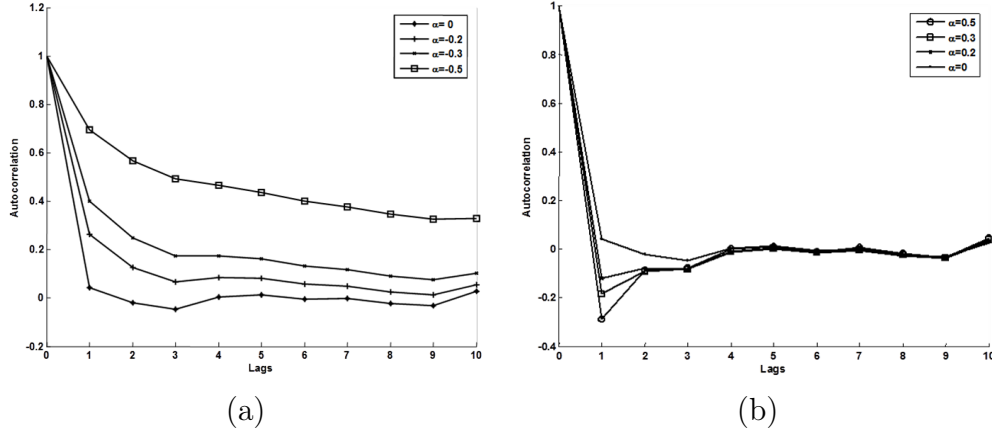


Figure 4.3: Example of application of a DFI to a zero mean white noise signal. (a): Autocorrelation increase with negative DFI order, (b): Autocorrelation decrease with positive DFI order.

4.2.3 The short-memory principle

For the interval $[n_0, n]$, where n_0 is the starting sample and n is the current sample, we can write the fractional integration as ${}_{n_0}J_n^\alpha X(n)$. However, it follows from the definition (4.2.4) that, for large number of samples n , the role of the history of the behavior of the coordinate function $X(n)$ near the starting point n_0 can be neglected under certain assumption. This observation leads us to the formulation of the "short-memory" principle. This principle means taking into account the behavior of $X(n)$ only in the recent few past samples, i.e. in the interval $[n - Hist, n]$, where $Hist$ is the history length. The short-memory principle allows one to accept the approximation expressed in (4.2.27):

$${}_{n_0}J_n^\alpha X(n) \approx {}_{n-Hist}J_n^\alpha X(n), \quad (n > n_0 + Hist) \quad (4.2.27)$$

The short-memory principle (4.2.27) leads to approximate the fractional integral with a fixed starting point by the fractional integral with moving lower limit $n - Hist$. Hence, the number of addends is always less than $[Hist/h]$. The disadvantage of this simplification is that the accuracy may degrade. If $X(n) \leq L$ for $n_0 \leq n \leq N$, then, using (4.2.2), we easily establish the estimate of the error introduced by short-memory principle as follows:

$$\Delta(n) = |{}_{n_0}J_n^\alpha X(n) - {}_{n-Hist}J_n^\alpha X(n)| \leq \frac{L \times Hist^{-\alpha}}{|\Gamma(1 - \alpha)|}, \quad (n_0 + Hist \leq n \leq N) \quad (4.2.28)$$

From (4.2.28) we can limit the acceptable error ϵ ,

$$\Delta(n) \leq \epsilon, \quad (n_0 + Hist \leq n \leq N), \quad (4.2.29)$$

therefore, determining the memory length $Hist$ according to the application required accuracy.

Finally, the short-memory length is determined by the equation (4.2.30):

$$Hist \geq \left(\frac{L}{\varepsilon |\Gamma(1 - \alpha)|} \right)^{\alpha^{-1}} \quad (4.2.30)$$

4.3 Our proposed method

In this section, we present a new method to solve the path prediction problem. The proposed method consists in adding on downstream the digital fractional integration operator to the classical prediction filters. Fig. (4.4) illustrates the principle of the proposed method.

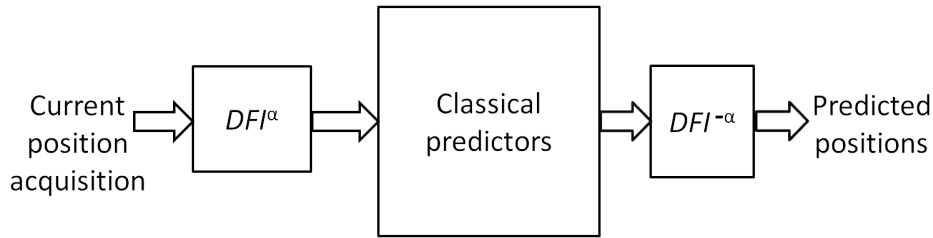


Figure 4.4: The principle of applying DFI to classical prediction filters.

The main idea takes advantage from the properties of the DFI to increase the performance without any complexity. The first step consists in applying the DFI with a positive order ($\alpha > 0$) to the current path, which forms the entry of any classical prediction filter. Reciprocally, we apply the DFI with a negative order ($\alpha < 0$) (that corresponds to digital fractional differentiation) to the output (estimated trajectory), which consists of the predicted locations of the MT. The second idea focuses on the archive size used in applying DFI to both original trajectory and estimated one.

We assume that MT location $P(i)$ is a positive function. Then, locations $P(i) = (X(i), Y(i))$ of a MT are decomposed into two positive coordinates trajectories $X(i)$ and $Y(i)$, where $X(i)$ expresses the abscissa trajectory, and $Y(i)$ is the ordinate one. Hereinafter, we define the differentiation of $X(i)$ ($Y(i)$ can be deduced easily).

Let $X(i) = \{X(1), X(2), \dots, X(N)\}$ be abscissa of the MT discrete trajectory locations. Then, the DFI of this trajectory, for a given negative DFI order $\alpha > 0$, is defined by the formula (4.2.20).

Then, we obtain $D^\alpha X(i) = \{D^\alpha X(1), D^\alpha X(2), \dots, D^\alpha X(N)\}$. Afterwards, we use $D^\alpha X(i)$ as input to a classical prediction filter to estimate the DFI of the future position $D^\alpha \widehat{X}(i)$. Then, to have MT positions, we differentiate with the same order as that used to integrate the predicted

path $D^\alpha \widehat{X}(i)$, then finally, we get the estimated positions of the MT. Similarly, we treat the ordinate trajectory $Y(i)$ to get the location ordinates.

The goal of applying the short-archive is to reduce the number of locations used in the prediction step, at the input as well as at the output, to generate the fractionally differentiated trajectory. That leads in many cases to suppression of the influence of accumulated rounding error during long-time tracking.

Based on the properties of the DFI seen in (4.2.2.2.b), the application to a function of the DFI with a positive order increases the autocorrelation of that function. Fig. (4.5)(b) illustrates the use of a linear prediction filter. One can see the small difference between a DFI path and its prediction (low prediction error). However, the prediction error is significant between the path and its prediction (see Fig. (4.5)(a)). The prediction errors occur between the original trajectory and its estimated one using only LP (linear predictor) of order 3, and the prediction error values with the estimated trajectory using DFI-LP are presented in Fig. (4.5)(c). One can notice that the variance of DFI estimated trajectory is less than the variance of the estimated trajectory using classical predictors only. More analysis and experiments will be presented in the following section.

Thus, instead of the original path, the input of prediction filters is the fractionally differentiated trajectory, therefore the prediction error value decreases (this property can be used in communication). The classical prediction filters, as Kalman filter (KF), and LP, have two main computational steps. The first step consists of the update time, while the second one is the measurement update. Table (4.1) presents these computational steps for KF, PF and LF, while Table (4.2) shows our contribution and the new computational steps of DFI prediction filters.

Table 4.1: Kalman filter, particle filter and linear filter: main computational steps.

Algorithm	KF	PF	LF
Time update	$x = Ax + B_u u$ $P = APA^T + B_{f_t} Q B_{f_t}^T$	$f^i \sim p_f$ $x^i = Ax^i + B_u u + B_f f^i$	$x(i) = \sum_{j=0}^N a_j x(j)$
Measurement update	$K = PC^T(CPC^T + R)^{-1}$ $x = x + K(y - Cx)$ $P = P - KCP$	$\omega^i = \omega^i p_e(y - h(x^i))$	

4.4 Results and discussion

In this section we present the obtained results using the proposed method. In order to provide to the reader a global vision of the advantage of using DFI, we show the results of two different

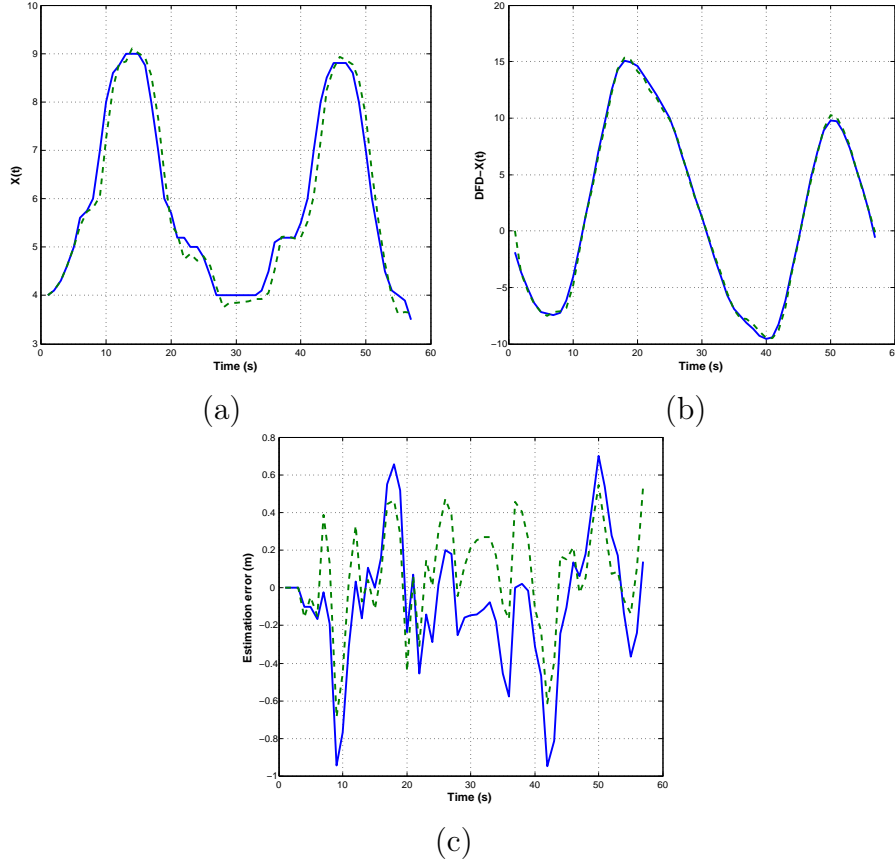


Figure 4.5: Illustration of using LP and DFI-LP on given path, (a): original trajectory (solid line) and its estimation using LP (dashed line), (b): DFI of the path and its estimation with $\alpha = -0.5$, (c): Prediction error values using LP (solid line) and prediction error using DFI-LP (dashed line).

Table 4.2: DFI-KF, DFI-PF and DFI-LF: main computational steps.

Algorithm	DFI-KF	DFI-PF	DFI-LF
Differentiation	$D_i^\alpha x = \sum_{j=0}^N \omega_j^{(\alpha)} x(i-j)$		
Time update	$D_i^\alpha x = AD_i^\alpha x + B_u u$ $P = APA^T + B_{f_t} QB_{f_t}^T$	$f^i \sim p_f$ $D_i^\alpha x^i = AD_i^\alpha x^i + B_u u + B_f f^i$	$D_i^\alpha x = \sum_{j=0}^N a_j D_j^\alpha x(j)$
Measurement update	$K = PC^T(CPC^T + R)^{-1}$ $D_i^\alpha x = D_i^\alpha x + K(y - Cx)$ $P = P - KCP$	$\omega^i = \omega^i p_e(y - h(D_i^\alpha x^i))$	
Integration	$x(i) = J_i^\alpha(D_i^\alpha x)$		

experiments: the goal of the first is to show the provided enhancement of the performance when DFI is used before the predictor. The second experiment concerns the efficiency of DFI

when using small archive (saving few past measurements) to predict the future position of the MT. For all our experiments, we simulated different scenarios in order to have an idea about the behavior of our proposed method in all situations. These scenarios are : two scenarios of indoor trajectories inspired from daily life promenades (museum visit (57 points or positions) and hospital doctor walk (102 points)) (Fig. (4.6) (a) and (b)), and two other scenarios (spiral (58 points) and sinusoidal (45 points)) (Fig. (4.6) (c) and (d)). The performances of the proposed method are compared to those obtained using LP alone and KF alone.

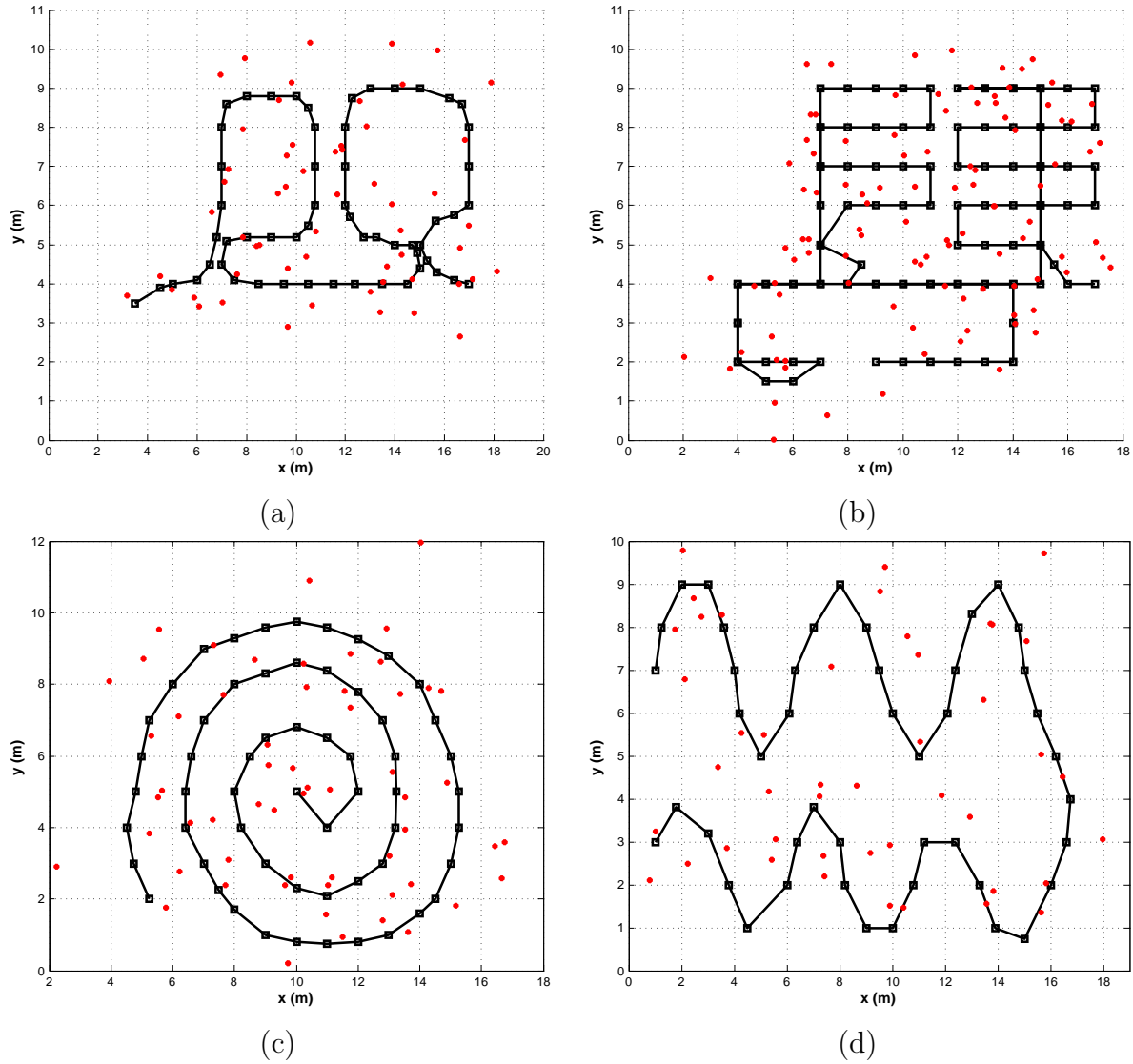


Figure 4.6: Four simulated paths scenarios: MT real trajectories (solid lines) and the observations (dots). Scenarios of daily promenades and noisy measurements, (a): Museum visit, (b): Hospital doctor walk, (c): Spiral trajectory, and (d): Sinusoidal trajectory.

4.4.1 Enhancement of the path prediction using DFI

We did several experimentations (we considered different paths) to show the efficiency of the association of DFI to the other predictors over using classical predictors alone. We distinguished two cases : noiseless and noisy, the noisy case is obtained by adding a Gaussian white noise of variance 2 to the path or to the observation. In Fig. (4.6)(a), (b), (c) and (d) the corresponding noisy paths are depicted using dots. We start by presenting the obtained results on the linear predictor (LP), then those on Kalman filter (KF).

In each future MT location, we exploited the last half observations of the traveled path. In Table (4.3), we summarize the obtained results of applying DFI to the linear predictor (LP). In the column $Acc(m)$ we show the obtained accuracy, in meter, using LP, while α_x column is the best DFI order on the abscissa axis (\overrightarrow{OX}), and α_y column is the best DFI order on the axis \overrightarrow{OY} . The $\Delta Var \%$ column shows the provided enhancement in terms of the variance of the prediction error expressed in percent. The $DFIAcc(m)$ shows the new accuracy when the DFI is used and the "Enhancement" column presents the global enhancement using DFI on the corresponding path. For each path, we presented the two cases: noiseless and noisy. Regarding the noiseless case, it is easy to see that enhancement of the accuracy can reach 57.2 % (in the case of museum path) and for worst case 14.04 %, in the sinusoidal case. This can be explained by the fact that path changes its orientation after four observations. Indeed, the museum and hospital scenarios don't have non derivable points, and the difference is not significant between the variation of the abscissa and the ordinates (see Fig. (4.6)(a) and (c)). While in the noisy case, the DFI allows also to enhance the prediction of the mobile with at least 3.8 %.

Table 4.3: Illustration of the enhancement using DFI in the case of LP. The cases noiseless and noisy measurements are considered.

Scenario		Acc(m)	α_x	α_y	$\Delta Var \%$	DFI Acc(m)	Enhancement %
Museum	Noiseless	0.56	1.02	1.07	72.28	0.29	49.00
	Noisy	1.52	0.01	0.01	20.15	1.38	9.20
Hospital	Noiseless	0.69	1.01	0.01	44.23	0.49	28.85
	Noisy	1.77	0.01	0.01	11.81	1.65	6.71
Spiral	Noiseless	0.65	1.00	0.38	67.74	0.28	57.02
	Noisy	1.77	0.01	0.06	32.92	1.46	17.82
Sinusoidal	Noiseless	0.67	1.02	0.01	21.37	0.58	14.04
	Noisy	1.67	0.01	0.01	0.90	1.60	3.87

In the museum visit scenario, the proposed method achieves an average prediction error of 30 cm, while in the case of the LP alone, it is of 56 cm, thus the enhancement is around 49 %.

Besides, the enhancement in terms of the variance of the prediction error using DFI is 72.28 %. As noisy measurements degrade the accuracy, the performance of the LP decreases drastically: the accuracy becomes 1.52 *m*. Despite that the DFI allows to have an accuracy of 1.38 *m* that corresponds to 9.2 %.

In the other scenarios (hospital and sinusoidal noisy measurements), the accuracy achieved when the DFI is added is better than that achieved by the LP alone. Thus, in all cases, the proposed method has achieved the best performance.

The second predictor used to illustrate the enhancement of the performance is the well known Kalman filter (KF). It is known that the performance of the KF depends on its two parameters: the system covariance (Q) and the observation covariance (R), see (1.3.2) for more details. So, we compare results obtained by applying KF and DFI-KF, to all cited scenarios to predict the MT path (the museum visit, the hospital promenade, the spiral, and the sinusoidal path). Tables (4.4) and (4.5) present the experimental results with varying the parameters of KF ($Q \in \{0.01, 0.1\}$ and $R \in \{5, 10, 100\}$), this choice is arbitrary, one can choose other values. The proposed method achieved at least a good performance in all scenarios with different parameters (Q and R). Fig. (4.7) presents the predicted MT trajectory in the museum visit scenario, using DFI-KF (KF preceded by the DFI) and KF alone. Looking to the Table (4.4) the best enhancement for museum path is around 21 % and it starts from 0.45 % with $R = 5$ and $Q = 0.01$. These results show that the DFI allows to increase performance even of a robust predictor as KF. The same remark can be made about the second case where $Q = 0.1$ (Table (4.5)), where we can notice that, in the test of museum path with $R = 10$ and $Q = 0.1$, the DFI does not allow to enhance the performance because the KF was already optimal. From these experiments, we can say that the obtained results confirm what we expect by increasing the autocorrelation by the DFI. Consequently, the proposed method enhances the performance of the classical predictors for all scenarios. As we said that we increase the autocorrelation, is it possible to reduce the order of the linear predictor? and is it possible to reduce the number of observations in the case of KF to predict the position? In next section, we answer these two questions.

4.4.2 On the decrease of archive size

The use of small archive leads to the use of a lower number of positions that will be taken into account to predict the location of the TM: in our experiments, we took 5, 10, 15, and 25 past points, as shown in Fig. (4.8).

To illustrate the decrease of the archive size to predict the position of a MT path, a performance analysis has been done, using the four simulated scenarios exposed in Fig (4.6). The

Table 4.4: Q and R , impact: Comparison of Kalman filter with DFI-Kalman filter, $Q = 0.01, R \in \{5, 10, 100\}$.

Scenario	R	Acc(m)	α_x	α_y	ΔVar %	DFIAcc(m)	Enhancement %
Museum	5	1.56	1.27	0.30	1.85	1.55	0.45
	10	1.29	0.37	0.56	28.18	1.02	21.03
	100	1.74	1.38	1.50	4.35	1.73	0.83
Hospital	5	1.59	0.64	0.01	3.98	1.56	1.75
	10	1.78	0.59	0.04	3.82	1.75	2.02
	100	2.33	0.83	0.34	14.22	2.20	5.45
Spiral	5	2.47	0.01	0.80	7.97	2.37	4.11
	10	2.79	0.03	1.04	10.75	2.65	5.28
	100	3.51	0.21	1.50	20.50	3.15	10.18
Sinusoidal	5	1.46	0.01	0.87	0.31	1.46	0.46
	10	1.75	0.01	0.97	0.27	1.74	0.43
	100	3.64	0.15	1.47	12.50	3.11	14.52

Table 4.5: Comparison of Kalman filter with DFI-Kalman filter, $Q = 0.1, R \in \{5, 10, 100\}$.

Scenario	R	Acc(m)	α_x	α_y	ΔVar %	DFIAcc(m)	Enhancement %
Museum	5	0.87	0.95	0.01	0.71	0.87	0.80
	10	1.07	0	0	0	1.07	0
	100	2.01	0.28	0.43	17.70	1.79	11.21
Hospital	5	0.99	0.47	0.02	3.12	0.98	1.02
	10	1.18	0.52	0.01	4.34	1.16	1.62
	100	1.87	0.72	0.16	20.26	1.76	5.79
Spiral	5	1.23	0.01	0.28	1.27	1.22	0.72
	10	1.61	0.01	0.38	2.72	1.59	1.51
	100	2.88	0.03	0.85	12.71	2.71	5.98
Sinusoidal	5	0.90	0.01	1.50	0.72	0.89	0.49
	10	1.02	0.01	0.06	0.04	1.02	0.19
	100	1.77	0.02	0.01	0.04	1.74	1.48

obtained results concerning LP and DFI-LP, are presented in Table (4.6). While the comparison to KF is depicted in : Tables (4.7) to (4.10).

4.4.2.1 The linear predictor (LP) case

To compare the proposed predictor (DFI-LP) to the linear predictor (LP), the different responses to noisy and noiseless measurements are presented. In the noisy case: the provided enhancement varies from 0 % in the case of the sinusoidal path with LP order equal to 5 to

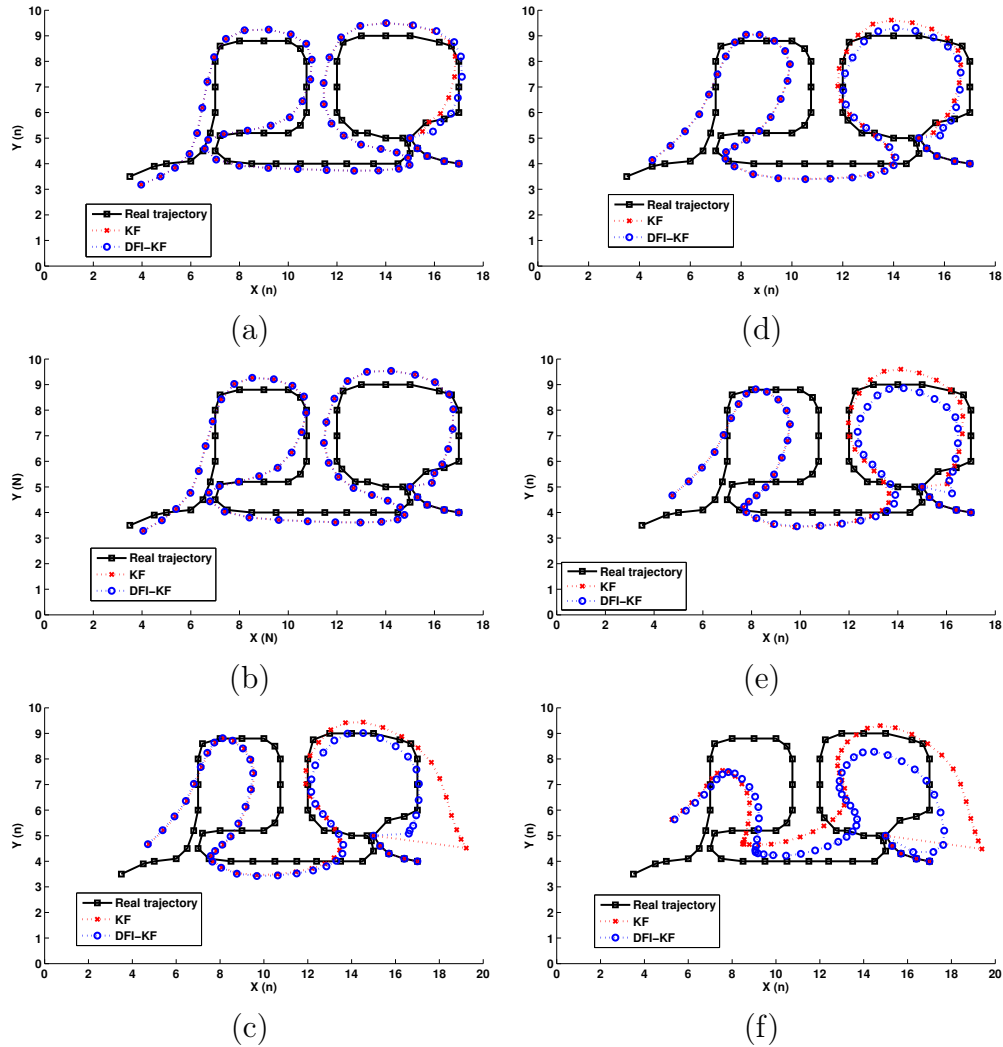


Figure 4.7: Illustration of the performance of KF and DFI-KF predictors for different KF parameters. (a): $Q = 0.01, R = 5$, (b): $Q = 0.01, R = 10$ and (c): $Q = 0.01, R = 100$. (d): $Q = 0.1, R = 5$, (e): $Q = 0.1, R = 10$ and (f): $Q = 0.1, R = 100$.

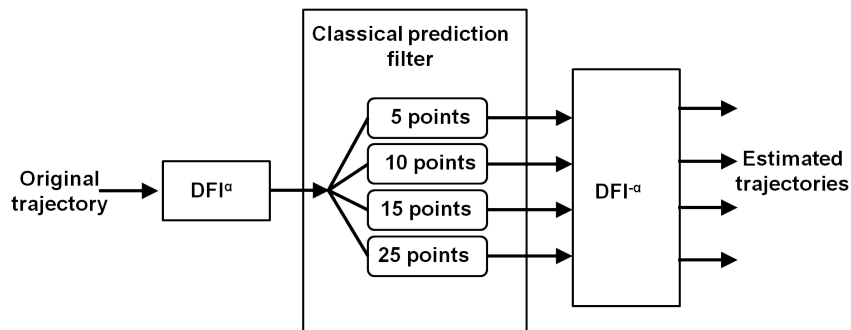


Figure 4.8: Schema of the experimentations using different orders of prediction.

13.26 % in the case of the spiral path with the LP order equal to 25 (Table (4.6)). In the case of the hospital doctor promenade scenario, the best enhancement is when the LP order is equal

to 25: 5.64 %.

In the noiseless case, one can remark that the best performance in the first scenario is obtained for an archive size of 15 where the enhancement is equal to 51.9 %. For the hospital scenario, the best score is 25.87 % and for the spiral scenario it is of 56.28 %, all these scores are obtained with an LP of order 25 (Table (4.6)).

Then, in the case of LP, the addition of DFI allows to have a good enhancement with the decrease of the archive size to predict the position of the mobile. The obtained paths are presented in Fig. (4.9).

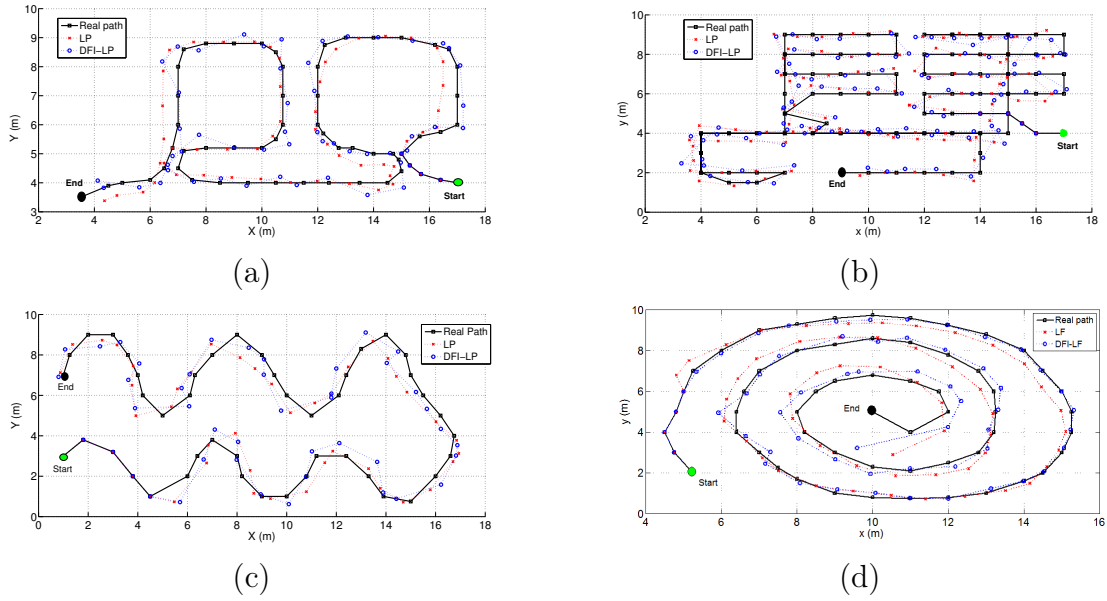


Figure 4.9: Illustration of the performance of the LP of order 25 preceded with DFI. (a) Museum scenario, (b) Hospital scenario, (c) Sinusoidal scenario, (d) Spiral scenario.

4.4.2.2 The Kalman filter case

To confirm the performance of the short archive on a robust predictor, we compare DFI-KF to KF alone by varying the R and Q values. As in previous experiments, we did for $Q \in \{0.1, 0.01\}$, $R \in \{5, 10, 100\}$, and the archive size $m \in \{5, 10, 15\}$. Tables (4.7) to (4.10) depict the obtained results. One can notice that, for $Q = 0.01$ and $m = 5$, the performance increases with the increase of R in most cases. For example, in the museum scenario, the enhancement is 17 %, 24 %, and 36 % for $R = 5$, $R = 10$, and $R = 100$, respectively (see the table (4.7)). The results presented in the tables (4.9) and (4.10), and illustrated in Fig. (4.10), show the usefulness of the DFI before a predictor. To have a more accurate idea about the enhancement of the performance, we present in Fig. (4.10) the different results of the enhancement for the four scenarios. Fig. (4.10)(a), (d), (g) and (j) show pseudo linear dependency between the increase

of the archive and the enhancement. So, the enhancement increases with the decrease of the archive size. Fig. (4.10)(b), (c), (e), (f), (h), (i), (k) and (l) show the prediction error on (\overrightarrow{OX}) axis and \overrightarrow{OY} axis, where the archive size is equal to 5. One can remark that, in all cases, the amplitude of the prediction error in the case of DFI-KF is lower than that in the case of KF alone; this is flagrant in the case of the museum scenario. However, in some cases, the DFI does not provide a significant enhancement, as for example in the case of $Q = 0.1, R = 5$ and $m = 10$.

4.4.3 The short-memory principle

To finish our discussion, the short-memory experiments have been done. The use of short memory length leads to use a lower number of last positions that will be taken into account to calculate the fractional integral of the original path. To prove the efficiency of the short-memory principle, we take only the last 5 positions and compare the obtained results to those obtained by taking all past positions. For Kalman filter, the noise R varies between 5, 10, and 100, while $Q = 0.01$. Our experiments schema is shown in Fig. (4.11) and Table (4.11) summarizes the obtained results and the achieved enhancements. As we have seen in previous experiments, the enhancements increase with greater values of R in most cases. The best enhancement is achieved with 62 % for the spiral scenario and for $R = 100$, while the smallest enhancement is of 6 % for the hospital scenario and $R = 5$. The obtained results show the superiority of the short-memory principle, due to suppression of the influence of accumulating rounding error, during long-time mobile tracking.

4.5 Conclusion

In this chapter, we showed and proved, under some assumptions, that the digital fractional integration allows to increase the autocorrelation of a path. This means to increase the similarity between observations as a function of the time separation between them. Then, we exploited this property in order to track a mobile in an indoor setting. Indeed, we presented the ability of enhancing the prediction of a path of a MT, using classical predictors by using the paradigm of digital fractional integration (DFI). The obtained results for different simulated scenarios, inspired from realistic personal indoor mobility patterns, are very promising, particularly in the noisy environments. The comparison study between the linear predictor and the Kalman filter demonstrates the performance of fractional integrals to enhance the performance of classical predictors. We also found that using DFI allows to reduce the archive size and that the short-memory principle, in many cases, leads to a decrease in the influence of accumulated rounding

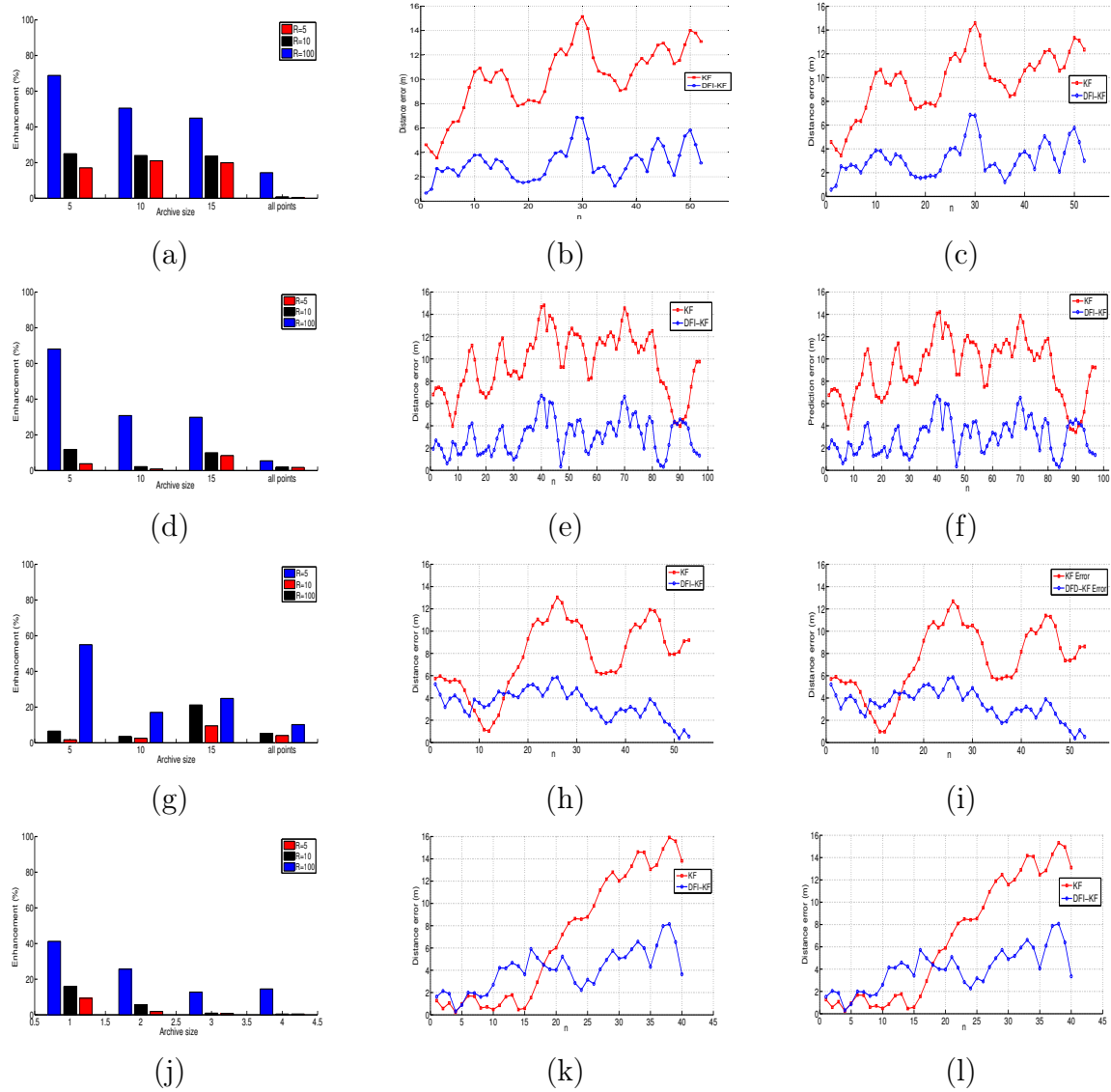


Figure 4.10: Enhancements of the prediction for different scenarios (a): Enhancements for museum scenario, (b) prediction error on (OX) with $Q = 0.01, R = 100$ and $m = 5$, (c) prediction error on (OY) with $Q = 0.1, R = 100$ and $m = 5$ (d): Enhancements for hospital doctor walk, (e) prediction error on (OX) with $Q = 0.01, R = 100$ and $m = 5$, (f) prediction error on OY with $Q = 0.1, R = 100$ and $m = 5$ (g): Enhancements for spiral scenario, (h) prediction error on (OX) with $Q = 0.01, R = 100$ and $m = 5$, (i) prediction error on (OY) with $Q = 0.1, R = 100$ and $m = 5$ and (j): Enhancements for sinusoidal scenario, (k) prediction error on (OX) with $Q = 0.01, R = 100$ and $m = 5$, (l) prediction error on (OY) with $Q = 0.1, R = 100$ and $m = 5$.

error, during long-time tracking. This is due to smaller number of addends. Additionally, the short-memory principle leads to faster algorithms. In works under progress, there is the design of an algorithm to optimize the DFI order and short-memory length as well.

Table 4.6: Archive size reducing. Comparison between LP and DFI-LP using noiseless and noisy measurements, and the archive size ($m \in \{5, 10, 15, 25\}$).

Scenario		m	Acc(m)	α_x	α_y	ΔVar %	DFIAcc(m)	Enhancement %
Museum	Noiseless	5	0.67	1.01	0.96	68	0.36	46.5
		10	0.66	1.02	1.04	72	0.33	50.3
		15	0.65	1.02	1.02	74	0.31	51.9
		25	0.58	0.01	0.01	71	0.3	48.3
	Noisy	5	1.82	0.16	0.03	6.4	1.75	3.5
		10	1.79	0.13	0.01	9.7	1.70	4.8
		15	1.71	0.10	0.01	13.1	1.59	7.3
		25	1.59	0.01	0.01	0.1	1.42	10.7
Hospital	Noiseless	5	0.88	0.28	0.09	38.37	0.63	28
		10	0.82	0.27	0.02	34.66	0.61	25.33
		15	0.81	0.27	0.01	33.68	0.61	24.47
		25	0.79	0.25	0.01	35.29	0.59	25.87
	Noisy	5	2.10	0.01	0.01	3.72	2.07	1.66
		10	2.03	0.01	0.01	7.21	1.97	2.94
		15	2.03	0.01	0.01	6.91	1.96	3.30
		25	1.95	0.01	0.01	10.53	1.84	5.64
Spiral	Noiseless	5	0.69	0.82	0.45	63.09	0.33	52.43
		10	0.65	0.65	0.40	64.07	0.31	52.04
		15	0.66	1.05	0.39	65.04	0.31	52.50
		25	0.65	1.02	0.40	67.48	0.29	56.28
	Noisy	5	2.01	0.01	0.02	11.58	1.86	7.51
		10	1.98	0.01	0.02	18.57	1.73	12.92
		15	1.93	0.01	0.03	21.36	1.69	12.42
		25	1.81	0.01	0.04	27.02	1.57	13.26
Sinusoidal	Noiseless	5	0.75	1.29	0.01	11.57	0.67	10.73
		10	0.73	0.91	0.01	12.34	0.67	9.19
		15	0.71	1.01	0.01	16.68	0.61	13.59
		25	0.67	1.02	0.01	19.44	0.57	14.93
	Noisy	5	1.92	0	0	0	1.92	0
		10	1.78	0.01	0.01	2.87	1.75	1.63
		15	1.77	0.01	0.01	7.39	1.65	6.63
		25	1.64	0.01	0.01	6.45	1.54	6.1

Table 4.7: Archive size reducing. Comparison between KF and DFI-KF, where archive size (m) $\in \{5, 10, 15, all\}$, and $R \in \{5, 10, 100\}$, and $Q = 0.01$.

Scenario	R	m	Acc(m)	α_x	α_y	$\Delta Var \%$	DFIAcc(m)	Enhancement %
Museum	5	5	1.28	0.19	0.01	4.04	1.06	17.09
		10	1.29	0.37	0.56	28.18	1.02	21.03
		15	1.37	0.85	0.01	43.17	1.10	19.94
		all	1.56	1.27	0.30	1.85	1.55	0.45
	10	5	1.94	0.23	0.01	7.70	1.46	24.79
		10	1.63	0.36	0.57	28.93	1.24	23.96
		15	1.65	0.86	0.01	49.21	1.26	23.71
		all	1.74	1.38	1.50	4.35	1.73	0.83
	100	5	10.20	0.54	0.60	66.87	3.18	68.83
		10	4.58	0.35	0.55	38.45	2.27	50.51
		15	3.40	0.92	0.01	60.26	1.88	44.91
		all	2.48	1.50	1.50	24.22	2.13	14.35
Hospital	5	5	1.21	0.04	0.01	0.23	1.16	3.81
		10	1.37	0.07	0.11	0.33	1.35	0.91
		15	1.48	0.62	0.01	21.72	1.36	8.41
		all	1.59	0.64	0.01	3.98	1.56	1.75
	10	5	1.73	0.10	0.01	1.33	1.52	11.79
		10	1.62	0.08	0.08	0.60	1.59	2.19
		15	1.74	0.64	0.01	21.46	1.56	9.98
		all	1.78	0.59	0.04	3.82	1.75	2.02
	100	5	9.64	0.44	0.41	40.70	3.08	68.09
		10	3.74	0.22	0.02	5.56	2.59	30.79
		15	3.14	0.70	0.01	22.75	2.20	29.83
		all	2.33	0.83	0.34	14.22	2.20	5.45

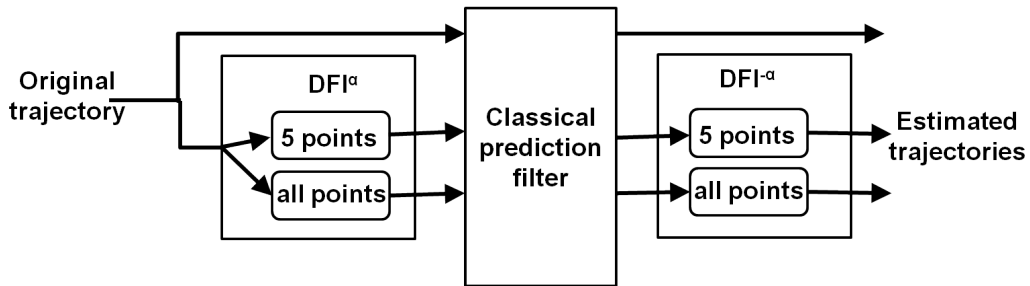


Figure 4.11: Schema of the experimentations using the short-memory principle.

Table 4.8: Archive size reducing. Comparison between KF and DFI-KF, where archive size (m) $\in \{5, 10, 15, all\}$, and $R \in \{5, 10, 100\}$, and $Q = 0.01$.

Scenario	R	m	Acc(m)	α_x	α_y	ΔVar %	DFIAcc(m)	Enhancement %
Spiral	5	5	1.30	0.03	0.02	0.15	1.27	1.71
		10	1.60	0.01	0.53	15.29	1.56	2.55
		15	2.11	0.01	0.61	23.51	1.91	9.55
		all	2.47	0.01	0.80	7.97	2.37	4.11
	10	5	1.91	0.11	0.12	2.31	1.79	6.54
		10	2.00	0.01	0.56	15.86	1.93	3.61
		15	2.60	1.40	0.61	32.13	2.05	21.19
		all	2.79	0.03	1.04	10.75	2.65	5.28
	100	5	7.71	0.53	0.64	53.55	3.47	54.99
		10	4.20	0.14	0.59	13.78	3.48	17.07
		15	4.01	1.36	0.59	41.16	3.01	24.85
		all	3.51	0.21	1.50	20.50	3.15	10.18
Sinusoidal	5	5	1.44	0.16	0.21	6.63	1.31	9.34
		10	1.24	0.04	0.01	0.19	1.21	1.87
		15	1.40	0.01	0.33	3.35	1.38	0.79
		all	1.46	0.01	0.87	0.31	1.46	0.46
	10	5	2.01	0.23	0.15	13.89	1.69	15.90
		10	1.49	0.10	0.01	1.73	1.41	5.69
		15	1.64	0.01	0.31	1.40	1.62	0.92
		all	1.75	0.01	0.97	0.27	1.74	0.43
	100	5	6.91	0.61	0.01	63.79	4.06	41.25
		10	3.89	0.29	0.01	33.25	2.89	25.64
		15	3.15	1.03	0.22	6.85	2.74	12.74
		all	3.64	0.15	1.47	12.50	3.11	14.52

Table 4.9: Archive size reducing. Comparison between KF and DFI-KF, where archive size (m) $\in \{5, 10, 15, all\}$, and $R \in \{5, 10, 100\}$, and $Q = 0.1$.

Scenario	R	m	Acc(m)	α_x	α_y	$\Delta Var \%$	DFIAcc(m)	Enhancement %
Museum	5	5	1.22	0.17	0.01	3.12	1.03	15.60
		10	1.07	0.36	0.56	24.16	0.86	19.38
		15	1.01	0.77	0.01	49.75	0.76	24.61
		all	0.87	0.95	0.01	0.71	0.87	0.80
	10	5	1.85	0.22	0.01	6.67	1.41	23.44
		10	1.44	0.37	0.59	26.86	1.11	23.07
		15	1.33	0.81	0.01	52.95	0.98	26.32
		all	1.07	0.01	0	0	1.07	0
	100	5	9.73	0.52	0.58	64.42	3.14	67.67
		10	4.14	0.35	0.57	37.58	2.15	48.03
		15	3.08	0.92	0.01	61.94	1.75	43.36
		all	2.01	0.28	0.43	17.70	1.79	11.21
Hospital	5	5	1.15	0.03	0.01	0.15	1.12	2.87
		10	1.16	0.01	0.05	0.03	1.16	0.08
		15	1.09	0.33	0.01	4.11	1.06	2.88
		all	0.99	0.47	0.02	3.12	0.98	1.02
	10	5	1.65	0.09	0.01	1.11	1.48	10.50
		10	1.45	0.04	0.02	0.15	1.44	0.90
		15	1.36	0.44	0.01	6.74	1.28	5.94
		all	1.18	0.52	0.01	4.34	1.16	1.62
	100	5	9.11	0.43	0.39	37.43	3.02	66.81
		10	3.39	0.19	0.01	4.69	2.52	25.55
		15	2.78	0.67	0.01	19.26	2.08	25.17
		all	1.87	0.72	0.16	20.26	1.76	5.79

Table 4.10: Archive size reducing. Comparison between KF and DFI-KF, where archive size $(m) \in \{5, 10, 15, all\}$, and $R \in \{5, 10, 100\}$, and $Q = 0.1$.

Scenario	R	m	Acc(m)	α_x	α_y	ΔVar %	DFIAcc(m)	Enhancement %
Spiral	5	5	1.24	0.02	0.01	0.06	1.22	1.14
		10	1.24	0.01	0.48	10.26	1.23	0.66
		15	1.29	0.01	0.45	6.99	1.23	5.25
		all	1.23	0.01	0.28	1.27	1.22	0.72
	10	5	1.83	0.10	0.11	1.85	1.72	5.91
		10	1.69	0.01	0.53	12.65	1.65	2.08
		15	1.77	0.01	0.54	13.39	1.64	7.69
		all	1.61	0.01	0.38	2.72	1.59	1.51
	100	5	7.39	0.52	0.61	50.71	3.45	53.37
		10	3.92	0.10	0.60	13.21	3.41	12.94
		15	3.71	1.36	0.63	33.20	2.95	20.28
		all	2.88	0.03	0.85	12.71	2.71	5.98
Sinusoidal	5	5	1.38	0.15	0.21	5.87	1.27	8.44
		10	1.10	0.01	0.09	0.51	1.09	1.02
		15	1.05	0.01	0.06	0.22	1.05	0.21
		all	0.90	0.01	1.50	0.72	0.89	0.49
	10	5	1.93	0.22	0.15	12.53	1.65	14.92
		10	1.36	0.07	0.02	0.94	1.31	3.75
		15	1.29	0.01	0.10	0.49	1.28	0.40
		all	1.02	0.01	0.06	0.04	1.02	0.19
	100	5	6.70	0.59	0.01	62.45	3.99	40.44
		10	3.55	0.26	0.01	28.44	2.73	23.07
		15	2.77	0.01	0.24	0.20	2.73	1.42
		all	1.77	0.02	0.01	0.04	1.74	1.48

Table 4.11: Short-memory principle. Comparison between KF and DFI-KF, where memory length (ML) $\in \{5, all\}$, and $R \in \{5, 10, 100\}$, and $Q = 0.01$.

Scenario	R	Acc(m)	ML	α_x	α_y	$\Delta Var \%$	DFIAcc(m)	Enhancement %
Museum	5	1.56	5	0.29	0.66	1.82	1.41	10
			all	1.27	0.30	1.85	1.55	0.45
	10	1.74	5	0.28	0.78	2.16	1.5	14
			all	1.38	1.50	4.35	1.73	0.83
	100	2.48	5	0.33	1.2	2.27	1.55	38
			all	1.50	1.50	24.22	2.13	14.35
Hospital	5	1.59	5	0.31	0.45	2.15	1.49	6
			all	0.64	0.01	3.98	1.56	1.75
	10	1.78	5	0.35	0.51	2.54	1.63	8
			all	0.59	0.04	3.82	1.75	2.02
	100	2.33	5	0.44	0.67	3.66	2.06	12
			all	0.83	0.34	14.22	2.20	5.45
Spiral	5	2.47	5	0.35	0.64	1.95	1.57	36
			all	0.01	0.80	7.97	2.37	4.11
	10	2.79	5	0.74	0.75	1.94	1.53	45
			all	0.03	1.04	10.75	2.65	5.28
	100	3.51	5	1.13	1.15	1.49	1.32	62
			all	0.21	1.50	20.50	3.15	10.18
Sinusoidal	5	1.46	5	0.49	0.37	1.37	1.23	16
			all	0.01	0.87	0.31	1.46	0.46
	10	1.75	5	0.58	0.44	1.52	1.31	25
			all	0.01	0.97	0.27	1.74	0.43
	100	3.64	5	0.86	0.62	2.3	1.7	53
			all	0.15	1.47	12.50	3.11	14.52

Conclusion and perspectives

In this thesis, we have presented a new hybrid coordinate clustering approach for indoor geo-location, with TOA and AOA in multipath environment. The used coordinate clustering in this approach helps to restrict the geo-location process, by reducing the number of observations at each coordinate level. As highlighted in chapter 2, too few ray tracings have direct LOS between the base stations and the mobile terminal to be located. Most ray tracings suffer of one or more reflections, due to the existing obstacles in the environment. Besides walls and furniture in the case of $2D$ environments, there are also the floor and the ceiling reflections in the case of $3D$ environments. The proposed method does not need any prior knowledge or prior mitigation technique to correct the error caused by the multipath ray tracings. In most cases, the proposed method proved efficient and the achieved accuracy showed its robustness. However, in real world conditions, many blind or dead zones exist, because most indoor environments are not prepared for geo-location issue. The small number or bad distribution of the base stations, and the continually changing (open/closed doors, prefabricated walls, rearrangement of furniture, and moving people) represent key reasons of performance degradation. The combination of RTT and RSS information could be useful to develop approaches which overcome the limitations in blind or dead zones of indoor environments.

This latter conclusion led us to the comparative study which has been performed in chapter 3. Two range-free techniques, learning ANN and deterministic KNN techniques, proved their performance and robustness for indoor geo-location process. We demonstrated that KNN positioning technique is more robust for higher fingerprint database resolution. Building the fingerprint database in offline phase is costly in terms of time. Continually changing indoor environments implies regular updates of the pre-built database. For ANN technique, many parameters have to be re-adjusted: the network topology, the learning method, the number of hidden layers and the hidden units in each hidden layer, the learning iterations and the transfer functions. Similarly, for KNN technique, parameters are the number of nearest neighbors K , the chosen metric or distance. Optimal parameter adjustment for each technique leads to better performance.

Using the infrastructure that is already installed in the indoor environment without any

extra requirements makes these methods favorable. Although their performance is not as good as our coordinate clustering method presented in chapter 2, these techniques tend to be more effective in case of lack of information or in situations of blind or dead zones.

Locating an indoor moving user in a real-world environment, buildings, or urban canyons is an essential requirement for dynamic tracking applications. However, in lack of critical input information for triangulation calculation, the system needs to rely on a prediction model to improve the accuracy of the positioning task. We showed and proved, under some assumptions, that the digital fractional integration allows to increase the autocorrelation of a path. Then, we exploited this property in order to track a mobile. Indeed, we presented the ability of enhancing the prediction of a path of a MT, using classical predictors, by using the paradigm of digital fractional integration (DFI). We also found that using the DFI allows to reduce the archive size and the short-memory principle. This leads, in many cases, to decrease the influence of accumulated rounding error during long-time tracking, due to smaller number of addends. Besides, the short-memory principle leads to faster algorithms.

Our experiments have been done using simulated environments produced by Radiowave Propagation Simulator software [GmbH 08]. However, our experimental results should be confirmed in a real indoor environment. In order to do this, we have started to develop a client/server application on iPhone/Macintosh platform using (Objective C) as programming language and Postgres as SQL database engine. The student library of the University Paris-Est Créteil (UPEC) has been chosen as our test-bed, in which our experiments would be performed. This library has two floors of $36 \times 22 m^2$. The first floor is equipped with 7 access points, while the second floor has 6 access points. Spiral stairs link the first floor to the second one.

So far, the performed tasks for this client/server application are:

- **Offline phase:** fingerprints have been collected using NetStumbler software in 14 different locations over all the second floor. Then, we completed the fingerprint database using a path loss model (see equation (1.2.5)).
- **Online phase:** the client-side module (iPhone) has been developed. The connection between the client-side module and the server-side module has been performed via WALN. In executing the client-side module, and once the connection to the server is performed, the library map has to be downloaded from the server-side module and displayed on the client-side module. Manual tests have been done to locate the mobile terminal (iPhone) using KNN technique with K-nearest neighbors as a parameter.

In perspective, completing this promising client/server application and developing an Android-compatible version are real challenges.

In certain conditions, it is not possible to geo-position all the mobile terminals active in the test-bed, so the location of certain terminals must be calculated using estimates of their distances to neighboring ones whose position is known. In a recent research work [Dakk 12b] we proposed to use the dependence of associated errors of inaccurate distances between unknown terminal positions and well-known terminal positions. This would allow the system to correct the imprecise measured distances to be more accurate. Then, we can use the corrected distances in the process of positioning the target mobile terminals. The main step is to define Cayley-Menger determinant, which describes the geometric relations of relative distances between well-known and unknown terminal positions. Further, to estimate the error, we will use an optimization algorithm as particle swarm optimization (PSO). A possible future work is too to experiment with other metaheuristics, and to introduce a dynamic optimization for mobile tracking in closed environments.

Each of the presented approaches in this thesis depends on one or more parameters. We have achieved good performances when we adjust these parameters to the optimal values. Therefore, the perspectives of this work consist in resolving optimization problems. As a potential future research direction, the critical parameters δ_x and δ_y , of the coordinate clustering approach, may be auto-adapted to facilitate their usage in our algorithm. In this case, a design of an algorithm to optimize these parameters could be useful. Another future research direction could consist in studying the robustness of our approach for indoor environments in which the obstacles are neither horizontal nor vertical.

Another future work consists in optimizing the ANN by using genetic algorithms for weight computation, and then testing the algorithm over a larger area, to assess the efficiency of the algorithm, in terms of robustness and accuracy.

Finally, in respect to the dynamic mobile location, an interesting future research direction could be to design an algorithm to optimize the DFI order.

References

- [Abhi 07] R. Abhishek, K. D. Sajal, and B. Kalyan. “A Predictive Framework for Location-Aware Resource Management in Smart Homes”. *IEEE Transactions on Mobile Computing*, Vol. 6, No. 11, pp. 1270–1283, 2007.
- [Achu 09] K. Achutegui, L. Martino, J. Rodas, C. Escudero, and J. Miguez. “A Multi-Model Particle Filtering Algorithm for Indoor Tracking of Mobile Terminals Using RSS Data”. In: *Proceedings of IEEE on Control Applications, (CCA) Intelligent Control, (ISIC)*, pp. 1702–1707, Saint Petersburg, Russia, July 8-10, 2009.
- [Achu 12] K. Achutegui, J. MiGuez, J. Rodas, and C. Escudero. “A Multi-Model Sequential Monte Carlo Methodology for Indoor Tracking: Algorithms and Experimental Results”. *Signal Processing*, Vol. 92, No. 11, pp. 2594–2613, 2012.
- [Ash 04] J. Ash and L. Potter. “Sensor Network Localization via Received Signal Strength Measurements with Directional Antennas”. In: *Proceedings of Allerton Conference on Communication, Control, and Computing*, pp. 1861–1870, Monticello, IL, USA, September 29-October 1, 2004.
- [Baal 09a] O. Baala, Z. You, and A. Caminada. “The Impact of AP Placement in WLAN-Based Indoor Positioning System”. In: *Proceedings of IEEE International Conference on Networks*, pp. 12–17, Gosier, Gaudeloupe, France, March 1-6, 2009.
- [Baal 09b] O. Baala, Z. You, and A. Caminada. “Toward Environment Indicators to Evaluate WLAN-Based Indoor Positioning System”. In: *Proceedings of IEEE/ACS International Conference on Computer Systems and Applications (AICCSA)*, pp. 243–250, Rabat, Maroc, May 10-13, 2009.
- [Bahi 09] A. Bahillo and S. Mazuelas. “Indoor Location Based on IEEE 802.11 Roundtrip Time Measurements with Two-Step NLOS Mitigation”. *Progress In Electromagnetics Research (PIER)*, Vol. 15, pp. 285–306, 2009.
- [Bahl 00a] P. Bahl, A. Balachandran, and V. Padmanabhan. “Enhancements to the RADAR User Location and Tracking System”. Microsoft Research TechReport, MSR-TR-2000-12, 2000.
- [Bahl 00b] P. Bahl and V. Padmanabhan. “RADAR: an In-Building RF-Based User Location and Tracking System”. In: *Proceedings of IEEE International Conference on Computer Communications (INFOCOM)*, pp. 775–784, Tel Aviv, Israel, March 26-30, 2000.
- [Batt 01] J. Battaglia, O. Cois, L. Puigsegus, and A. Oustaloup. “Solving an Inverse Heat Conduction Problem Using a Non-Integer Identified Model”. *International Journal of Heat and Mass Transfer*, Vol. 44, No. 14, pp. 2671–2680, 2001.
- [Bish 95] C. M. Bishop. *Neural Networks for Pattern Recognition*. Oxford University Press, 1995.
- [Bore 08] M. Borenovic, A. Neskovic, D. Budimir, and L. Zezelj. “Utilizing Artificial Neural Networks for WLAN Positioning”. In: *Proceedings of IEEE International Symposium on Personal, Indoor and Mobile Radio Communications (PIMRC)*, pp. 1–5, Cannes, France, September 15-18, 2008.
- [Boue 09] M. Bouet and G. Pujolle. “L-VIRT: Range-Free 3-D Localization of RFID Tags Based on

- Topological Constraints”. *Computer Communications*, Vol. 32, No. 13-14, pp. 1485–1494, 2009.
- [Bria 10] F. Brian, W. Kari, and B. Alan. “Location-Aware Tools for Improving Public Transit Usability”. *IEEE Pervasive Computing*, Vol. 9, No. 1, pp. 13–19, 2010.
- [Brun 05] M. Brunato and R. Battiti. “Statistical Learning Theory for Location Fingerprinting in Wireless LANs”. *Computer Networks*, Vol. 47, No. 6, pp. 825–845, 2005.
- [Chen 06] Y. Chen, Q. Yang, J. Yin, and X. Chai. “Power-Efficient Access-Point Selection for Indoor Location Estimation”. *IEEE Transactions on Knowledge and Data Engineering*, Vol. 18, No. 7, pp. 877–888, 2006.
- [Chen 11] C.-S. Chen and J.-M. Lin. “Applying Rprop Neural Network for the Prediction of the Mobile Station Location”. *Sensors*, Vol. 11, No. 4, pp. 4207–4230, 2011.
- [Chen 91] S. Chen, C. Cowan, and P. Grant. “Orthogonal Least Squares Learning Algorithm for Radial Basis Function Networks”. *IEEE Transactions on Neural Networks*, Vol. 2, No. 2, pp. 302–309, 1991.
- [Chen 99] P. Chen. “A Non-Line-Of-Sight Error Mitigation Algorithm in Location Estimation”. In: *Proceedings of IEEE on Wireless Communications and Networking Conference (WCNC)*, pp. 316–320, New Orleans, LA, USA, September 21-24, 1999.
- [Cong 04] L. Cong and W. Zhuang. “Non-Line-Of-Sight Error Mitigation in Mobile Location”. In: *Proceedings of IEEE International Conference on Computer Communications (INFOCOM)*, pp. 1–10, Hong Kong, China, March 7-11, 2004.
- [Corr 03] N. Correal, S. Kyperountas, Q. Shi, and M. Welborn. “An Ultra Wideband Relative Location System”. In: *Proceedings of IEEE on Ultra Wideband Systems Technologies Conference*, pp. 394–397, Reston, VA, USA, November 16-19, 2003.
- [Cris 00] N. Cristianini and J. Shawe-Taylor. *An Introduction to Support Vector Machines*. Cambridge University Press, 2000.
- [Daac 12] B. Daachi, T. Madani, and A. Benallegue. “Adaptive Neural Controller for Redundant Robot Manipulators and Collision Avoidance with Mobile Obstacles”. *Neurocomputing*, Vol. 79, No. 1, pp. 50–60, 2012.
- [Dakk 11a] M. Dakkak, A. Nakib, B. Daachi, P. Siarry, and J. Lemoine. “Indoor Localization Method Based on RTT and AOA Using Coordinates Clustering”. *Computer Networks*, Vol. 55, No. 8, pp. 1794–1803, 2011.
- [Dakk 11b] M. Dakkak, A. Nakib, B. Daachi, P. Siarry, and J. Lemoine. “Méthode Hybride de Localisation à l’Intérieur d’un Bâtiment via la Classification de Coordonnées”. In: *ROADEF 2011 - 12e congrès annuel de la Société française de Recherche Opérationnelle et d’Aide à la Décision*, pp. I–411, Saint-Etienne, France, March 2-4, 2011.
- [Dakk 12a] M. Dakkak, B. Daachi, A. Nakib, and P. Siarry. “Neural Networks and Nearest Neighbor Range-Free Techniques for Indoor Localization”. *Under submission*, 2012.
- [Dakk 12b] M. Dakkak, A. Nakib, B. Daachi, and P. Siarry. “Localisation de Capteurs Sans Fil. Parallélisation sur GPGPU”. In: *ROADEF 2012 - 13e congrès annuel de la Société française de Recherche Opérationnelle et d’Aide à la Décision*, pp. 160–161, Angers, France, April 11-13, 2012.
- [Dakk 12c] M. Dakkak, A. Nakib, B. Daachi, P. Siarry, and J. Lemoine. “Mobile Indoor Location Based on Fractional Differentiation”. In: *Proceedings of IEEE on Wireless Communications and Networking Conference (WCNC)*, pp. 2003–2008, Paris, France, April 1-4, 2012.
- [Dawe 11] B. Dawes and K.-W. Chin. “A Comparison of Deterministic and Probabilistic Methods for Indoor Localization”. *Journal of Systems and Software*, Vol. 84, No. 3, pp. 442–451,

- 2011.
- [Dran 98] C. Drane, M. Macnaughtan, and C. Scott. “Positioning GSM Telephones”. *IEEE Communications Magazine*, Vol. 36, No. 4, pp. 46–54,59, April, 1998.
- [Ebli 10] M. Ebling and R. Cáceres. “Gaming and Augmented Reality Come to Location-Based Services”. *IEEE Pervasive Computing*, Vol. 9, No. 1, pp. 5–6, 2010.
- [Even 05] F. Evennou, F. Marx, and E. Novakov. “Map-Aided Indoor Mobile Positioning System Using Particle Filter”. In: *Proceedings of IEEE on Wireless Communications and Networking Conference (WCNC)*, pp. 2490–2494, New Orleans, LA, USA, March 13-17, 2005.
- [Even 07] F. Evennou. *Techniques et Technologies de Localisation Avancées pour Terminaux Mobiles dans les Environnements Indoor*. PhD thesis, Université Joseph Fourier - Grenoble I, France, January 22, 2007.
- [Fang 08] S. Fang and T. Lin. “Indoor Location System Based on Discriminant-Adaptive Neural Network in IEEE 802.11 Environments”. *IEEE Transactions on Neural Networks and Learning Systems*, Vol. 19, No. 11, pp. 1973–1978, 2008.
- [Fang 90] B. Fang. “Simple Solution for Hyperbolic and Related Position Fixes”. *IEEE Transactions on Aerospace and Electronic Systems*, Vol. 26, No. 5, pp. 748–753, 1990.
- [Ferd 00] Y. Ferdi, J. P. Herbeuval, and A. Charel. “Un Filtre Numérique Basé sur la Dérivation Non-Entière pour l’Analyse du Signal Electrocardiographique”. *Journal de l’Innovation et Technologies en Biologie et Médecine*, Vol. 21, No. 4, pp. 205–209, 2000.
- [Ferd 11] Y. Ferdi. “Fractional order calculus-based filters for biomedical signal processing”. In: *Proceedings of Middle East Conference on Biomedical Engineering (MECBME)*, pp. 73–76, Sharjah, February 21-24, 2011.
- [Fisc 10] C. Fischer and H. Gellersen. “Location and Navigation Support for Emergency Responders: A Survey”. *IEEE Pervasive Computing*, Vol. 9, No. 1, pp. 38–47, 2010.
- [GmbH 08] A. GmbH. “Radiowave Propagation Simulator (RPSim)”. Version 5.4, Build (457), Student Edition, <http://www.actix.com/>, 1997-2008.
- [Grau 07] D. Graupe. *Principles of Artificial Neural Networks*. Second Edition, World Scientific Publishing Co., Inc., 2007.
- [Gunt 05] A. Gunther and C. Hoene. “Measuring Round Trip Times to Determine the Distance Between WLAN Nodes”. In: *Proceedings of Networking*, pp. 768–779, Waterloo, Canada, May 2-6, 2005.
- [Guo 08] F. Guo, C. Zhang, M. Wang, and X. Xu. “Research of Indoor Location Method Based on the RFID Technology”. In: *Proceedings of the 11th Joint Conference on Information Sciences (JCIS)*, pp. 1–6, Shenzhen, China, December 15-20, 2008.
- [Gure 11] E. Guresen, G. Kayakutlu, and T. Daim. “Using Artificial Neural Network Models in Stock Market Index Prediction”. *Expert Systems with Applications*, Vol. 38, No. 8, pp. 10389–10397, 2011.
- [Gust 00] F. Gustafsson. *Adaptive Filtering and Change Detection*. John Wiley & Sons, Ltd, 2000.
- [Gust 02] F. Gustafsson, N. Bergman, U. Forssell, J. Jansson, R. Karlsson, and P.-J. Nordlund. “Particle Filters for Positioning, Navigation and Tracking”. *IEEE Transactions on Signal Processing*, Vol. 50, No. 2, pp. 425–437, 2002.
- [Haeb 04] A. Haeberlen, E. Flannery, A. Ladd, A. Rudys, D. Wallach, and L. Kavraki. “Practical Robust Localization Over Large-Scale 802.11 Wireless Networks”. In: *Proceedings of the 10th Annual International Conference on Mobile Computing and Networking (MobiCom)*, pp. 70–84, Philadelphia, PA, USA, September 26- October 1, 2004.
- [Haga 94] M. Hagan and M. Menhaj. “Training Feedforward Networks with the Marquardt Algo-

- rithm”. *IEEE Transactions on Neural Networks*, Vol. 5, No. 6, pp. 989–993, 1994.
- [Hami 10] M. Hamid, K. Nitin, and T. Taravudh. “Indoor Positioning System Using Artificial Neural Network”. *Journal of Computer Science*, Vol. 6, No. 10, pp. 1219–1225, 2010.
- [Henr 78] P. Henrici. “Fast Fourier Methods in Computational Complex Analysis”. *Society for Industrial and Applied Mathematics (SIAM), Journal on Applied Mathematics*, Vol. 21, No. 4, pp. 481–527, 1978.
- [Hoss 07] A. Hossain, M. Mahtab, H. Van, Y. Jin, and W.-S. Soh. “Indoor Localization Using Multiple Wireless Technologies”. In: *Proceedings of IEEE International Conference on Mobile Adhoc and Sensor Systems*, pp. 1–8, Pisa, Italy, October 8-11, 2007.
- [Juli 97] S. Julier and J. Uhlmann. “A New Extension of the Kalman Filter to Nonlinear Systems”. In: *Proceedings of AeroSense, the 11th International Symposium on Aerospace/Defence Sensing, Simulation and Controls*, pp. 182–193, Orlando, FL, USA, April 20-25, 1997.
- [Jung 05] I.-S. Jung, T. Devinder, and G.-N. Wang. “Neural Network Based Algorithms for Diagnosis and Classification of Breast Cancer Tumor”. In: *Proceedings of International Conference of Computational Intelligence and Security (CIS), Part I*, pp. 107–114, Xian, China, December 15-19, 2005.
- [Kaem 04] K. Kaemarungsi and P. Krishnamurthy. “Properties of Indoor Received Signal Strength for WLAN Location Fingerprinting”. In: *Proceedings of International Conference on Mobile and Ubiquitous Systems: Networking and Services (MobiQuitous)*, pp. 14–23, Boston, MA, USA, August 22-26, 2004.
- [Kaem 05] K. Kaemarungsi. *Design of Indoor Positioning Systems Based on Location Fingerprinting Technique*. PhD thesis, University of Pittsburgh Pittsburgh, PA, USA, February 16, 2005.
- [Kail 00] T. Kailath, A. Sayed, and B. Hassibi. *Linear Estimation*. Vol. 1, Prentice Hall NJ, 2000.
- [Kana 04] M. Kanaan and K. Pahlavan. “A Comparison of Wireless Geolocation Algorithms in the Indoor Environment”. In: *Proceedings of IEEE on Wireless Communications and Networking Conference (WCNC)*, pp. 177–182, Atlanta, GA, USA, March 21-25, 2004.
- [Kecm 01] V. Kecman. *Learning and Soft Computing: Support Vector Machines, Neural Networks, and Fuzzy Logic Models*. MIT Press, Cambridge, MA, USA, 2001.
- [Khan 10] S. Khan, B. Daachi, and K. Djouani. “Enhanced Sensor Localization Through Compensation of Battery Level Decay”. In: *Proceedings of IEEE International Conference on Broadband and Biomedical Communications (IB2Com)*, pp. 1–5, Malaga, Spain, December 15-17, 2010.
- [Khan 11] S. Khan, B. Daachi, and K. Djouani. “Overcoming Localization Errors Due to Node Power Drooping in a Wireless Sensor Network”. *International journal of electronics and telecommunications*, Vol. 57, No. 3, pp. 341–346, 2011.
- [Kolo 06] K. W. Kolodziej and J. Hjelm. *Local Positioning Systems. LBS Applications and Services*. CRC Press, Taylor & Francis Group LLC, 2006.
- [Kont 04] P. Kontkanen, P. Myllymaki, T. Roos, H. Tirri, K. Valtonen, and H. Wettig. “Topics in Probabilistic Location Estimation in Wireless Networks”. In: *Proceedings of the 15th IEEE Symposium on Personal, Indoor, Mobile Radio Communications*, pp. 1052–1056, Barcelona, Spain, September 5-8, 2004.
- [Koss 00] M. Kossel, H. Benedickter, R. Peter, and W. Bachtold. “Microwave Backscatter Modulation Systems”. In: *Proceedings of IEEE MTT-S International Microwave Symposium Digest*, pp. 1427–1430, Boston, MA, USA, June 11-16, 2000.
- [Kruc 92] V. Kůrková. “Kolmogorov’s Theorem and Multilayer Neural Networks”. *Neural Networks*, Vol. 5, No. 3, pp. 501–506, 1992.

-
- [Kush 06] A. Kushki, K. Plataniotis, and A. Venetsanopoulos. “Location Tracking in Wireless Local Area Networks with Adaptive Radio Maps”. In: *Proceedings of IEEE International Conference on Acoustics, Speech, and Signal Processing (ICASSP)*, pp. 741–744, Toulouse, France, May 14-19, 2006.
- [Kush 07] A. Kushki, K. Plataniotis, and A. Venetsanopoulos. “Kernel-Based Positioning in Wireless Local Area Networks”. *IEEE Transactions on Mobile Computing*, Vol. 6, No. 6, pp. 689–705, 2007.
- [Ladd 02] A. Ladd, K. Bekris, A. Rudys, G. Marceau, L. Kavradi, and D. Wallach. “Robotics-Based Location Sensing Using Wireless Ethernet”. In: *Proceedings of the 8th Annual International Conference on Mobile Computing and Networking (MobiCom)*, pp. 227–238, Atlanta, GA, USA, September 23-28, 2002.
- [Ladd 04] A. Ladd, K. Bekris, A. Rudys, D. Wallach, and L. Kavradi. “On the Feasibility of Using Wireless Ethernet for Indoor Localization”. *IEEE Transactions on Robotics*, Vol. 20, No. 3, pp. 555–559, 2004.
- [Leve 44] K. Levenberg. “A method for the Solution of Certain Problems in Least Squares”. *Quarterly of Applied Mathematics*, Vol. 2, pp. 164–168, 1944.
- [Li 00] X. Li, K. Pahlavan, M. Latva-aho, and M. Ylianttila. “Comparison of Indoor Geolocation Methods in DSSS and OFDM Wireless LAN”. In: *Proceedings of IEEE Vehicular Technology Conference*, pp. 3015–3020, Boston, MA, USA, September 24-28, 2000.
- [Liu 05] H. Liu, A. Kshirsagar, J. Ku, D. Lamb, and C. Niederberger. “Computational Models of Intracytoplasmic Sperm Injection Prognosis”. In: *Proceedings of the 13th European Symposium Artificial Neural Networks*, pp. 115–120, Bruges, Belgium, April 27-29, 2005.
- [Liu 07] H. Liu, H. Darabi, P. Banerjee, and J. Liu. “Survey of Wireless Indoor Positioning Techniques and Systems”. *IEEE Transactions on Systems, Man and Cybernetics, Part C (Applications and Reviews)*, Vol. 37, No. 6, pp. 1067–1080, 2007.
- [Maro 05] M. Maroti, B. Kusy, G. Balogh, P. Volgyesi, A. Nadas, K. Molnar, S. Dora, and A. Ledeczki. “Radio Interferometric Geolocation”. In: *Proceedings of ACM 3rd Conference on Embedded Networked Sensor Systems (SenSys)*, pp. 1–12, San Diego, CA, USA, November 2-4, 2005.
- [Marq 63] D. Marquardt. “An Algorithm for Least-Squares Estimation of Nonlinear Parameters”. *Society for Industrial and Applied Mathematics (SIAM), Journal on Applied Mathematics*, Vol. 11, No. 2, pp. 431–441, 1963.
- [Math 03] B. Mathieu, P. Melchior, A. Oustaloup, and C. Ceyral. “Fractional Differentiation for Edge Detection”. *Signal Processing*, Vol. 83, No. 11, pp. 2421–2432, 2003.
- [Mazu 09] S. Mazuelas, F. Lago, J. Blas, A. Bahillo, P. Fernandez, R. Lorenzo, and E. Abril. “Prior NLOS Measurement Correction for Positioning in Cellular Wireless Networks”. *IEEE Transactions on Vehicular Technology*, Vol. 58, No. 5, pp. 2585–2591, 2009.
- [Merw 00] R. V. D. Merwe, A. Doucet, N. D. Freitas, and E. Wan. “The Unscented Particle Filter”. Technical report *cued/f-infeng/tr 380*, Cambridge University Engineering Department, August, 2000.
- [Mike 04] H. Mike, S. James, and K. John. “Location-Aware Computing Comes of Age”. *IEEE Computer*, Vol. 37, No. 2, pp. 95–97, 2004.
- [Mill 93] K. Miller and B. Ross. *An Introduction to Fractional Calculus and Fractional Differential Equations*. John Wiley & Sons, Inc., 1993.
- [Mish 12] S. Mishra and S. Savarkar. “Image Compression Using Neural Network”. In: *Proceedings of International Conference and Workshop on Emerging Trends in Technology (ICWET)*, pp. 18–21, New York, NY, USA, 2012.
-

-
- [Mous 08] A. Moustapha and R. Selmic. “Wireless Sensor Network Modeling Using Modified Recurrent Neural Networks: Application to Fault Detection”. *IEEE Transactions on Instrumentation and Measurement*, Vol. 57, No. 5, pp. 981–988, 2008.
- [Nicu 03] D. Niculescu and B. Nath. “Ad Hoc Positioning System (APS) Using AOA”. In: *Proceedings of IEEE International Conference on Computer Communications (INFOCOM)*, pp. 1734–1743, San Francisco, CA, USA, March 30– April 3, 2003.
- [Oldh 74] K. Oldham and J. Spanier. *The Fractional Calculus*. Academic Press Inc., 1974.
- [Otte 93] B. Ottersten, M. Viberg, P. Stoica, and A. Nehorai. *Exact and Large Sample ML Techniques for Parameter Estimation and Detection in Array Processing. Radar Array Processing*, Springer Verlag, 1993.
- [Oust 96] A. Oustaloup and H. Linares. “The CRONE Path Planning”. *Mathematics and Computers in Simulation*, Vol. 41, No. 3-4, pp. 209–217, 1996.
- [Pahl 02] K. Pahlavan, X. Li, and J. Makela. “Indoor Geolocation Science and Technology”. *IEEE Communications Magazine*, Vol. 40, No. 2, pp. 112–118, 2002.
- [Pahl 09] K. Pahlavan and P. Krishnamurthy. *Networking Fundamentals: Wide, Local and Personal Area Communications*. John Wiley & Sons, 2009.
- [Pan 06] J. Pan, J. Kwok, Q. Yang, and Y. Chen. “Multidimensional Vector Regression for Accurate and Low-Cost Location Estimation in Pervasive Computing”. *IEEE Transactions on Knowledge and Data Engineering*, Vol. 18, No. 9, pp. 1181–1193, 2006.
- [Paol 09] B. Paolo, L. Stefano, C. Stefano, and G. Gaetano. “Virtual Calibration for RSSI-Based Indoor Localization with IEEE 802.15.4”. In: *Proceedings of IEEE International Conference on Communications (ICC)*, pp. 5–10, Dresden, Germany, June 14-18, 2009.
- [Para 02] P. Parasithsangaree, P. Krishnamurthi, and P. Chrysanthis. “On Indoor Position Location with Wireless LANs”. In: *Proceedings of IEEE International Symposium on Personal Indoor Mobile Radio Communications*, pp. 720–724, Pavilhao Atlantico, Lisboa, Portugal, September 15-18, 2002.
- [Parl 94] A. Parlos, K. Chong, and A. Atiya. “Application of the Recurrent Multilayer Perceptron in Modeling Complex Process Dynamics”. *IEEE Transactions on Neural Networks*, Vol. 5, No. 2, pp. 255–66, 1994.
- [Paul 08] A. Paul and E. Wan. “Wi-Fi Based Indoor Localization and Tracking Using Sigma-Point Kalman Filtering Methods”. In: *Proceedings of IEEE/ION on Position, Location and Navigation Symposium*, pp. 646–659, Monterey, CA, USA, May 5-8, 2008.
- [Pete 98] B. Peterson, C. Kliecik, R. Hartnett, P. Thompson, J. Mendoza, and H. Nguyen. “Spread Spectrum Indoor Geolocation”. *Institute’s Journal, Navigation*, Vol. 45, No. 2, pp. 97–102, 1998.
- [Pras 02] P. Prasithsangaree, P. Krishnamurthy, and P. Chrysanthis. “On Indoor Position Location with Wireless LANs”. In: *Proceedings of the 13th IEEE International Symposium on Personal, Indoor, and Mobile Radio Communications*, pp. 720–724, Los Alamitos, CA, USA, September 15-18, 2002.
- [Prod 02] I. Prodlubny. “Geometric and Physical Interpretation of Fractional Integration and Fractional Differentiation”. *Fractional calculus and applied analysis*, Vol. 5, No. 4, pp. 367–386, 2002.
- [Ramu 02] C. Ramus-Serment, X. Moreau, M. Nouillant, A. Oustaloup, and F. Levron. “Generalised Approach on Fractional Response of Fractal Networks”. *Chaos, Solitons and fractals*, Vol. 14, No. 3, pp. 479–488, 2002.
- [Ried 93] M. Riedmiller and H. Braun. “A Direct Adaptive Method for Faster Backpropagation
-

- Learning: the RPROP Algorithm”. In: *Proceedings of IEEE International Conference on Neural Networks*, pp. 586–591, San Francisco, CA, USA, March 28– April 1, 1993.
- [Roos 02] T. Roos, P. Myllymäki, H. Tirri, P. Misikangas, and J. Sievänen. “A Probabilistic Approach to WLAN User Location Estimation”. *International Journal of Wireless Information Networks*, Vol. 9, No. 3, pp. 155–164, 2002.
- [Rume 86] D. Rumelhart, G. Hintont, and R. Williams. “Learning Representations by Back-Propagating Errors”. *Nature*, Vol. 323, No. 6088, pp. 533–536, 1986.
- [Saha 03] S. Saha, K. Chaudhuri, D. Sanghi, and P. Bhagwat. “Location Determination of a Mobile Device Using IEEE 802.11b Access Point Signals”. In: *Proceedings of IEEE on Wireless Communications and Networking Conference (WCNC)*, pp. 1987–1992, New Orleans, LA, USA, March 16–20, 2003.
- [Sall 10] J. Sallai, A. K. Lédeczi, I. Amundson, X. Koutsoukos, and M. Maróti. “Using RF Received Phase for Indoor Tracking”. In: *Proceedings of the 6th Workshop on Hot Topics in Embedded Networked Sensors*, pp. 1–5, Killarney, Ireland, June 28–29, 2010.
- [Seow 08] C. Seow and S. Tan. “Localization of Omni-Directional Mobile Device in Multipath Environments”. *Progress In Electromagnetics Research (PIER)*, Vol. 85, pp. 323–348, 2008.
- [Serg 09] S. Sergi, F. Pancaldi, and G. Vitetta. “Cluster-Based Ranging for Accurate Localization in Wireless Sensor Networks”. In: *Proceedings of IEEE International Conference on Communications (ICC)*, pp. 1–5, Dresden, Germany, June 14–18, 2009.
- [Sidd 12] U. Siddhaling. “Multilayer Feed-Forward Neural Network Integrated with Dynamic Learning Algorithm by Pruning of Nodes and Connections”. *International Journal of Computer Applications*, Vol. 47, No. 2, pp. 7–17, 2012.
- [Simp 95] P. Simpson. *Neural Networks Theory, Technology and Applications*. First Edition, IEEE Technology Update Series, 1995.
- [So 03] H. So and E. Shiy. “Performance of TOA-AOA Hybrid Mobile Location”. *Transactions on Fundamentals of Electronics, Communications and Computer Sciences IEICE Transactions*, Vol. E86-A, No. 8, pp. 2136–2138, 2003.
- [Stat 06] D. Stathakis and A. Vasilakos. “Satellite Image Classification Using Granular Neural Networks”. *International journal of remote sensing*, Vol. 27, No. 18, pp. 3991–4003, 2006.
- [Stoi 97] P. Stoica and R. L. Moses. *Introduction to Spectral Analysis*. First Edition, Prentice Hall, 1997.
- [Suro 11] D. Suroso, P. Cherntanomwong, P. Sooraksa, and J. Takada. “Fingerprint-Based Technique for Indoor Localization in Wireless Sensor Networks Using Fuzzy C-Means Clustering Algorithm”. In: *Proceedings of IEEE International Symposium on Intelligent Signal Processing and Communications Systems (ISPACS)*, pp. 1–5, Chiang Mai, Thailand, December 7–9, 2011.
- [Swan 08] N. Swangmuang and P. Krishnamurthy. “An Effective Location Fingerprint Model for Wireless Indoor Localization”. *Pervasive and Mobile Computing*, Vol. 4, No. 6, pp. 836–850, 2008.
- [Taye 09] A. Tayebi, J. Gomez, F. S. de Adana, and O. Gutierrez. “The Application of Ray-Tracing to Mobile Localization Using the Direction of Arrival and Received Signal Strength in Multipath Indoor Environments”. *Progress In Electromagnetics Research (PIER)*, Vol. 91, pp. 1–15, 2009.
- [Teub 06] A. Teuber and B. Eissfeller. “A Two-Stage Fuzzy Logic Approach for Wireless LAN Indoor Positioning”. In: *Proceedings of IEEE/ION on Position Location and Navigation Symposium*, pp. 730–738, San Diego, CA, USA, April 24–27, 2006.

-
- [Torr 84] D. Torrieri. “Statistical Theory of Passive Location Systems”. *IEEE Transactions on Aerospace and Electronic Systems*, Vol. 20, No. 2, pp. 183–197, 1984.
- [Vapn 99] V. Vapnik. *The Nature of Statistical Learning Theory. Statistics for Engineering and Information Science*, Second Edition, Springer, 1999.
- [Vars 07] A. Varshavsky, E. de Lara, J. Hightower, A. LaMarca, and V. Otsason. “GSM Indoor Localization”. *Pervasive and Mobile Computing*, Vol. 3, No. 6, pp. 698–720, 2007.
- [Veen 88] B. Veen and K. Buckley. “Beamforming: A Versatile Approach to Spatial Filtering”. *IEEE Acoustics, Speech, and Signal Processing Magazine*, Vol. 5, No. 2, pp. 4–24, 1988.
- [Wang 08] H. Wang, A. Szabo, J. Bamberger, D. Brunn, and U. Hanebeck. “Performance Comparison of Nonlinear Filters for Indoor WLAN Positioning”. In: *Proceedings of International Conference on Information Fusion*, pp. 1–7, Cologne, Germany, June 30- July 3, 2008.
- [Welc 01] G. Welch and G. Bishop. “An Introduction to the Kalman Filter”. Technical report, University of North Carolina, Chapel Hill, 2001.
- [Werb 88] P. Werbos. “Backpropagation: Past and Future”. In: *Proceedings of IEEE International Conference on Neural Networks*, pp. 343–353, San Diego, CA, USA, July 24-27, 1988.
- [Wi F 08] *Wi-Fi Location-Based Services 4.1 Design Guide, (Chapter 2)*. Cisco Systems, Inc., <http://www.cisco.com/>, 2008.
- [Wu 04] C. Wu, L. Fu, and F. Lian. “WLAN Location Determination in e-Home via Support Vector Classification”. In: *Proceedings of IEEE International Conference on Networking Sensing and Control*, pp. 1026–1031, Taipei, Taiwan, March 21-31, 2004.
- [Yin 08] J. Yin, Q. Yang, and L. Ni. “Learning Adaptive Temporal Radio Maps for Signal-Strength-Based Location Estimation”. *IEEE Transactions on Mobile Computing*, Vol. 7, No. 7, pp. 869–883, 2008.
- [Yous 03] M. Youssef, A. Agrawala, and U. Shankar. “WLAN Location Determination via Clustering and Probability Distributions”. In: *Proceedings of IEEE International Conference on Pervasive Computing and Communications*, pp. 143–150, Fort Worth, TX, USA, March 23-26, 2003.
- [Yous 05] M. Youssef and A. K. Agrawala. “The Horus WLAN Location Determination System”. In: *Proceedings of the 3rd International Conference on Mobile Systems, Applications, and Services (MobiSys)*, pp. 205–218, Seattle, WA, USA, June 06-08, 2005.
- [Yu 10] H. Yu and B. Wilamowski. *Levenberg Marquardt Training, (Chapter 12, pp. 1-16)*. Vol. 5, Industrial Electronics Handbook, Intelligent Systems 2nd Edition, CRC Press, 2010.
- [Yun 09] S. Yun, J. Lee, W. Chung, E. Kim, and S. Kim. “A Soft Computing Approach to Localization in Wireless Sensor Networks”. *Expert Systems with Applications*, Vol. 36, No. 4, pp. 7552–7561, 2009.
- [Zhe 04] X. Zhe, S. Song, C. Jin, W. Hao, H. Jian, and G. Xingxin. “A Wireless LAN-Based Indoor Positioning Technology”. *IBM Journal of Research and Development*, Vol. 48, No. 5-6, pp. 617–626, 2004.
- [Zhen 04] J. Zhen and S. Zhang. “Adaptive AR Model Based Robust Mobile Location Estimation Approach in NLOS Environment”. In: *Proceedings of IEEE Vehicular Technology Conference*, pp. 2682–2685, Milan, Italy, May 17-19, 2004.
- [Zhou 05] J. Zhou, K.-K. Chu, and J.-Y. Ng. “Providing Location Services Within a Radio Cellular Network Using Ellipse Propagation Method”. In: *Proceedings of the 19th International Conference on Advanced Information Networking Applications*, pp. 559–564, Tamkang University, Taiwan, March 28-30, 2005.
- [ZYou 10] Z.You, O. Baala, and A. Caminada. “Efficient Design of Indoor Positioning Systems
-

Based on Optimization Model". In: *Wireless Days (WD), International Federation for Information Processing (IFIP)*, pp. 1–5, Venice, Italy, October 20-22, 2010.